TAL TECH

DOCTORAL THESIS

Molecularly Imprinted Polymer-modified Electrodes for Electrochemical Sensing of Emerging Aqueous Pollutants

Vu Bao Chau Nguyen

TALLINNA TEHNIKAÜLIKOOL
TALLINN UNIVERSITY OF TECHNOLOGY
TALLINN 2025

Molecularly Imprinted Polymer-modified Electrodes for Electrochemical Sensing of Emerging Aqueous Pollutants

VU BAO CHAU NGUYEN

TAL
TECH
PRESS

TALLINN UNIVERSITY OF TECHNOLOGY
School of Engineering
Department of Materials and Environmental Technology
This dissertation was accepted for the defence of the degree 02/07/2025

Supervisor: Dr. Vitali Syritski
                                   Leading Researcher, Head of Laboratory
                                   School of Engineering
                                   Tallinn University of Technology
                                   Tallinn, Estonia

Co-supervisor: Dr. Jekaterina Reut
                                   School of Engineering
                                   Tallinn University of Technology
                                   Tallinn, Estonia

Opponents: Prof. Sergey A. Piletsky
                                   Research Director for School of Chemistry
                                   Chemistry Department, University of Leicester
                                   Leicester, United Kingdom

                                   Prof. Toonika Rinken
                                   Associate Professor in Environmental Chemistry
                                   Institute of Chemistry
                                   University of Tartu
                                   Tartu, Estonia

Defence of the thesis: 12/09/2025, Tallinn

Declaration:
Hereby I declare that this doctoral thesis, my original investigation and achievement, submitted for the doctoral degree at Tallinn University of Technology has not been submitted for doctoral or equivalent academic degree.

Vu Bao Chau Nguyen

                                   _____
                                                        signature

Molekulaarselt jäljendatud polümeeriga modifitseeritud elektroodid esilekerkivate veesaasteainete elektrokeemiliseks tuvastamiseks

VU BAO CHAU NGUYEN

Contents

List of publications

The list of author's publications, on the basis of which the thesis has been prepared:

I **V.B.C. Nguyen**, J. Reut, J. Rappich, K. Hinrichs, V. Syritski, Molecularly Imprinted Polymer-Based Electrochemical Sensor for the Detection of Azoxystrobin in Aqueous Media, Polymers 16 (2024) 1394.

II **V.B.C. Nguyen**, A.G. Ayankojo, J. Reut, J. Rappich, A. Furchner, K. Hinrichs, V. Syritski, Molecularly Imprinted Co-Polymer for Class-Selective Electrochemical Detection of Macrolide Antibiotics in Aqueous Media, Sens. Actuators B Chem. 374 (2023) 132768.

III **V.B.C. Nguyen**, J. Reut, A.G. Ayankojo, V. Syritski, Direct Electrochemical Sensing of Ampicillin in Aqueous Media by a Ruthenium Oxide Electrode Decorated with a Molecularly Imprinted Polymer, Talanta 287 (2025) 127580.

In addition, the author has contributed to a review article relevant to the molecular imprinting technique for detecting antibiotic pollutants in aqueous environments. Although not included in the main research of this thesis, the following publication provides a comprehensive overview of recent advancements and supports the broader scientific context of the work:

A.G. Ayankojo, J. Reut, **V.B.C. Nguyen**, R. Boroznjak, V. Syritski, Advances in Detection of Antibiotic Pollutants in Aqueous Media Using Molecular Imprinting Technique—A Review, Biosensors 12 (2022) 441.

Author's contribution to the publications

Contribution to the papers in this thesis are:

I   Major role in experimental work and data processing, writing manuscript with assistance from co-authors.

II Major role in experimental work, participating in data processing and in manuscript writing.

III Major role in experimental work and data processing, writing manuscript with assistance from co-authors.

Introduction

Water pollution is a growing global concern that endangers both environmental and human health. Among the emerging contaminants, fungicides and antibiotics are particularly alarming due to their extensive use and persistence in aquatic environments. Fungicides account for 23–25% of the 2.7 million tons of pesticides used globally in 2020, reflecting their widespread application in agriculture [1]. Likewise, global antibiotic consumption increased by 65% between 2000 and 2015 with a prediction of a further rise up to 200% by 2030 [2]. Both of these compounds frequently escape into water through wastewater disposal [3], [4], [5], where they can accumulate, disrupt ecosystems, and pose health risks such as toxicity or DNA damage [6], [7]. The situation is exacerbated when nearly 8,500 tonnes of antibiotics are released into river water annually, with 3,300 tonnes reaching the oceans, making over 6 million kilometres of rivers worldwide experiencing antibiotic concentrations above ecological safety thresholds [8]. This significantly contributes to antimicrobial resistance, a major threat predicted to cause 10 million deaths annually by 2050 [9]. Therefore, the urgent need for effective detection and monitoring strategies to safeguard the environment and public health cannot be overstated.

Conventional analytical techniques, including high-performance liquid chromatography, mass spectrometry, immunoassays, have been widely used to detect fungicides and antibiotics. Nonetheless, they required expensive equipment and skilled operators, which are impractical for in-field analysis. As a result, attention has shifted toward sensor-based approaches, such as biosensors and chemical sensors, which offer portability and enable daily environmental monitoring [10], [11]. Despite their advantages, many of them rely on natural receptors or nanomaterials, which limit their stability or selectivity. To overcome these limitations, the development of synthetic recognition elements has gained increasing interest [12], [13].

Among such materials, molecularly imprinted polymers (MIPs) have emerged as effective candidates a recognition element for sensor development. MIPs are stable, crosslinked polymer network that contain molecular recognition sites specific to target analytes. They have distinguished themselves as versatile biomimetic receptors in analytical chemistry, offering promising alternatives to biological receptors for the selective detection of target analytes [14]. When interfaced with sensor transducers, molecular recognition events occurring within MIPs can be translated into measurable electrical signals, enabling the development of versatile tools for a wide range of sensor applications. Electrochemical transducers, in particular, offer an attractive platform due to their simplicity, sensitivity, and compatibility with miniaturized formats. In this context, MIPs act as synthetic recognition elements that provide high selectivity toward target analytes, supporting the development of portable sensors for accurate and rapid in-situ environmental analysis. Inevitably, their applications have been expanded to the selective detection of plenty environmental water pollutants [15].

In most cases, the working principle of MIP-based electrochemical sensors involves using an external redox probe (e.g., ferricyanide) to monitor the adsorption-dependent changes in the diffusion of redox probe ions through the target-specific cavities preformed on the MIP surface [16], [17]. Nevertheless, the dependence on external redox probes complicates sensor design, can introduce stability issues due to potential interference from other electroactive species, and produces an indirect signal that reflects not only target presence but also changes in polymer during sample interaction

[18]. These limitations motivate the exploration of alternative approaches, including the incorporation of internal redox centers into the polymer matrices or electrode materials, to remove the need for external redox probes and enhance signal stability [19], [20].

Meanwhile, ruthenium oxide (RuO_2) electrodes are exceptionally suited for achieving high sensitivity in electrochemical detection applications as they are esteemed for their steadfast catalytic efficacy [21]. Also, it demonstrates remarkable thermodynamic stability, ensuring consistent performance of RuO_2 electrodes even under challenging experimental conditions [22]. The expansive potential window of RuO_2 electrodes allows for their exploration in diverse redox processes [23]. Additionally, the porous structure of RuO_2 electrodes provides a large surface area [24], which is crucial for enhancing charge-transfer characteristics and sensitivity in electrochemical measurements [25] (e.g., pH sensing in water [26]). Moreover, RuO_2 exhibits versatile electrochemical behaviour when possessing multiple accessible oxidation states [27], [28], particularly valuable in MIP-based sensor configuration, as a single RuO_2 electrode can serve a dual purpose: an electrochemical transducer and an internal redox probe. This enables MIP-based electrochemical sensors to measure signals directly, and reduce contamination risks, thus ensuring more reliable results.

Despite extensive research on MIP-based electrochemical sensors, practical implementation for detecting fungicide and antibiotic pollutants in water remains limited, mostly due to challenges in maintaining reliable performance in complex real-world samples, such as tap or natural water [29]. For instance, the synthesis of MIPs tailored for agriculture fungicide azoxystrobin (AZO) recognition and their subsequent application in electrochemical sensing platforms have not been previously reported. Additionally, the possibility of class-selective detection can be of great advantage for monitoring environmental pollutants since they are presented together at varying concentrations. Moreso, the development of MIP-based electrochemical sensors that operate without the need of external redox probe remains underexplored, despite their potential to reduce contaminant risk. Thus, further studies are essential to advance MIP-based electrochemical sensors for in-field applications.

This thesis aims to develop MIP-based electrochemical sensors for the fast and reliable detection of both individual pollutants—such as AZO and AMP—and pollutant classes, specifically ML class of antibiotics. The AZO-MIP-based electrochemical sensor (AZO sensor) is designed to address the current lack of reported MIPs for AZO recognition, thereby filling a critical gap in fungicide detection. Furthermore, the synthesis and implementation of an ML-selective MIP will, for the first time, enable the development of a sensor capable of cooperatively detecting multiple macrolide antibiotics, including erythromycin (ERY), clarithromycin (CLA), and azithromycin (AZI). In addition, the elimination of external redox probe solutions—through the use of inherently redox active materials such as RuO_2 electrodes—represents a novel and rational advancement in the design of MIP-based electrochemical sensors, particularly for applications targeting antibiotic-origin contaminants in environmental water samples. The successful implementation of these electrochemical sensors, which could be capable of operating in complex aqueous environments such as tap and river water, could provide valuable tools for portable, in-field monitoring of fungicides and antibiotics. This advancement could facilitate early detection and timely mitigation of potential environmental and public health risks associated with their presence.

Abbreviations

AMP	Ampicillin
ANI	Aniline
APBA	3-Aminophenylboronic Acid
AZI	Azithromycin
AZO	Azoxystrobin
CLA	Clarithromycin
CV	Cyclic Voltammetry
DPV	Different Pulse Voltammetry
EIS	Electrochemical Impedance Spectroscopy
ERY	Erythromycin
HPLC	High-Performance Liquid Chromatography
IRSE	Infrared Spectroscopic Ellipsometry
LOD	Limit of Detection
LOQ	Limit of Quantification
LSV	Linear Sweep Voltammetry
MIP	Molecularly Imprinted Polymer
MS	Mass Spectrometry
NIP	Non-Imprinted Polymer
ML	Macrolide
mPD	m-Phenylenediamine
PANI	Poly(Aniline)
P(ANI-co-mPD)	Poly(Aniline-co-m-Phenylenediamine)
PBS	Phosphate-Buffered Saline
PmPD	Poly(m-Phenylenediamine)
P(mPD-co-ABPA)	Poly(m-Phenylenediamine-co-3-Aminophenylboronic Acid)
QM	Quantum Mechanic
RR	Relative Response
SD	Standard Deviation
SPE	Screen-Printed Electrode
TFME	Thin Film Metal Electrode

1 Literature review

1.1 Water pollution

Environmental pollution has become a critical issue of global concern, endangered ecosystems and threatening public health. Rapid industrialization and urbanization have significantly contributed to the increased emission of harmful chemicals into air, water, and soil [30], [31]. This widespread contamination has severe implications: air pollution exacerbates respiratory illnesses, while pollutants in soil and water disrupt natural ecosystems, leading to the environmental and public health problems [32], [33]. The global scale impact of pollution contributes heavily to climate change and biodiversity loss, affecting global ecosystems with disproportionately severe impacts on developing countries [34].

A majority of air and land pollutants ultimately find their way into water systems through atmospheric deposition, surface runoff, and soil erosion [35]. Agricultural and industrial activities release a wide range of hazardous substances—such as heavy metals, toxic chemicals, pesticides, and untreated wastewater—into rivers, lakes, and oceans [36]. This makes water bodies particularly vulnerable and reduces water safety for daily human activities such as drinking, cooking, and sanitation [37], causing various human health issues, from gastrointestinal disorders to neurological diseases [38], [39].

The effects of polluted water do not stop at human; they disturb the balance of water organisms. For example, pollutants can accumulate in fish tissue, which are then consumed by other large animals and humans. The process, known as biomagnification, concentrates toxic substances at higher levels within the food chain, leading to various health issues such as developmental disorders and chronic diseases [40], [41]. Moreover, such chemicals as mercury and polychlorinated biphenyls are dangerous since they accumulate in animals, leading to the death of pieces [42]. The latter can have a domino effect on human health and a shift in food chains, which is challenging to correct.

Furthermore, the costs incurred in the treatment of water pollution are so high that many developing nations struggle to resolve [43]. In addition, the erosion of the environment and the loss of species significantly damage future generations. Thus, it is necessary to monitor pollutants within water bodies frequently to ensure the water sources safety for both human and other species [41]. It is more cost-effective to prevent and control pollutants than to address the latter occurred damage.

1.2 Pesticides and antibiotics as emerging pollutants

Compounds such as fungicides and antibiotics, originally developed to enhance agricultural productivity and prevent disease in crops and livestock, have now become widespread pollutants that threaten aquatic ecosystems. Their intense usage made them become pervasive contaminants and emerging pollutants in aquatic habitats, raising concern about the long-term effects on living species. Increasing agricultural and healthcare practices further worsen the issue of water pollutants, as fertilizers and medications are usually washed into water systems, contributing to water quality degradation. Several reports demonstrated that most pollutants reaching wastewater treatment plants were incompletely eliminated during the treatment process and released into the environment [44], [45], [46]. In particular, eighteen fungicide classes and nine antibiotic classes are identified across various aquatic environments [47], [48].

1.2.1 Fungicides

Fungicides are used to control fungal infections in agriculture. The high consumption makes them the second most globally sold category of agricultural pesticides, with 31% of the sales attributed to European consumers [1]. It is unfortunate that fungicides often find their way into nearby water systems through runoff [49] and improper disposal in treatment plants [50]. Their prolonging persistence in aquatic environments poses risks to non-target microorganisms (e.g., macrophytes, invertebrates, and vertebrates) [48], [51]. The disruption of these organisms can have cascading consequences across ecosystems and reduce biodiversity.

Fungicides pose potential risks directly to human health, including long-term exposure to certain fungicides, which results in toxic effects [52], genotoxicity, DNA damage, and cancer risk [53]. They can associate with reproductive issues, including decreased fertility, hormonal changes, congenital malformations [54], and severe chronic conditions within respiratory system functions [55]. Additionally, research proved evidence of neurodevelopmental disorders, attention deficit hyperactivity disorder (ADHD), and poor developmental brain performance in children [56], [57].

Azoxystrobin

Among common fungicide used in agriculture, azoxystrobin (AZO)—belongs to the strobilurin class—is renowned for its broad-spectrum effectiveness against a wide range of fungal pathogens [58]. The methoxyacrylate moiety, specifically the methoxy ($-OCH_3$) and acrylate groups (Figure 1), allows AZO to suppress the respiratory chain in fungi, halting energy production in fungal cells and thereby impeding their growth and reproduction [59].

Maximize Market Research predicted that global AZO market experienced significant growth, from USD 1.09 billion in 2023 to a remarkable number of USD 2.12 billion by 2030 with the biggest share from North Ameria, Asia-Pacific, and Europe [60]. Consequently, the presence of AZO contamination detected in water systems (as shown in Table 1) has triggered profound concerns about its environmental impact globally [61], [62], [63], [64]. One major concern associated with AZO is its significant threat to aquatic ecosystems due to its highly toxic nature toward a wide range of non-target aquatic
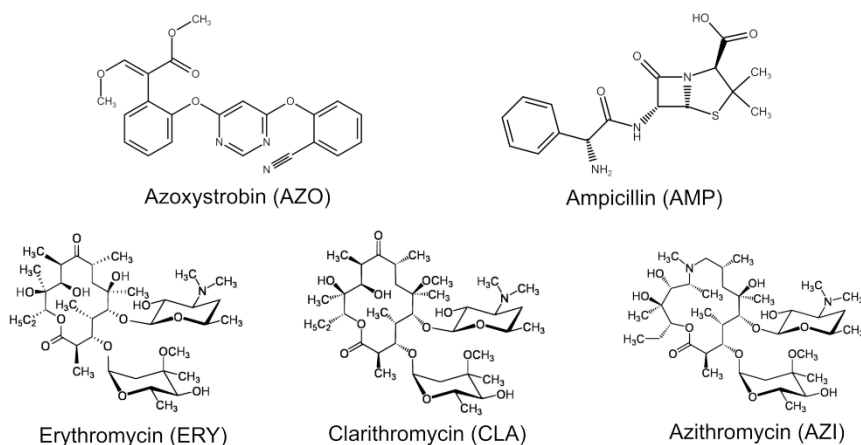
Figure 1. Molecular structures of AZO, AMP and 3 members of macrolide class: ERY, CLA, AZI.

organisms [65]. This alarming toxicity level causes adverse effects on fishes, including physiological disruptions, reduced growth rates, reproductive disorders, and even mortality [65], [66], [67], [68]. Additionally, AZO exhibits high environmental persistence, with half-life values ranging from 143 to 158 days in water across pH 4 to 9 [69], disrupts aquatic ecosystems in long-term exposure, including inhibiting eukaryotic algae growth and damaging aquatic plants by suppressing antioxidant enzymes [70], [71]. AZO contamination in water also poses human health risks, such as mitochondrial oxidative respiration suppression, neuronal lipid alterations, and genotoxic effects [72], [73]. Therefore, monitoring this fungicide in water is important to mitigate its potential impacts, managing pesticide pollution and maintain water quality.

1.2.2 Antibiotics

Nowadays, antibiotics are the most prescribed agents among pharmaceuticals used for inhibiting pathogen growth through disrupting protein synthesis and cell wall formation. In EU/EEA countries alone spend USD 1.5 billion annually to treat more than 670,000 antibiotic-resistant infections [82]. Much of this burden stems from the incomplete metabolism of antibiotics in humans and animals, leading to their excreted into wastewater [83], [84]. These residues continue entering water systems via improper pharmaceutical disposal [85], agricultural runoff [86], and inadequate wastewater treatment [87]. Consequently, varying concentrations of antibiotics have been detected in surface water and wastewater across nations, contributing to the emergence and spread of antibiotic-resistant bacteria [88], [89].

Table 1. *Representative data on environmental concentrations of AZO, MLs, and AMP reported in various water matrices.*

Compound	Water type	Location	Concentration (nM)	Reference
AZO	Stream water	Germany	73.6	[74]
ERY	Wastewater effluent	Hong Kong	4.1	[75]
	Sea water		2.4	
	Wastewater effluent	Germany	8.2	[76]
	Surface water		2.3	
CLA	Wastewater effluent	Germany	0.3	[76]
	Surface water		0.4	
	Wastewater effluent	Switzerland	0.8	[77]
AZI	Surface water	South Africa	0.03	[78]
	Sea water	Iran	0.01	[79]
	Wastewater effluent		1.2	
AMP	Wastewater	Egypt	202,057	[80]
	Wastewater effluent	Mid-Atlantic	121	[81]

The antibiotic residues reported in water bodies are of diverse genera, with fluoroquinolones being the most abundant with a frequency of 49%, followed by sulfonamides with a 30% frequency [90]. Other antibiotics classes have also been found in water, including tetracyclines, macrolides, and beta-lactams. Such compounds exhibit long-lasting persistence from several months to years [91]. Conventional water treatment facilities fail to eradicate them from water completely, hence advanced technologies integrated membrane and oxidation processes have been proven effective in solving this problem. However, they are not fully developed for large-scale applications due to high costs and difficulties in engineering [92].

In aquatic ecosystems, antibiotics can disrupt microbial communities critical for nutrient cycling and water purification. Their chemical activity may interfere with essential biological functions, potentially producing toxic effects on humans, animals, plants, and microorganisms [93]. Research has increasingly linked antibiotic pollution to DNA damage [94], alterations in enzyme activity [95], disruptions in protein synthesis [96] and photosynthesis [97]. Additionally, exposure to certain antibiotic pollutants can alter the composition of the gut microbiome, leading to microbial imbalances and increasing the susceptibility of animals and humans to diseases [98].

This situation is exacerbated by the development of resistant bacterial strains due to their exposure to antibiotic residues in the environment, raising substantial public health concerns with 4.95 million deaths in 2019 [99] and predicted to cause about 10 million deaths per year by 2050 [9]. As spreading in clinics and environment, antibiotic-resistant bacterial strains threaten the effectiveness of the treatment regimens, leading to increased hospitalization times, higher healthcare expenses, and untreatable illnesses in some cases. This issue rises healthcare costs and reduces workforce productivity due to prolonged illness. It was predicted that global GDP will decrease 1.1–3.8% by 2050, with low-income countries potentially experiencing a 5% decline in GDP [100].

Macrolide class

Macrolide (ML) is a class of antibiotic that are characterized by a large macrocyclic lactone ring and widely used in human and veterinary medicine due to their effectiveness in treating bacterial infections [101]. They specifically target the bacterial ribosome, the molecular machine responsible for translating genetic instructions into proteins. ML interfere ribosome's function by binding to the 50S ribosomal subunit, preventing the forming of new amino acids to the growing protein chain. This inhibition of protein synthesis stops the bacteria from growing and replicating, particularly effective against gram-positive bacteria and some gram-negative bacteria [102], [103]. They are commonly used to treat respiratory infections, skin infections, and sexually transmitted infections [104]. Unfortunately, this intend used of them leads to their presence in natural water and drinking water [105]. Among ML antibiotics commonly found in aqueous ecosystems, erythromycin (ERY), clarithromycin (CLA), and azithromycin (AZI) (Figure 1,Table 1) have been included in the EU surface water watch list of emerging pollutants [106]. ERY has been reported to exhibit a half-life of approximately 42 days in a natural aquatic system [107]. Similarly, CLA has demonstrated seasonal variability in degradation rates, with an estimated half-life up to 40 days under clear-sky conditions [108]. The half-life data for AZI remain limited, although it is known for its high persistence in soil and biosolid matrices [109]. Since they remain active in aqueous environments for lengthy periods of time, certain bacterial strains develop genetic mutations after exposure to MLs, albeit at low concentrations [110].

Ampicillin

Ampicillin (AMP), a β-lactam antibiotic, ranks third among the top ten most frequently sold fixed-dose antibiotic combinations globally [111]. Its function target on the bacterial cell wall, peptidoglycan layer, particularly important in gram-positive bacteria. AMP inhibits the capability to form a stable cell wall, leading to their death by rupturing of the bacterial cell [112]. AMP can exhibit a half-life of up to 27 days in water at pH 7 and 25 $^{\circ}$C, indicating its potential to persist in aqueous environments for extended periods [113]. The high utilization rate, coupled with improper disposal practices, has resulted in the environmental contamination of water sources with elevated AMP concentrations (Table 1) [114], raising concerns about the development of antibiotic-resistant bacteria, especially when up to 40% of certain bacterial isolates in different parts of the world are currently resistant [115]. Therefore, monitoring AMP pollution plays a key role in limiting the spread of AMP resistance.

1.3 Traditional methods for detecting emerging water pollutants

Since the persistence of them in aquatic environments poses serious risks to both ecosystems and human health, the development of accurate and sensitive methods for detecting antibiotics in water is essential for effective monitoring and mitigating these threats. Traditionally, fungicides and antibiotics in water samples have been detected using analytical techniques such as high-performance liquid chromatography (HPLC) [116], [117] and mass spectrometry (MS) [118], [119]. HPLC separates chemical compounds based on their interaction with a stationary phase and a mobile phase, while MS provides molecular identification by measuring the mass-to-charge ratio of ionized compounds. Also, coupling HPLC with MS (HPLC-MS) further enhances detection capabilities for environmental pollutants [120]. These methods are highly valued for their sensitivity, specificity, and ability to identify and quantify a broad spectrum of molecules. However, they are usually time-consuming, require complex sample preparation on expensive instruments with highly skilled operators [121]. These limitations impede them for routine in-field applications.

In recent years, portable devices for the detection of emerging pollutants in environmental waters have been developed but remain largely at researching phase. While some commercially available platforms offer real-time monitoring capabilities, they primarily target general water quality parameters (e.g., pH, conductivity), and do not provide specific detection of pharmaceuticals or pesticides contaminants at trace level [122], [123], [124]. This underscores a critical gap in current in-field monitoring technologies. In response, recent research has focused on developing portable sensor systems employing electrochemical strategies and advanced biosensing or nanomaterials to enable detection of these pollutants in complex water matrices [125]. Immunoassay- [126], [127], DNA- [128] and aptamer-based sensors [129], [130] detection mechanisms have offered a practical balance between sensitivity and operational simplicity. They rely on the interaction between antigen and antibody, generating measurable signals allowing for the rapid detection of target compounds, such as antibiotic residues and pesticides, at low concentrations [131]. Even so, they face challenges such as cross-reactivity and the natural instability of antibodies [132], [133].

Beyond that, chemical sensors have been widely explored for environmental monitoring due to their portable size, ability to provide rapid analysis with higher stability over biosensors, suitable for in-field detection [11]. They determine the presence of

analytes, and transform chemical information, such as concentration, into analytically usable signals [134]. For instance, NH_2-UiO-66 metal-organic framework and reduced graphene oxide composites as the sensing material on an electrochemical transducer is developed for the detection of antibiotic ciprofloxacin in water, offering low detection limit of 6.67 nM, and excellent reproducibility [135]. Unfortunately, chemical sensors are still at the developmental stage with limited selectivity remaining as a major drawback, compromising their reliability [13].

Promising results have been also reported using microfluidic sensor platforms for electrochemical detection specific emerging pollutants, garnering particular interest due to their capacity for rapid analysis, compact design, low reagent consumption, and in-situ operation [136]. For example, Kling et al. developed a microfluidic platform integrated with electrochemical detection of tetracycline in water, achieving a limit of detection of 14.24 nM [137]. However, sensor platforms often encounter limitations related to bubbles, clogging, and challenges in integrating selective detection mechanisms for complex environmental samples [136], [138]. Therefore, there is still a need to develop systems that offer not only high sensitivity and portability but also enhanced selectivity and stability for in-field detection. Incorporating synthetic recognition elements onto electrochemical electrodes presents a promising approach that is more reliable for environmental monitoring. One such class of recognition materials—molecularly imprinted polymers (MIPs)—offers custom-designed binding sites capable of mimicking natural molecular recognition with enhanced selectivity and chemical stability.

1.4 Molecularly imprinted polymers

The concept of molecular imprinting started early in the 20th century and gained significant recognition in the 1980s. Wulff and colleagues demonstrated that polymers could be tailored to incorporate specific binding sites for target molecules through template molecules during polymerization [139]. This discovery laid the groundwork for the development of MIPs that are functional materials mimic biological receptors in discriminating between molecules but surpassing them in lower preparation cost and environmental stability [140]. Since then, there have been substantial advancements in MIP technology, including improvements in synthesis methods, characterization techniques, and their applications across diverse fields. These innovations have enabled MIPs to be produced in various shapes, such as membranes, thin layers, nanoparticles, regular spherical particles, irregularly ground particles, and composites [141]. MIPs have become highly versatile materials and are employed in numerous fields such as determine selected target in analytical chemistry [142], monitoring contaminants in environmental/ milk/ food samples [143], [144], [145], and enhance the efficiency of therapeutic compounds in drug delivery [146].

1.4.1 Principle of molecular imprinting

The fundamental concept of MIPs is based on the formation of a polymer network containing specific binding sites that are complementary toward a target template molecule. This is achieved by polymerizing suitable functional monomers in the presence of a target analyte, or similar molecule, acting as a template molecule. The template molecule is chosen depending on application purpose with a wide variety of them are available, covering from large molecules (e.g., protein) to smaller organic compounds (e.g., vitamin) [147], [148]. The suitable functional monomers interact initially with

template to form a pre-polymerization complex. During the subsequent polymerization, the template is embedded within the polymer matrix. By removing the template, cavities that are chemical complementary to the original target molecules are revealed, enabling highly selective recognition of the target molecules (Figure 2). Based on how templates interact with functional monomers, molecular imprinting approaches are categorized as covalent, non-covalent, semi-covalent, and meta-ion interaction.
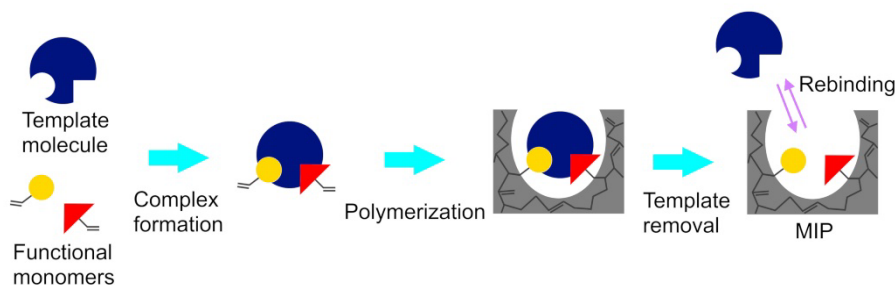
Figure 2. *A schematic representation of molecular imprinting.*

The covalent approach involves the formation of reversible covalent bonds between the template and functional monomers during the polymerization process. The stability of template-monomer(s) complexes under a broad range of conditions for polymerization are the main advantages of this approach. However, this approach has limited numbers of suitable monomers (e.g., alcohols, aldehydes, ketones, amines or carboxylic acids) and could be challenging to remove the template during template removal [149]. This approach may not be ideal for applications requiring fast kinetics [150].

On the other hand, non-covalent approach is favoured for its simplicity with the variety of possible functional groups and fast template removal [151]. It relies on weak interactions such as hydrogen bonding, van der Waals forces, and electrostatic interactions to form the pre-polymerization complex [152]. This makes it widely used in various application. However, the specificity of the binding sites is compromised due to the heterogeneity resulting from the formation of various pre-polymerization complexes, as well as the direct competition from the solvent and the cross-linker [149].

The third approach, semi-covalent, is the combination of both covalent and non-covalent binding. Covalent and noncovalent interactions are jointly exploited between the template and the functional monomer throughout the polymerization and rebinding processes [153]. Imprinting semi-covalent owns the advantages of both approaches while counterbalancing their disadvantages, may balance stability and flexibility.

Lastly, the metal-ion interaction approach utilizes coordination bonds to form highly specific recognition sites, typically preferred for imprinting metal ions or molecules with strong metal affinity. However, it is limited to strategies involving complex-forming groups with metals [154], [155].

Building on these foundational imprinting approaches, researchers have extended MIP functionality beyond single-analyte recognition. For instant, group-selective or class-selective MIPs were developed, offering the capability to recognize many structurally similar molecules [156], [157]. During the synthesis process, the use of a single template as a substitute for a whole class takes full advantage of similar molecular

structures among compounds. This method optimizes the preparation stage by reducing the required template amount, particularly advantageous in applications where imprinting for each member of a class is unnecessary. This phenomenon is useful in environmental monitoring, pharmaceuticals, or food safety, where detecting entire classes of contaminants, drugs, or toxins can be more practical and efficient. For example, class-selective MIPs could result in their enrichment and detection simultaneously for polychlorinated aromatic compounds that often exist in similar forms, known as congeners or homologs [158]. However, designing class-selective MIPs requires a profound comprehension of the complex molecular features that define the target class. The potential of cross-reactivity toward unwanted molecules is also another challenge. Thus, further development and optimization of template design and functional monomers composition are required to improve the class-selective MIPs' performance for real-world applications.

1.4.2 Computational approaches for selecting functional monomers for MIP synthesis

The effectiveness of MIPs primarily depends on the strength of the interactions between the template molecule and the functional monomers [159]. These interactions facilitate the formation of molecular memory within the MIP by capturing both the shape and spatial arrangement of functional groups in the template molecule. Therefore, the choice of functional monomers is a critical factor in achieving the optimal performance of a MIP. It can be accomplished by conducting a preliminary study of molecular complexes between monomers and template molecule to design MIP with optimal performance. Traditionally, this selection process has been largely involving experimental screening; however, in recent years, computational approaches have emerged as powerful tools to rationalize and optimize the choice of functional monomers in MIP research.

By simulating and estimating the interactions between template and monomer molecules, computational software helps replace trial-and-error steps, reducing reagent consumption and saving time in experimental work [160]. Different computational approaches—including molecular mechanics (MM), molecular dynamics (MD), and quantum mechanics (QM)—were reported to provide insights into the molecular interactions, guide the selection of suitable functional monomers, ultimately optimize the overall efficiency [161], [162].

Molecular mechanics (MM), refers to the use of Newtonian mechanics to model molecular systems and is generally preferred for assessing large numbers of molecular interactions. More than twenty functional monomers can be efficiently evaluated based on their electrostatic interaction energies and optimal geometries, requiring relatively small number of computational resources [163]. In classical MM modelling, molecules are represented as assemblies of atoms, and their behaviour is determined by force fields that define the system's potential energy [164]. For example, the selection of monomers for the synthesis of MIP that is selective for paracetamol were supported by calculating the interaction energies using Merck molecular force field (MMFF94) [165].

While MM focuses on static structures, molecular dynamics (MD) captures the dynamic behaviour of monomer-template complexes over time by solving Newton's equations of motion for atoms and molecules in a system. This is particularly valuable for understanding the stability of interactions and how they behave under realistic

conditions, such as the solvents influence and temperature fluctuations [166]. Pavel et al. successfully predicted suitable monomers for the template molecules theophylline, its derivatives [167], and chemical warfare agents [168] using Cerius^2 version 4.10 and Materials Studio. Unfortunately, MD simulations are computationally demanding over long time periods.

While MM and MD simulations offer valuable insights into molecular conformations and dynamic behaviour, their reliance on classical Newtonian mechanics limits their ability to precisely describe electronic interactions. In contrast, quantum mechanics (QM) approaches, particularly those based on density functional theory (DFT), allow for a more detailed and accurate estimation of chemical binding energies by explicitly considering electron density and quantum effects [169]. This makes QM especially suited for modelling the weak non-covalent interactions—such as hydrogen bonding—that are critical in the selective recognition processes of MIPs. For instance, binding energy calculations at the PM3 level have been applied by Luliński et al. to design dopamine-imprinted polymers, demonstrating the effectiveness of QM methods in MIP development [170]. Another example involves screening functional monomers for MIP fabrication by calculating the binding energies between theophylline and various monomers via DFT at the B3LYP/6-31+G level [171]. In this work, QM calculations were employed to evaluate the binding affinities between template molecules and functional monomers, guiding the monomer selection.

1.4.3 Electrochemical synthesis of MIPs

MIPs are usually prepared by free radical polymerization using a variety of methods, such as bulk, suspension, precipitation, emulsion polymerizations. Even though these methods are well-established, they may not precisely control the thickness of polymer and can be challenging for template removal [146]. Meanwhile, electropolymerization allows for direct deposition of the polymer onto an electrode surface, enabling precise control over the thickness, which are critical for sensor applications [172]. Moreover, this synthesis method has superior properties with respect to adherence to the transducer surface (e.g., gold, carbon, platinum), along with simplicity and possibility of operation in aqueous solutions at room temperature [173], [174].

The film thickness is governed by the amount of charge transferred during electropolymerization under galvanostatic, potentiostatic, or potentiodynamic conditions [172]. It involves the anodic oxidation of an electropolymerizable monomer employing different modes of potential stimulus to form radical cation [175]. These unstable radicals quickly react with other monomers thereby forming oligomers and subsequently the final polymer chain [176]. Such polymerization requires an electrolyte in the form of a solvent containing a doping salt or an ionically conducting medium [177].

To achieve optimal imprinting efficiency, it is crucial to preserve the structural integrity of the template molecules during electrosynthesis by preventing template oxidation during electropolymerization [178], [179], [180]. A wide range of electropolymerizable monomers is available, among which commonly used examples are pyrrole [181], aniline [182], thiophene [183], phenol [184], phenylenediamine [185], 3,4-ethylenedioxythiophene (EDOT) [186], and aminophenylboronic acid [187].

1.5 MIP-based electrochemical sensors for environmental monitoring

The integration of MIPs with electrochemical transducers has emerged as a promising approach to develop sensitive, selective, and field-deployable sensors for environmental monitoring. Electrochemical sensors are widely favoured in chemical sensor technology due to their low cost of manufacture, simple experimental set-up, ease in achieving miniaturisation and wireless control, and adaptability for a wide range of applications [145], [188]. By coupling MIPs with electrochemical platforms, the highly selective molecular recognition capability of the imprinted polymer is combined with the sensitive transduction offered by electrochemical techniques. In a typical MIP-based electrochemical sensor, the polymer is deposited on the surface of working electrodes through either spin-coating, electropolymerization, or other surface-initiated polymerization technique [189].

The sensing mechanism of a MIP-based electrochemical sensor depends on the nature of the analyte. For non-electroactive compounds, detection is often achieved indirectly using external redox probes to measure changes in electrochemical reactions that occur when the target analyte interacts with MIP. Upon binding of the analyte to specific recognition sites within MIP layer, the accessibility of redox species to the electrode surface is altered. This interaction typically leads to a measurable change in electrochemical signals (e.g., shift in current, potential, or impedance) due to hindered ion diffusion, enabling quantification of the analyte (Figure 3) [190]. To evaluate the permeation of redox-active markers, electrochemical techniques, such as cyclic voltammetry (CV), electrochemical impedance spectroscopy (EIS), and different pulse voltammetry (DPV) can be used [191]. In contrast, electroactive analytes may directly participate in redox reactions at the electrode surface, generating faradaic currents that serve as measurable analytical signals [192]. While both direct and indirect electrochemical transduction mechanisms are possible with MIP-based sensors, indirect detection approach is more commonly reported, likely due to the prevalence of non-electroactive target analytes in environmental monitoring applications.
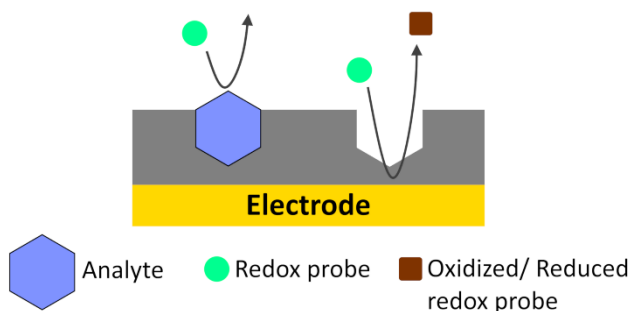

Figure 3. Schematic illustration of non-electroactive analyte molecule binding within imprinted cavities, hindering the diffusion of the redox probe into the MIP layer.

The combination of MIPs and electrochemical transducers has proven to be a highly efficient synergy, offering cost-effective and robust solutions for real-time monitoring [193], [194]. It has also demonstrated a growing interest in development of MIP-based electrochemical sensors for the detection and quantification of fungicides and antibiotics in aqueous media, as evidenced by the increasing number of peer-reviewed articles over

the last decade (Figure 4). Although MIP-based electrochemical sensors show great potential, they still have certain limitations that must be considered. One of the limitations is the binding affinity and kinetics of MIPs, which may be less efficient than those of biological recognition elements like antibodies or enzymes. This can sacrifice sensor sensitivity, especially at ultra-low analyte concentrations [145]. Increasing the specific surface area of the MIP layer by integrating it with nanostructures (e.g., nanoparticles, or nanospheres) may help address this issue by improving sensitivity and operational efficiency [195], [196]. Vu et al. integrated gold nanoparticles into the MIP layer aiming to detect norfloxacin in aquaculture samples showing excellent sensitivity and a wide linear detection range of the resulting sensor [197].

The actual sensing environment presents another challenge. Complex environmental matrices often introduce interfering substances, which can negatively impact sensor performance. Several studies have attempted to evaluate sensor reliability in such challenging conditions by testing their performance in complex matrices. For example, Motia et al. utilized acrylamide as functional monomer and bisacrylamide as cross-linker to deposit the MIP on the surface of Au SPE for the detection of triclosan, an antimicrobial agent, in wastewater [198]. Similarly, functional monomer indole-3-acetic acid was used to obtain MIP on boron-doped diamond electrode for the detection of antibiotic cefalexin in river water [199]. Despite the ongoing research, the limited real-world validation under complex environmental conditions raises concerns about sensor reliability, necessitating extensive field testing before widespread adoption as commercial products. The scalability of MIP-based electrochemical sensors also remains areas for improvement, as translating laboratory-scale designs into commercial products facing technical and economic obstacles, such as long-term storage for transportation, and affordability in markets [200]. Coming studies thus are expected to focus on improving polymer design that is suitable for real sample testing, improving sensor efficiency prior to transition toward commercialization.
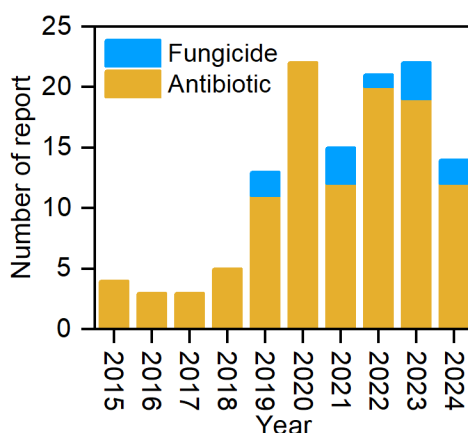
Figure 4. Shares of peer-reviewed articles on MIP-based electrochemical sensors for the detections of fungicides and antibiotics in aqueous samples from 2015 to 2024.

1.5.1 MIP-Based electrochemical sensors for fungicide and antibiotic detection

Detection of azoxystrobin

MIP-based electrochemical sensor has been developed for detection of several fungicides in water, including enrofloxacin [201], carbendazim [202], and indoxacarb [203]. Nevertheless, the synthesis of MIPs tailored for AZO recognition and their subsequent application in electrochemical sensing platforms have not been previously reported. This gap is particularly concerning due to AZO's widespread use and its persistence in the environment, which contribute to its accumulation in water bodies. Indeed, AZO have been detected in environmental waters at concentrations up to approximately 30 µg/L (74 nM) [74], which exceed the aquatic Maximum Acceptable Concentration-Environmental Quality Standard (MAC-EQS) value for AZO (1.8 µg/L or 4.5 nM) [204]. Therefore, the development AZO sensor facilitates more effective environmental monitoring and risk management of AZO contamination.

Detection of macrolides

There are numerous studies have reported efforts to imprint ERY, CLA and AZI. To illustrate, Syritski's group formed ERY-MIP by electrochemically deposited poly(mPD) on an Au electrode, with the purpose of detecting ERY in tap water samples [205]. CLA-imprinted poly(arylene phthalide) was obtained using the phase inversion method on the surface of a glassy carbon electrode for electrochemical detection of the target molecule [206]. Pan et al. generated AZI-MIP on glassy carbon electrode, adopting benzothiophene-3-boronic acid as functional monomer [183]. However, no subsequent demonstration has been reported on the preparation of MIPs capable of detecting an entire class of ML compounds in a single measurement, aimed at signalling antibiotic pollution in water. This is notable limitation, especially considering that MLs are often coexist and share common mechanisms of biological effects. A class-selective sensor would offer a practical and efficient approach for monitoring antibiotic pollution in environmental water.

Detection of ampicillin

AMP imprinting has been applied with various MIP-based electrode modifications to develop electrochemical sensors capable of selectively detecting AMP. For example, Shi and colleagues electrochemically deposited poly(o-phenylenediamine) in the presence of AMP to design MIP on a single-walled carbon nanotube modified glassy carbon electrode [207]. Similarly, Sun et al. developed a MIP-based sensor using pyrrole as functional monomer, fabricated on a ZrO_2 nanofiber-modified Au electrode [208]. Also, Liu's group employed bulk polymerization to generate AMP-MIP on Fe_3N-Co_2N modified carbon electrode using N,N'-dimethylacrylamide as the functional monomer and ethylene glycol dimethacrylate as the cross-linker [209]. Yet in another report, AMP-MIP was synthesized, using dopamine as a functional monomer, onto a modified gold electrode as an electrochemical sensor for analysing AMP in various media [210]. Despite the outstanding performance of the reported sensors, their reliance on ferricyanide as a redox mediator to transduce molecular interactions at the electrode-electrolyte interface remains a drawback. Thus, the development of a ferricyanide-free AMP sensor would reduce contamination risks and simplify analysis, offering a practical approach for in-situ monitoring of aquatic antibiotic pollution.

1.6 Summary of the literature review and objectives of the study

The widespread use of fungicides and antibiotics, coupled with inadequate treatment and disposal methods, has led to their persistent presence in water bodies and posed significant risks to not only human health but also ecosystem balance. Many studies have demonstrated that exposure to these pollutants, both short-term and long-term, leads to a range of detrimental effects for human and aquatic biota. Notably, chronic exposure to fungicides is associated with DNA damage and cancer risk, while prolonged antibiotic exposure has been linked to the emergence of antibiotic-resistant bacteria. The cumulative impact can manifest in prolonging illnesses, increasing healthcare costs, and even mortality. Therefore, monitoring water pollutants, including fungicides and antibiotics, is crucial to ensure ecosystem and human safety, as prevention is more cost-effective than remediation.

For decades, conventional detection methods (e.g., HPLC-MS) remain gold standard for detection. However, they are usually expensive, time-consuming, and require skilful operators. Although latter biosensors and chemical sensors are suitable for in-field applications of environmental monitoring, they are often accompanied by unstable natural receptors or limited selectivity.

Meanwhile, highly selective MIPs combined with sensitive electrochemical transducers, offer portable sensing solutions for in-field detection of fungicides and antibiotics. Unfortunately, their practical implementation remains limited due to challenges in ensuring reliable performance when measuring real-world samples. For instance, the design of MIP-based electrochemical sensing platform to detect AZO in complex water samples has not been previously reported. Additionally, the possibility of class-selective detection can further advantage environmental monitoring since pollutants usually exist together in water samples. Furthermore, the development of electrochemical sensors without the need of external redox probes remains underexplored, despite their potential to simplify sensor design and improve overall performance.

This study aims to address these challenges by designing MIP-based electrochemical sensors capable of fast and reliable detection of both individual targets such as AZO and AMP, and broader pollutant classes such as the ML class of antibiotics (Figure 5). To achieve this goal, the following specific objectives are outlined:

1. To design and synthesize a fungicide selective MIP (targeting AZO), integrated with a miniaturized electrode system for electrochemical detection AZO in water.
2. To develop and synthesize a MIP selective for ML antibiotics, and to integrate it with a miniaturized electrode system for portable electrochemical detection of macrolides in aqueous environments.
3. To explore the possibility of combining a MIP layer with an inherently redox-active electrode material (RuO_2), aiming to simplify the electrochemical assay for the target antibiotic (AMP) by enabling reliable detection - eliminating the need of an external redox probe solution.

The above-mentioned objectives should include but not limited to the following stages:

- Evaluation of the binding affinity and selectivity of the prepared MIP-based electrochemical system toward the designated target analytes using electrochemical techniques.
- Optimization of the polymerization conditions (e.g., monomer-template ratio, thickness) for enhanced imprinting efficiency and sensor performance.

- Characterization of the physicochemical properties of the synthesizing ultrathin MIP layers using spectrochemical techniques aiming to confirm the relevance of used imprinting strategy.
- Assessment of the analytical performance of the developed MIP-based sensors, including selectivity, linear range, limit of detection (LOD), and reproducibility.
- Validation of the developed sensors in real water samples (e.g., tap water or natural surface waters) spiked with the above-mentioned antibiotics and fungicide.
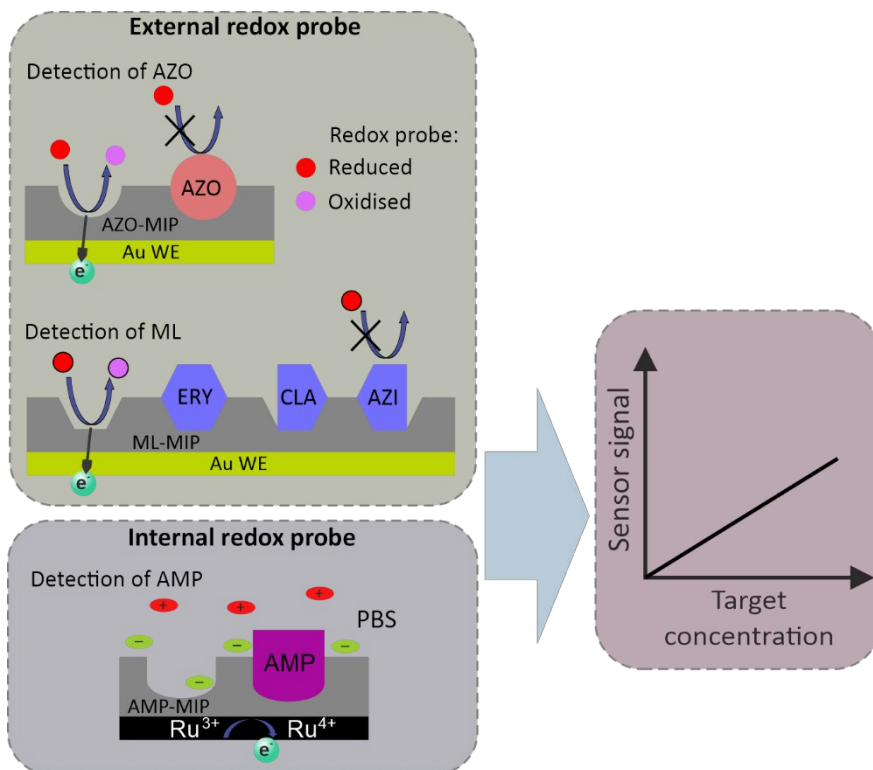
Figure 5. *A graphical representation of the thesis goal.*

2 Experimental

2.1 Selection of functional monomer

The suitable functional monomers for AZO-MIP and AMP-MIP preparation were selected from several electropolymerizable candidates (Table 2) using computational modelling based on binding energy estimations obtained through density functional theory (DFT) calculations. First, a functional monomer candidate and a template molecule underwent geometric optimization using the Universal Force Field for energy minimization with Avogadro 1.2.0 software with a 1:1 ratio. Subsequently, potential energies were computed utilizing the DFT method at the B3LYP/6-31+G(d,p) level of Gaussian'09 software. Binding energies, as the difference between the energy of the complex and the energy of each molecule, were calculated by the equation:

$$\Delta E = E_{T+M} - (E_T + E_M) \tag{1}$$

where E_{T+M}, E_T and E_M are the potential energies of the complex and its isolated molecular components, template and monomer, respectively.

This approach provided insights into the strength of the hydrogen bonding interactions between template and functional monomer, guiding the selection of the most suitable candidate for stable complexes formation with the target molecules.

In Paper II, the interaction between the monomer, 3-APBA, and the antibiotic, ERY, was additionally studied using ^{13}C nuclear magnetic resonance (NMR) spectroscopy with a Bruker SMART X2S benchtop diffractometer to confirm covalent bond formation. Sample solutions of 3-APBA, ERY, and their 1:1 molar ratio mixture were prepared in PBS.

Table 2. *List of electropolymerizable monomers evaluated for functional monomers suitability.*

Template	Monomers
AZO (Paper I)	2-methyl-4-nitroaniline (2M4N), 3-aminothiophenol (3ATP), aniline (ANI), m-phenylenediamine (mPD), pyrazole (PRZ), and pyrrole (PYR)
AMP (Paper III)	1,8-diaminonaphthalene (1,8-DAN), 3,4-ethylenedioxythiophene (EDOT), ANI, mPD, and PYR

2.2 Preparation of MIP-based electrochemical sensors

In this study, AZO-, AMP-, and ML-selective MIP films were formed via electrochemical polymerization on different electrochemical transducer platforms resulting in three electrochemical sensors: AZO sensor, AMP sensor, and ML sensor.

For AZO sensor the AZO-MIP film was electrochemically deposited on the working electrode (WE) of a thin-film metal electrode (TFME) acquired from MicruX Technologies (Gijón, Spain). The TFME configuration included a 1 mm diameter (approximately 0.785 mm²) circular gold (Au) WE, along with Au counter electrode (CE) and reference electrode (RE). For ML sensor, the ML-MIP was prepared on the Au WE surface of a screen-printed electrode (SPE) obtained from BVT Technologies, a.s. (Brno, Czech Republic). The SPE consisted of a 1 mm diameter circular Au WE, an Au CE, and a silver electrode coated with AgCl serving as the RE. In the case of AMP sensor, the AMP-MIP

film was electrodeposited on the RuO₂ WE of the DRP-810 SPE, purchased from Metrohm DropSens (Oviedo, Spain). The DRP-810 SPE featured a 4 mm diameter (approximately 12.56 mm²) RuO₂ WE, a silver RE, and a carbon CE.

All electrodes were interfaced with an electrochemical workstation (Reference series, Gamry Instruments, Inc., USA). The applied potentials during the electrochemical deposition process were referenced against the external reference electrode Ag/AgCl/3 M KCl. The parameters of electrochemical polymerization are described in Table 3. Similar synthesis parameters were used for the reference non-imprinted polymer (NIP), films preparation, with the polymerization carried out in the absence of template molecules.

The entrapped template molecules were removed from the electrodeposited polymer films by immersing the modified electrodes in appropriate solutions under vortex agitation for 30 minutes, thereby revealing the imprinted binding sites. A 5% acetic acid solution was used for AZO and ERY, while a mixture of acetic acid and methanol (volume ratio 1:19) was used for AMP. After thoroughly rinsing with ultrapure water, the MIP film-modified electrodes—denoted as AZO sensor, ML sensor and AMP sensor—were subjected to rebinding studies. A similar treatment process was used for NIP-modified electrodes.

Table 3. *Parameters for electrochemical polymerization are used in this work.*

Template	Polymerization solution*	Electrochemical technique	WE material	Setup parameters*
AZO (Paper I)	10 mM ANI, 5mM mPD, and 2mM AZO in PBS	Galvanostatic	Au	current 0.3 µA, time 131 s
ERY (Paper II)	10 mM mPD, 5 mM APBA, and 2 mM ERY in PBS	Chronocoulometry	Au	potential 0.5 V, charge density limit 5mC/cm²
AMP (Paper III)	10 mM mPD and 2 mM AMP in PBS	Cyclic voltammetry	RuO₂	scan range 0.2 to 0.4 V, scan rate 100 mV/s, 5 cycles

* Optimized values.

2.3 Characterization of the MIP films

2.3.1 Infrared Spectroscopic Ellipsometry

Infrared Spectroscopic Ellipsometry (IRSE) is a powerful, polarization-sensitive, and non-destructive technique for characterizing thin polymer films with high precision. By utilizing vibrational absorption bands in the infrared region, IRSE provides enhanced spectral contrast between chemical components within the polymer film. This makes it particularly well-suited for analysing complex polymer structures such as MIPs, enabling simultaneous assessment of film thickness, uniformity, and chemically relevant changes occurring during MIP formation. These structural and compositional insights are critical, as they directly influence sensor's performance and selectivity [211].

In Paper I, IRSE was used to confirm the coexistence of both ANI and mPD within P(ANI-co-mPD) as well as to evaluate the efficiency of the template removal process. A custom-built, dry-air purged IR spectroscopic ellipsometer externally coupled to a Fourier-transform infrared spectrometer (Vertex 70, Bruker, Billerica, MA, USA) was used for this purpose. Measurements of tan Ψ were acquired in the mid infrared spectral range at incidence angles of 70° and 80°.

In Paper II, IRSE was applied to determine the thickness of electrodeposited polymer films, ensuring equal thickness between NIP and MIP films. The charges passed through the working electrode during electrosynthesis were correlated with film thickness values determined by spectroscopic ellipsometry (SE 850, Sentech Instruments GmbH, Berlin, Germany). The Ψ and Δ values were recorded in the wavelength range of 370–800 nm at incidence angles of 70°, 60°, and 50°. Further information regarding the instrument configurations and measurement procedures can be found in references [211], [212].

2.3.2 Electrochemical characterization

Electrochemical characterization of the modified electrodes was performed using cyclic voltammetry (CV), electrochemical impedance spectroscopy (EIS), or linear sweep voltammetry (LSV) to monitor surface modifications by assessing the electron transfer properties at the electrode/solution interface during different stages of MIP preparation. CV is a widely used electroanalytical technique that monitors electrochemical processes at the molecular level on conductive electrode surfaces, allowing rapid assessment of redox reaction thermodynamics and evaluation of charge transfer blocking by insulating films [213], [214]. Similarly, EIS offers a non-invasive, highly sensitive method for surface analysis and system monitoring, with the added benefits of easy operation and does not require the bulk size of materials [215], [216]. LSV provides a straightforward approach to analyse redox behaviour by sweeping the potential linearly, enabling clear identification of oxidation or reduction events.

In Papers I, CV was conducted in redox probe solution containing 0.3 M KCl and 4 mM redox couple $K_3[Fe(CN)_6]$/$K_4[Fe(CN)_6]$ within a potential range of −0.2 to 0.2 V at a scan rate of 50 mV/s. EIS was performed in the redox probe solution at open circuit potential with an amplitude of 10 mV over a frequency range of 0.1Hz to 5 kHz. In Papers II, CV was conducted in redox probe solution within a potential range of 0 to 0.5 V at a scan rate of 100 mV/s. EIS was performed in the redox probe solution at open circuit potential with an amplitude of 10 mV over a frequency range of 0.1 Hz to 100 kHz. In Paper III, LSV was carried out in PBS from −0.2 V to +0.5 V, using a scan rate of 50 mV/s and a step size of 1 mV.

2.4 Performance evaluation of MIP-based electrochemical sensors

2.4.1 Electrochemical signal generation

The electrochemical responses of the MIP-based sensors were generated using either Differential Pulse Voltammetry (DPV) or Linear Sweep Voltammetry (LSV). For this purpose, electrode systems modified with analyte-specific MIP layers were incubated for an optimized duration in solutions containing increasing concentrations of the target analyte. Following incubation, the electrodes were transferred to either an external redox probe solution (for AZO and ML sensors) or phosphate-buffered saline (PBS) in the case of the AMP sensor, where a redox mediator was pre-embedded within the electrode. These sensors detect changes in charge transfer through the MIP layer, which contains

selective imprinting cavities formed during polymerization. The binding of analyte molecules to these cavities hinders charge transfer, resulting in a concentration-dependent suppression of the current peak observed in DPV or LSV measurements.

The concentration-dependent sensor response, I_n, was expressed as the normalized suppression of the current peak obtained via DPV or LSV, according to the following equation:

$$I_n = (I_0 - I) / I_0 \tag{2}$$

where I_0 and I represent the current peak values measured after incubation in the blank (analyte-free) and analyte-containing samples, respectively.

In the case of AZO- and ML- sensors, the MIP-modified electrodes were incubated for an optimized time in solutions containing increasing concentrations of the analyte. Subsequently, DPV measurements were performed in 0.3 M KCl solution containing 4 mM redox probe $K_3[Fe(CN)_6]/K_4[Fe(CN)_6]$. For AZO sensor, the DPV curves were recorded at potential range of 0–0.4 V and a sample period of 0.5 s with pulse time of 40 ms, pulse size of 35 mV, step size of 7 mV. For ML sensor, the DPV curves were recorded at the same potential range and sample period, but with pulse time of 10 ms, pulse size of 25 mV, step size of 5 mV.

The AMP sensors were incubated in PBS containing increasing analyte concentrations, followed by LSV. The LSV was conducted in the potential range of −0.2–0.5 V, with a scan rate of 50 mV and a step size of 1 mV.

2.4.2 Analyte-induced relative response

The initial evaluation of the capability of the prepared MIPs, when attached to electrodes, to recognize their target molecules was conducted by calculating so-called Relative Response (RR). This was determined as the ration of the responses (In) obtained from MIP- and NIP-modified sensors:

$$RR = I_n(MIP)/I_n(NIP) \tag{3}$$

where $I_n(MIP)$ and $I_n(NIP)$ represent electrochemical responses of the MIP- and NIP-modified electrodes, respectively, measured using either DPV or LSV upon binding of the respective analytes.

RR was used in this thesis in a manner somewhat analogous to the commonly reported Imprinting Factor (IF). However, while IF typically characterizes the intrinsic properties of the MIP material itself, RR was employed here to assess the integrated performance of the MIP/transducer system in responding to target analytes. This approach acknowledges that the electrochemical signal may not be directly proportional to analyte binding. Furthermore, RR was also utilized to evaluate the selectivity of the MIP-based systems against non-target analytes, making it a more appropriate and versatile metric for the objectives of this study.

Although IF (RR) metric is commonly used to assess the success of molecular imprinting—indicating the presence of specific recognition sites in the MIP—it should be interpreted with caution. MIP and NIP are typically two morphologically distinct polymers, often differing in the number and nature of their binding sites, and IF (RR) value greater than 1 can indicate both that a MIP that is capable of binding more target molecules as compared to a corresponding reference material, NIP, but it can be also

connected with increased porosity introduced during the imprinting process. Also, the polymer matrix may exhibit significant interactions with target analyte even in NIP due to non-specific binding [217], and thus IF (RR) should be considered alongside other affinity binding characteristics to accurately evaluate success of molecular imprinting. For example, the equilibrium dissociation constants, K_D of MIP and NIP can be measured and compared.

In Paper II, RR was calculated at saturated analyte concentrations, where the maximal amount of adsorbed analyte is reached, corresponding to the following expression:

$$RR = I_m(MIP)/I_m(NIP) \qquad (4)$$

where I_m is the sensor response signals after adsorption of the analyte at its saturation value. I_m was extracted by fitting the data to models such as Langmuir (X1), Freundlich (X2), or the combined Langmuir-Freundlich model (X3):

$$I_n = I_m C/(K_D+C) \qquad (5)$$
$$I_n = I_m C^m \qquad (6)$$
$$I_n = I_m C^m/(K_D+C^m) \qquad (7)$$

where I_n is sensor responses at concentration C of an analyte in a solution; K_D is the equilibrium dissociation constant, m is the heterogeneity index, which ranges from 0 to 1.

2.4.3 Selectivity

Selectivity refers to a sensor ability to distinguish between a target analyte and other compounds. In MIP-based sensors, selectivity is imparted by the MIP layer, which formed through an imprinting process that creates recognition sites complementary in shape, size and functional groups to the target molecule. High selectivity is especially crucial when the sensor is intended for use in complex sample matrices, where the presence of multiple interferents can significantly compromise the sensor's performance compared to its behaviour in simplified or controlled matrices.

To assess selectivity, a set of comparison compounds is selected, including structurally similar analogues from the same chemical class and/or structurally dissimilar interferents likely to coexist in real-world samples. The sensor's response to each of these compounds is then measured under the same conditions used for the target analyte. A higher response to the target analyte compared to non-targets indicates effective molecular recognition and confirms the sensor's selectivity.

2.4.4 Limit of detection

The performance of MIP-based electrochemical sensors at low analyte concentrations is commonly evaluated using two parameters: the limit of detection (LOD) and the limit of quantification (LOQ). LOD refers to the lowest concentration of the analyte that can be detected, though not necessarily quantified with accuracy. LOQ, on the other hand, refers to the lowest concentration at which the analyte can be quantitatively determined with acceptable precision and accuracy. These values are determined from the linear regression of the sensor's response to low analyte concentrations in water samples, using following equations:

$$LOD = 3SD/b \tag{8}$$
$$LOQ = 10SD/b \tag{9}$$

where SD and b are the standard deviation of the residual and the slope of the regression line, respectively.

In this thesis, these parameters serve as indicators for practical performance of the MIP-based electrochemical sensor, validating their suitability for detecting low-level pollutants in complex water samples.

2.4.5 Recovery

Assessing recovery is essential to validate the reliability and accuracy of the MIP-based electrochemical sensor, especially in real sample samples. Known amounts of the target analyte were spiked into water samples and their normalized responses were recorded. Subsequently, the corresponding antibiotic concentrations were determined using a previously established linear regression of the sensor's response to low concentrations of the analyte in pond water (from Section 2.4.3). The recovery percentage (%R) was calculated by using equation (6):

$$\%R = (C_{estimated}/C_{spiked}) \times 100 \tag{10}$$

where $C_{estimated}$ is the concentration of the antibiotic estimated by the linear regression equation, and C_{spiked} is the initial concentration of the antibiotic spiked into the sample.

A recovery percentage (%R) closer to 100% confirms its reliable performance, indicates good accuracy of the MIP-based sensor for quantifying the target compound, as it shows that the estimated concentration ($C_{estimated}$) is nearly identical to the spiked concentration (C_{spiked}).

3 Results and discussions

3.1 AZO sensor

This section discusses the design of AZO sensor for the application of detection of fungicide AZO in water environments. The design includes the selection of suitable functional monomer, synthesis, and characterization, as well as the study of the sensor analytical performance in complex aqueous sample, such as tap water.

3.1.1 Functional monomer selection

Electropolymerizable monomers capable of engaging in hydrogen bonds with oxygen atoms of AZO molecule were examined: 2M4N, 3ATP, ANI, mPD, PRZ, and PYR (referred to Figure 1, Paper I for chemical structures). As can be seen from Table 4, AZO-ANI complex exhibited the highest binding energy, followed by the AZO-mPD. The results confirmed that ANI displayed the highest binding energies with AZO, highlighting its potential to form robust non-covalent interactions with the template. The binding interactions between ANI and the AZO template (Figure 6) involve hydrogen bonding from the ANI hydrogen atoms to five oxygen atoms (labelled O1-O5, red) of the AZO molecule.

However, ANI could compromise the stability and recognition capabilities of the resulting MIP when possessing only a single amino group. To address this concern, mPD was introduced as a co-monomer to ensure sufficient hydrogen bonding with AZO. It was found that phenylenediamines can serve as branching or cross-linking sites during copolymerization with ANI [218], [219], [220], and previous studies have demonstrated the successful formation of ANI and mPD during electrochemical polymerization [221], [222]. Additionally, π-π interactions between the aromatic moieties in the studied molecules also contribute significantly the strength of non-covalent interaction within prepolymerization complex as well as in the resulting MIP, resulting in its' selectivity and stability.
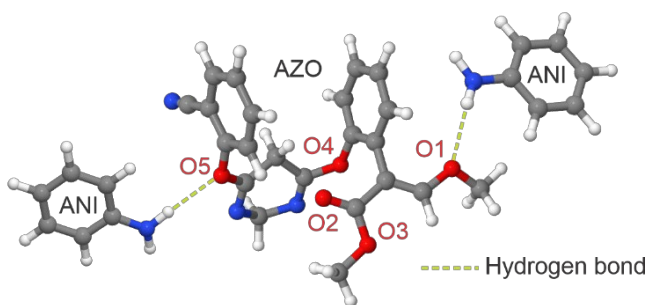
Figure 6. A schematic representation of possible binding interactions between ANI and mPD monomers with template AZO. The AZO structure is represented by five highlighted oxygen atoms (red color), carbon (gray), hydrogen (white), and nitrogen (purple).

		ANI	mPD	PYR	PRZ	2M4N	3-ATP
Binding energy (kJ/mol)	**O1**	−187	−144	−96	−75	−68	−71
	O2	−206	−149	−135	−121	−74	−12
	O3	−165	−163	−164	−141	−113	−90
	O4	−205	−135	−138	−138	−71	−133
	O5	−104	−89	−86	−87	−84	−86
	Total *	−867	−680	−619	−562	−410	−392

*A rough estimate of the overall binding energy was calculated as the sum of the individual binding energies in the 1:1 complex between AMP and the monomer.

3.1.2 Synthesis and characterization of AZO-MIP film

Electropolymerization, a well-established method for depositing a MIP film layer on a sensor transducer, was used to synthesis AZO-MIP. CV measurements were initially carried out (Figure 7) to determine the electrochemical potential for the synthesis of the co-polymer layer of ANI and mPD, denoted as P(ANI-co-mPD), and avoiding unwanted oxidation of the template molecules AZO. The fragment of first cycle of CV shows ANI oxidizes at approximately 300 mV and mPD at around 250 mV. This close oxidation potentials also reveal the feasibility of co-polymerizing these monomers through electrochemical synthesis, allowing chain growth. Thus, the oxidation of both monomers in a solution mixture is expected to occur higher than 300 mV.
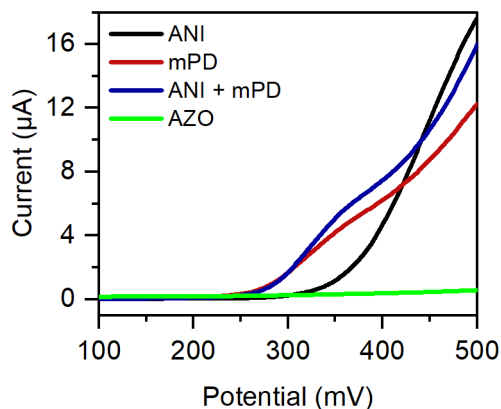
Figure 7. *A fragment of the first cycle of the cyclic voltammogram recorded on Au in PBS at the presence of 5 mM ANI, 5 mM mPD, or their mixture at a scan rate of 100 mV/s.*

The galvanostatic method was employed for AZO-MIP layer synthesis due to its capability to precisely control polymerization through current regulations to attain the required electrodeposition potential of above 300 mV. The polymer film thickness can be precisely controlled by adjusting time during galvanostatic to provide tunability in

the final MIP film efficiency. The superior performance of P(ANI-co-mPD) over the homopolymers P(ANI) and P(mPD) in AZO-MIP formation was clearly demonstrated by the significantly enhanced response of the sensor with the MIP synthesized from the co-polymer compared to those prepared from P(ANI) or P(mPD) (Figure 8a). In addition, the MIP-based electrochemical sensor, synthesized using co-monomers, consistently outperformed its reference non-imprinted polymer (NIP)-based counterpart across all tested concentrations, as depicted in Figure 8b. The difference in responses observed between the AZO-MIP and NIP, particularly evident in the RR values (calculated using Equation (3)), strongly indicates the successful implementation of the molecular imprinting process.
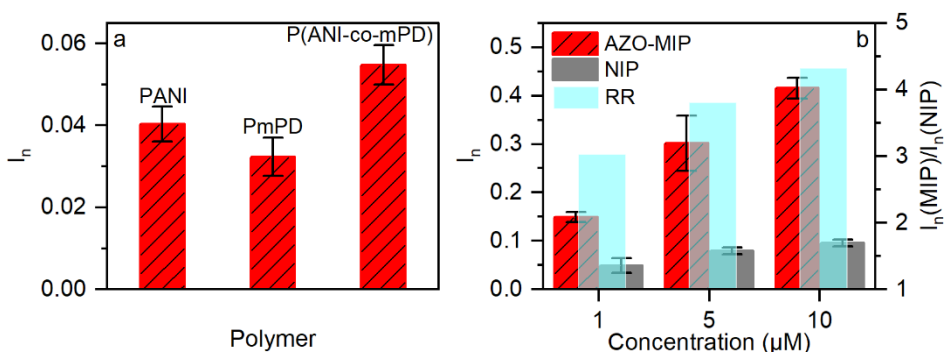
Figure 8. (a) Responses of AZO sensor based on AZO-MIPs formed from the different polymers upon incubation in 50 nM AZO solution in ultrapure water. (b) Responses of sensors modified with AZO–MIP and NIP layers formed from P(ANI-co-mPD) in ultrapure water. Error bars show the standard deviation of three measurements carried out by three independent AZO sensors.

The electrodeposited thin co-polymer film was characterized using IRSE. In Figure 2a, Paper I, the spectrum in the region of 1400-1700 cm^{-1} showed that P(ANI-co-mPD) displayed the characteristic bands of both P(ANI) (red arrows) and P(mPD) (blue arrow) at wavenumbers of 1498, 1515, and 1630 cm^{-1}, with a shoulder at 1600 cm^{-1}. This suggests that the synthesized co-polymer structure differs from the corresponding homopolymers structures.
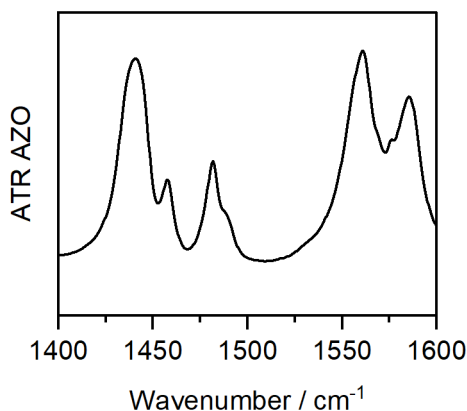
Figure 9. Attenuated total reflection (ATR) absorbance of AZO powder.

To prepare AZO-MIP, the polymer film synthesized in the presence of AZO, denoted as P(ANI-co-mPD)/AZO, was treated with removal solution (details in Section 2.2) to remove entrapped AZO from the polymer matrix. The film before and after the treatment was evaluated using IRSE to ensure the removal of AZO. As can be seen in Figure 2b, Paper I, there are changes in the frequency positions in the range 1400-1600 cm^{-1}. Specifically, the peak at 1447 cm^{-1} was attenuated, and peaks at 1463 and 1569 cm^{-1} vanished after washing. Since these peak positions are close to those of AZO (Figure 9), it can be concluded that the AZO present in the P(ANI-co-mPD)/AZO was removed after template removal treatment, resulting in the AZO-MIP layer formation.

The formation of AZO-MIP on the Au WE was further evaluated using electrochemical techniques, including CV and EIS, to monitor changes in charge transfer between the redox pair in solution and the Au WE surface at each modification stage. In the result of CV scans (Figure 10a), the reduction in both CV's anodic and cathodic current peaks indicated the electrodeposition of P(ANI-co-mPD)/AZO, signifying the development of a non-conductive film hindering charge transfer at the electrode-solution interface. The partial recovery of current peaks after template removal suggested improved permeability of the polymer layer due to the formation of imprinted cavities of AZO-MIP. Similar trends were observed in the EIS spectra (Figure 10b), where the semicircle diameter representing charge transfer resistance, R_{ct}, increased after polymer film electrodeposition (Table 5), and then decreased after subsequent treatment with template removal. The selective adsorption of AZO by AZO-MIP resulted in changes observed in both the CVs and the EIS spectra.

To optimize AZO-MIP performance, a series of experiments were conducted (see section 3.2.1, 3.2.2, 3.3.1, and 3.3.2 in Paper I). The results demonstrated that the sensor equipped AZO-MIP formed from film generated by concentration ratio of 2:10:5 mM (AZO:ANI:mPD) in the synthesis solution and charge density 5 mC/cm^2 demonstrated the highest responses and consequently selected as optimal for further study. Additionally, incubation time of 15 minutes in analyzed solution with pH value around 7 would benefit AZO-MIP the most to achieve optimal analyte binding.

Table 5. *Charge transfer resistance (R_{ct}) values obtained from fitting EIS spectra to a Randles equivalent circuit consisting of a solution resistance (R_s), a constant phase element (CPE), a charge transfer resistance (R_{ct}), and a Warburg impedance (W_d).*

Parameters	Au	P(ANI-co-mPD)/AZO	AZO-MIP	AZO on AZO-MIP
R_{ct} (kOhms)	0.6	7.5	3.2	7.3
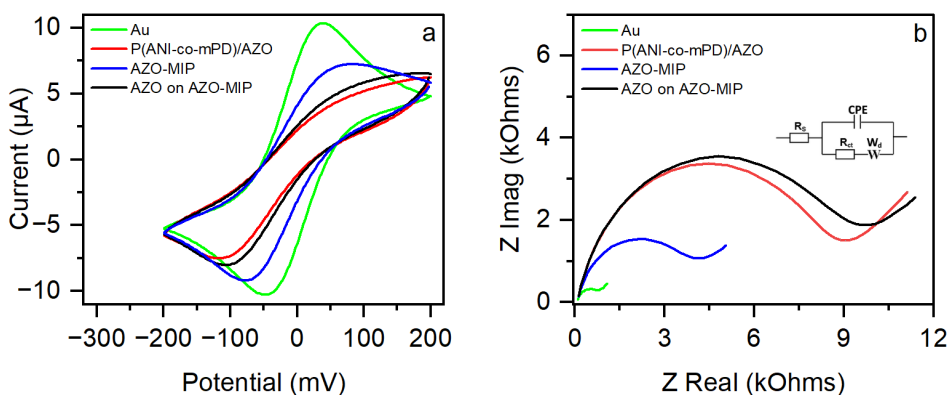
Figure 10. *CVs (a) and EIS (b) characterization of bare Au, P(ANI-co-mPD)/AZO, AZO-MIP and AZO on AZO-MIP that are prepared on Au TFME.*
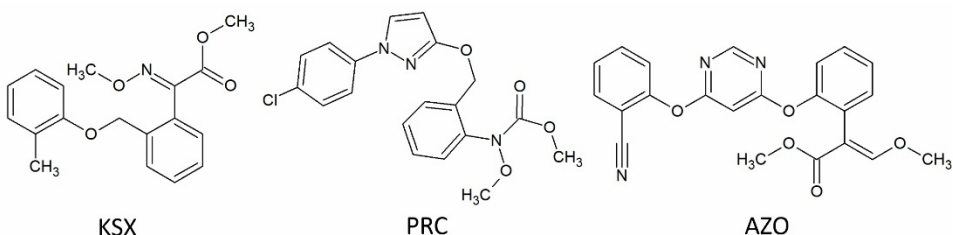
3.1.3 Performance of AZO sensor

Limit of detection

As shown in Figure 5, paper I, the responses of the AZO sensor exhibited a quasi-linear increase in response signal with rising analyte concentrations in the range of 6-50 nM for both ultrapure and tap water. The LOD and LOQ values, calculated using Equations (8) and (9), were 3.6 nM and 11.8 nM in tap water media, respectively. Since AZO concentration in the lowland stream water was found to be as high as 73.6 nM, the results of detection limits promise the practical utility of the AZO sensor for the analysis of environmental water [74].

Selectivity

Two fungicides, kresoxim-methyl (KSX) and pyraclostrobin (PRC), which belong to the same group of strobilurin fungicides as AZO, were chosen for evaluating the sensor's ability to distinguish between different compounds (refer to Figure 11 for molecular structures). As evident from Figure 6, Paper I, despite their structural similarities, the AZO sensor exhibited a stronger response to the target compound (AZO) compared to the other tested fungicides (KSX and PRC). The signal caused by AZO presence was approximately 2 and 4 times higher than the signals generated by PRC and KSX, respectively. Hence, the AZO sensor could discriminate between AZO and other similar molecules in the tap water.

Figure 11. *Fungicide molecules used in selectivity experiments, including KSX (313.3 g/mol) and PRC (387.8 g/mol).*

To validate the accuracy of the sensor's measurements and assess its practical utility, recovery experiments were conducted using AZO solutions of varying concentrations in tap water (as detailed in Table 1, Paper I). The sensor confirmed its robust performance with good recoveries within the range of 94% to 119%.

3.2 ML sensor

Although the previously developed ERY-selective MIP-based electrochemical sensor showed excellent performance towards ERY [205], it failed to detect other ML despite their similarity in molecule structure. Since many different pollutant molecules tend to exist together in water samples, it will be interesting and economically beneficial if a single sensor can detect more than 1 target molecule. This section describes the design of a ML-based electrochemical sensor that is capable to detect ML class, particularly 3 members ERY, CLA, and AZI that share similarities in molecule structure.

3.2.1 Rational design of the class-selective ML-MIP

Hereby, the double recognition approach combing both non-covalent and covalent was utilised to generate ML imprinting for class selective. The noncovalent approach relied on hydrogen bond formation between mPD and hydroxyl group of the ML. Meanwhile, the covalent approach aimed to form a reversible interaction between the boronic acid group of APBA and the 1,2-diols moiety of the macrocyclic lactone unique to all ML antibiotics (Figure 12). This well-known interaction has been employed in preparing multiple sensors to detect various analytes [223], [224], [225].
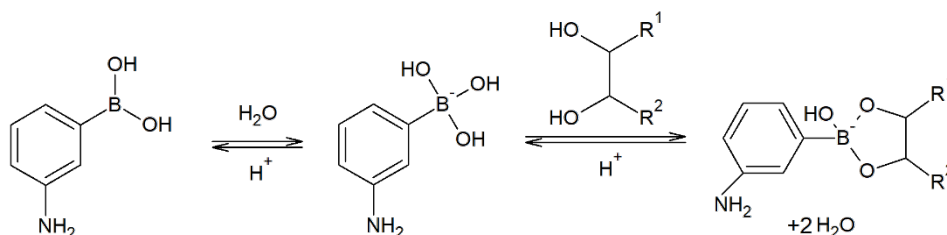
Figure 12. Scheme showing reversible covalent interactions between 3-APBA and 1,2-diols moiety.

To ensure the formation of covalent bond, ^{13}C nuclear magnetic resonance analysis was carried out on ERY, APBA, and their mixtures in PBS solutions at pH 7.4 and 4. In Figure 13, the characteristic spectra were clearly seen in the solution of individual molecules, while ERY spectra disappeared at a pH of 7.4 which re-emerges, albeit with lower intensity, at a pH of 4. This observation suggested the formation of boronate ester bonds between the molecules at a pH of 7.4 and their subsequent breakage at an acidic pH. The result agreed with previous reports where the formation and breakage of covalent boronate ester bonds in basic and acidic solutions [226].
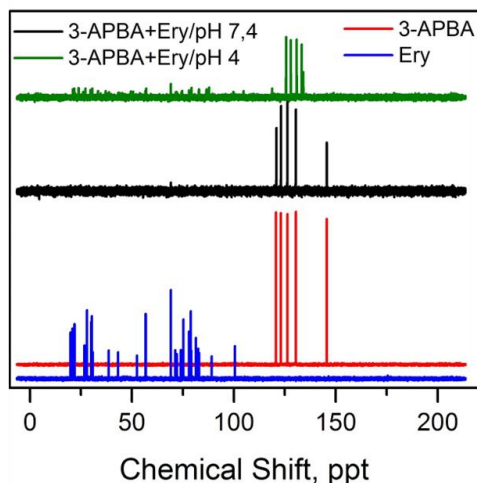
Figure 13. *Liquid-state ^{13}C NMR spectroscopy of ERY, 3-APBA and their mixture (molar ratio 1:1) at pH 7.4 and pH 4.*

Although the combination of APBA and mPD has previously been reported for the preparation of aerogels used in silver separation [227], to the best of the author's knowledge, this is the first time it has been applied in the preparation of ML-MIP for class antibiotic recognition. Using multiple functional monomers in ML-MIP synthesis allows interactions with various regions of the template molecule, thereby improving selectivity compared to MIPs synthesized with a single monomer.

### 3.2.2 Synthesis and characterization of ML-MIP film

Two functional monomers mPD and APBA with the presence of template ERY were electrochemically to synthesis MIP film. CV measurements were caried out to determine the electrochemical potential for the synthesis of the copolymer P(mPD-co-APBA), while avoiding unwanted oxidation of the ERY. The CV scans (Figure 1a, Paper II) showed that the electropolymerization potential of the co-polymer should be selected in the range of 0.4–0.6 V. Meanwhile, the IRSE spectra (Figure 1b, Paper II) showed no pronounced differences in the vibrational signatures of polymer films synthesized at either 0.5 or 0.6 V, although a slight increase in the thickness at 0.6 V. Therefore, a constant potential of 0.5 V was chosen for the electrodeposition of the P(mPD-co-APBA)/ERY co-polymer film. The presence of APBA-related IRSE absorption bands (1320 cm^{-1}, 1425 cm^{-1}, and 1475 cm^{-1} in Figure 1b, Paper II) and their linear increase in intensity with higher APBA:mPD ratios (Figure 1c, Paper II) confirm the successful incorporation of APBA into the copolymer, indicating the coexistence of both monomers in the poly(mPD-co-APBA) structure.

To monitor ML-MIP formation on the sensor surface, CV and EIS measurements were performed to correlate each modification stage with the observed changes in charge transfer between the Au WE surface and the redox pair. The significant depression of CV's anodic and cathodic current peaks, in Figure 14a, indicated the formation of a non-electroactive film P(mPD-co-APBA)/ERY obstructs charge transfer at the electrode/solution interface. However, after template removal treatment, a substantial

recovery of the peaks was observed, suggesting the increased permeability of the polymer layer to the redox probe ions via the imprinted cavities formed after the removal of entrapped ERY molecules from the polymer; hence, ML-MIP formation.

Similar behaviour was observed in EIS spectra (Figure 14b) where the semicircle diameter, which corresponds to the charge transfer resistance (R_{ct}) greatly increased after electrodeposition (Table 6), followed by a subsequent decrease after treatment in 5% acetic acid to form ML-MIP.

Nevertheless, the treatment of reference sensor (NIP) with acetic acid yielded much less changes in the measured parameters for both CV and EIS. This validated the suggestion that the removal of ERY from P(mPD-co-APBA)/ERY film resulted in the observed increase in charge transfer via the imprinted cavities created in the polymer. Furthermore, after the adsorption of 1.6 µM ERY, ML-MIP revealed more significant change in both CV voltammogram and R_{ct} value of EIS compared to the NIP (see Table 6), indicating an enhanced adsorption of the target on the ML-MIP based sensor.
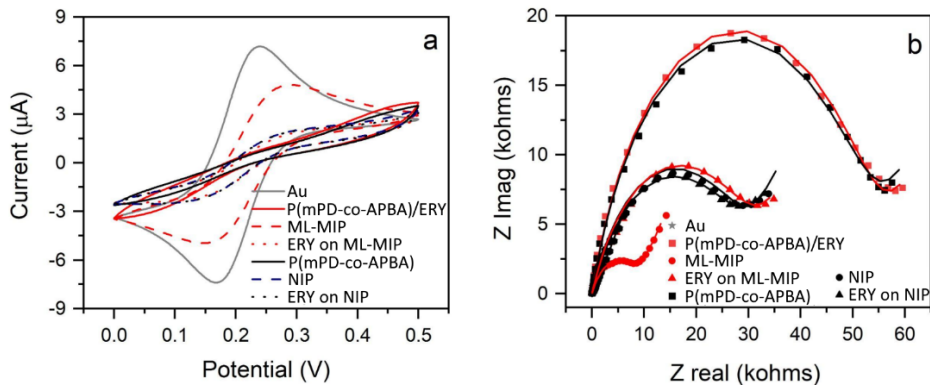
Figure 14. (a) CV and (b) EIS characterization of ML-MIP preparation on SPE.

To enhance ML-MIP performance, the optimal molar concentration ratio of Ery:mPD:APBA of 2:10:5 mM and a charge density of 5.0 mC/cm^2 were adopted for preparing mMIP films (see more section 3.2.1 and 3.2.2, Paper II). Furthermore, the solution with pH value close to 7 could be considered optimal for ML analysis (see more section 3.2.3, Paper II). This is especially beneficial for ML sensor in practical application, as environmental water typically exists at the pH ranging from 6.5 to 8.5 [228], [229].

Table 6. Charge transfer resistance (R_{ct}) values obtained from fitting EIS spectra to an equivalent circuit consisting of a solution resistance, R_s, a charge transfer resistance, R_{ct}, a constant phase element, CPE, and a Warburg impedance, W_d.

Parameter	Au	P(mPD-co-APBA)/ERY	ML-MIP	ERY on ML-MIP	P(mPD-co-APBA)	NIP	ERY on NIP
R_{ct} (kohms)	0.3	54.6	9.1	31.5	53.5	29.6	29.8

3.2.3 Performance of ML sensor

Evaluation of molecular recognition via RR

To evaluate the molecular recognition properties of the prepared ML-MIP toward target analytes, the responses of ML sensors to the increasing analyte concentration were plotted as an adsorption isotherm and fitted to common models, including Langmuir; Freundlich and LF (more detail in section 2.4.2). As observed in Figure 15 and Tables 7, the LF model accurately describes the experimental binding interactions between ML-MIP and analytes. These results lend credibility to the notion that the MIP preparation process introduces a certain degree of heterogeneity into the polymer layer which differs from either homogeneous or heterogeneous surfaces, as reported previously [230]. This aligns with literature reports showing that the LF model more accurately fits the practical adsorption isotherms of MIPs than either the Langmuir or Freundlich models [205], [231], and has been successfully applied to simulate metal ion adsorption [232], gas adsorption on surfaces [233], and adsorption on both MIP and NIP materials [234].

Consistent with the LF model-based analysis, ML sensor signaled about a 4-fold higher response (RR values of 3.8, 3.5 and 4.4 for ERY, CLA and AZI, respectively, in Table 7) than the NIP-based reference as saturation. Since the NIP differs from the ML-MIP solely by
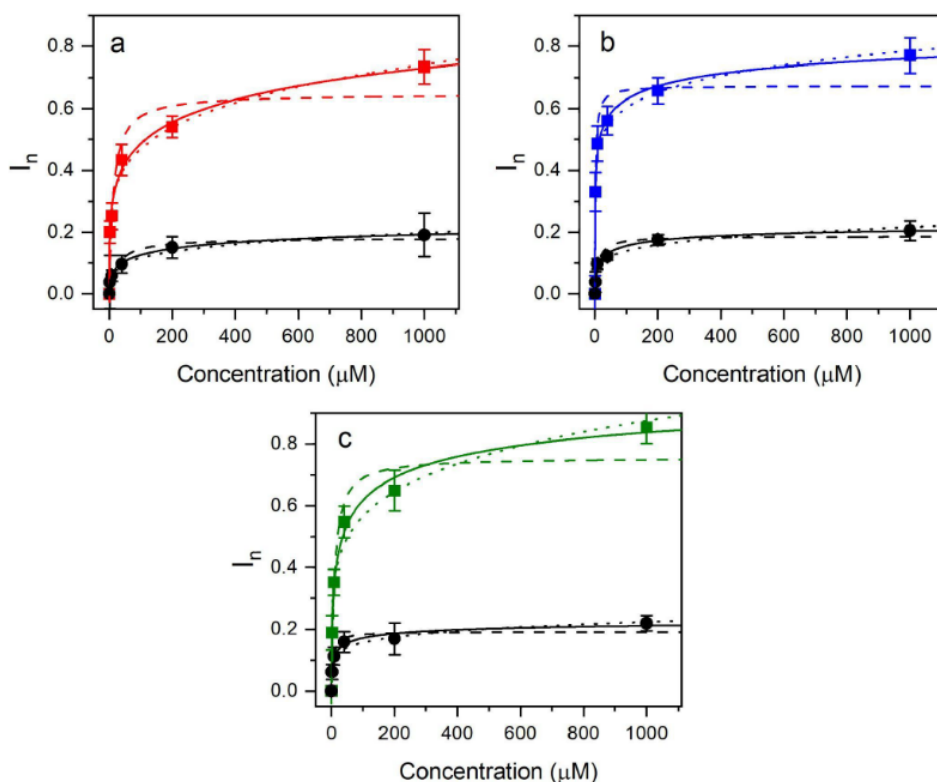
***Figure 15.** Adsorption isotherms of ML-MIP and NIP-based sensors upon binding of increasing concentrations of (a) ERY, (b) CLA, and (c) AZI. Fits to the Langmuir (L), Freundlich (F), and Langmuir-Freundlich (LF) isotherms are represented by dashed, short-dashed, and solid lines, respectively.*

the absence of ERY during polymerization, such a significant difference highlights the molecular recognition ability of ML-MIP, attributed to binding cavities formed in the presence of ERY during polymerization.

Table 7. *Parameters derived from fitting the adsorption isotherms of target analytes on ML-MIP and NIP to Langmuir, Freundlich and LF models.*

		Langmuir		Freundlich		LF	
		ML-MIP	**NIP**	**ML-MIP**	**NIP**	**ML-MIP**	**NIP**
ERY	Imax	0.6 ±0.1	0.2 ±0.1	0.20 ±0.01	0.04 ±0.01	0.84 ±0.06	0.22 ±0.02
	$K_D(\mu M)$	12.8	25.2	-	-	6.0	10.1
	m	-	-	0.2	0.2	0.5	0.6
	RR	3.0		5.0		3.8	
	R^2	0.919		0.992		0.993	
CLA	Imax	0.70 ±0.03	0.20 ±0.04	0.40 ±0.02	0.10 ±0.01	0.77 ±0.03	0.22 ±0.01
	$K_D(\mu M)$	2.2	9.7	-	-	2.0	6.0
	m	-	-	0.1	0.2	0.5	0.6
	RR	3.5		4.0		3.5	
	R^2	0.963		0.991		0.986	
AZI	Imax	0.80 ±0.04	0.20 ±0.04	0.20 ±0.02	0.08 ±0.02	0.96 ±0.05	0.22 ±0.01
	$K_D(\mu M)$	9.6	5.0	-	-	5.1	3.4
	m	-	-	0.2	0.2	0.5	0.6
	RR	4.0		2.5		4.4	
	R^2	0.952		0.980		0.990	

Limit of detection

In Figure 3d, Paper II, the response increases linearly with the analyte concentrations of each ML at a low analyte concentration range of 2-20 nM. The LOD and LOQ within the range of ca. 1–2 nM and 4–5 nM (Table 8), respectively, indicated a significant improvement over previously reported MIP-based electroanalytical sensors (Table 9) for macrolide antibiotic detection.

Table 8. *Parameters obtained from the linear regression of the sensor's response to low concentrations of the analytes as Figure 3d, paper II.*

Analyte	Slope	SD	LOD (nM)	LOQ (nM)	R^2
ERY	1.76E-3	6.7E-4	1.1	3.8	0.996
CLA	2.02E-3	9.5E-4	1.4	4.7	0.994
AZI	1.87E-3	0.001	1.6	5.3	0.992

Platform	Analyte	Interaction	LOD (nM)	LOQ (nM)	Ref
Surface plasmon resonance	ERY	non-covalent	400	Not found	[235]
Microcantilever	ERY	non-covalent	1000	3000	[236]
Electrochemical	AZI	non-covalent	120	340	[183]
Electrochemical	AZI	non-covalent	80	300	[237]
Electrochemical	ERY	non-covalent	0.1	0.4	[205]
Electrochemical	ERY, CLA, AZI	semi-covalent	1.1 – 1.6	3.4 – 5.3	This work

Selectivity

Three antibiotic candidates, including sulfamethizole (SMZ), ciprofloxacin (CIP), and amoxicillin (AMO) were chosen to test the sensor's selectivity (refer to Figure 16 for molecular structures). They belong to different antibiotic classes of penicillin, fluoroquinolones, and sulfonamides, respectively, which coexist with targets in the same environment due to their broad prescription and the possibility of being combined with ML. The result in Figure 4, Paper II demonstrated that ML sensors responded higher towards the three MLs than AMO, CIP, and SMZ in PBS.
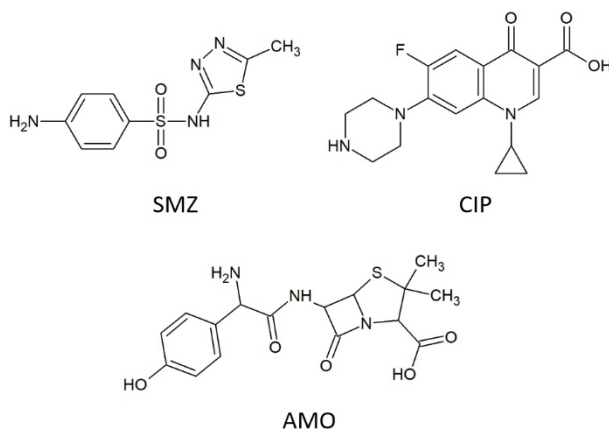
Figure 16. *Antibiotic molecules used in used in selectivity experiments, including SMZ (270.3 g/mol), CIP (331.3 g/mol), and AMO (365.4 g/mol).*

To test in a more complex matrix, tap water was spiked with the required amount of each analyte to prepare the sample solutions. Figure 5a, Paper II indicated that the sensor clearly distinguished between the recognition of MLs and other molecules. As the concentration of interfering analytes increases, there were no significant changes in the sensor's responses observed. In contrast, the responses exhibited a proportional increase with rising concentrations of ML. Thus, the sensor's selective property is preserved even in the intended media such as tap water, which contains multiple dissolved ions

Macrolide	Amount spiked (µM)	Found Ery (µM)	Recovery (%)
ERY	0.04	0.04±0.01	93±2
	0.20	0.19±0.03	95±2
	8.00	8.16±0.10	102±1
CLA	0.04	0.04±0.01	96±2
	0.20	0.20±0.03	98±2
	8.00	8.60±0.02	108±1
AZI	0.04	0.04±0.01	95±2
	0.20	0.19±0.02	96±2
	8.00±	7.92±0.05	99±1

(e.g., bicarbonate, calcium, sodium, potassium, manganese, sulphate, and fluoride), along with trace compounds that meet drinking water quality standards [238], [239].

Moreover, the sensor's response was studied in the exposure to an aqueous solution containing a mixture of MLs. Thus, tap water spiked with 0.04, 0.2 and 1 µM concentrations of MLs and their equimolar mixture were prepared, and the induced responses were analyzed. As shown in Figure 5b, Paper II, the responses generated by the mixtures were comparable with those caused by individual MLs at the same concentration (differences range from 3% to 10%). This observation suggested that the sensor selectively recognizes the parent macrocyclic lactone central to all MLs, thereby crediting the significance of the imprinting strategy.

The recoveries of the analytes were examined in tap water fortified with different concentrations of each ML. The results (Table 10) showed good recoveries ranging from 93% to 108%, indicating the sensor's adaptability for use in the intended media.
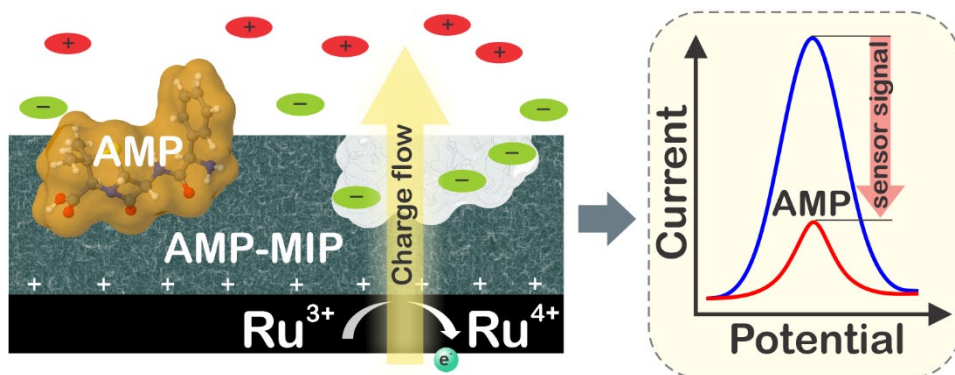
3.3 AMP sensor

This section describes the design of an AMP sensor, which employs RuO_2 electrode as both an electrochemical transducer and an intrinsic redox probe. This innovative approach eliminates the reliance of traditional MIP-based sensors on external redox probes. The working principle, rational design, key characteristics of the sensor, and its performance in natural complex aqueous samples are thoroughly examined.

3.3.1 AMP sensor working principle

The working principle of the AMP sensor is illustrated in Figure 17. During LSV, the RuO_2 electrode undergoes oxidation, prompting anions from the electrolyte to diffuse toward the electrode through the empty imprinted binding cavities of the AMP-MIP layer to compensate for the positive charge close to electrode's surface, thereby sustaining the current flow between the electrode and the solution within the electrochemical cell.

With the present of AMP in the solution, its molecule rebind to the imprinted cavities, obstructing the diffusion of ions and leading to a noticeable change in the measured current. Therefore, the sensor detects the presence and quantity of AMP by changing in peak current observed during LSV.

Figure 17. *Scheme of working principle of the AMP sensor, which utilizes RuO₂ as both a transducer and an internal redox probe material. In the absence of AMP, the charge is transferred through the binding cavity, providing a strong current peak (blue curve). After AMP rebinding, the non-conducting antibiotic molecules obstruct the charge transfer, resulting in a reduced current peak (red curve).*

3.3.2 Functional monomer selection

Electropolymerizable monomers, including 1,8-DAN, ANI, EDOT, mPD, and PYR (Figure 2, Paper III) were considered as potential functional monomers for MIP synthesis. Following the calculation of binding energies, the results (Table 1, Paper III) showed that mPD exhibited the greatest overall binding energy, signifying its capability to form robust hydrogen interactions with AMP. Therefore, further experimental work uses mPD as a functional monomer.

3.3.3 Synthesis and characterization of AMP-MIP films

The initial experiments to assess the performance of AMP-MIP for the detection of AMP were conducted on the Au slide, which is well-known for its stable surface chemistry and electrochemical properties [240], [241]. CV measurements were performed to determine the suitable electrochemical potential for synthesizing PmPD while avoiding the undesired oxidation of AMP. The fragment of the first cycle of CV scans (Figure 18a) revealed that mPD undergoes oxidation at approximately 250 mV, while AMP shows negligible activity. Based on this, a potential range of −0.2 to 0.4 V at a scan rate of 50 mV/s over 15 cycles was used to synthesize PmPD/AMP film on the Au slide (Figure 18b). The modified electrode was immersed in a washing solvent of acetic acid and methanol in a volume ratio of 1:19 and vortexed for 60 minutes to remove AMP, resulting in the formation of AMP-MIP. The results of CV characterization in redox solution (Figure 18c) indicated a decrease in both the anodic and cathodic current peaks after the electrodeposition of PmPD/AMP. This suggested the formation of a non-conductive film that hinders the charge transfer at the interface between the electrode and the solution. The increase in current peaks after the washing out process showed that the polymer layer has become more permeable, proving the formation of imprinted cavities on polymer film. Following AMP rebinding, a substantial depression of the current peaks could be observed. This is most likely indicative of the adsorption of AMP molecules on the preformed binding cavities on AMP-MIP resulting in the expected

reduction of the charge transfer. This experiment was crucial in the AMP sensor development process as it demonstrated the initial selectivity of AMP-MIP, suggesting its potential effectiveness when later combined with the RuO_2 WE.
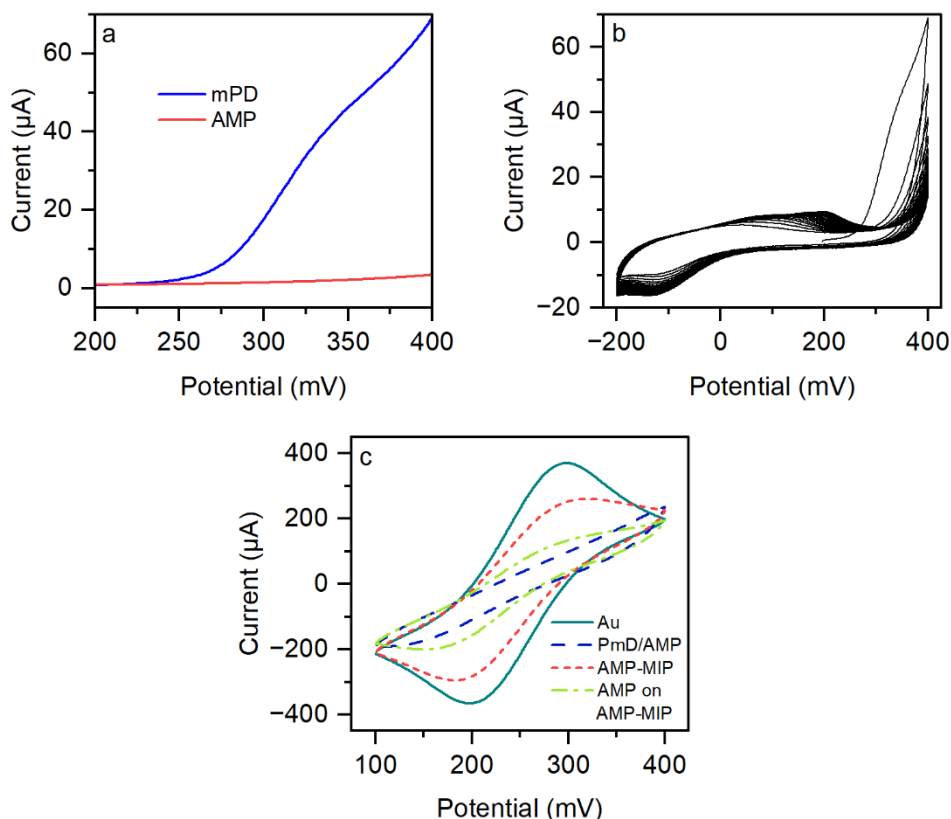
Figure 18. *CV recorded on the gold slides at a scan rate of 50 mV/s, showing (a) a fragment of the first cycle in PBS containing either 10 mM mPD or 2 mM AMP, and (b) their electrodepolimerization resulted in PmPD/AMP in PBS (c) the characterization of bare gold Au, PmPD/AMP modified Au, AMP-MIP modified Au before, and after AMP adsorption.*

The gradual decrease in redox peak currents upon the addition of mPD into PBS solution confirms the successful electropolymerization of a non-conductive PmPD film on the RuO_2 working electrode, as it increasingly hinders charge transfer (Figure 4, Paper III). To further modify the electrode with the PmPD/AMP layer, CV was employed, enabling precise control over film thickness. By adjusting the number of CV cycles to 5, the thickness of the layer ensured the optimal synergy between the AMP-MIP and the RuO_2 WE, enhancing the sensor's performance (see Section 3.3.1, Paper III). The AMP sensor's incubation time of 30 minutes was used for further experiments (see Section 3.3.2, Paper III).

Each stage of the AMP sensor preparation process was closely monitored by LSV, where the modifications of the RuO_2 electrode surface were expected to induce changes in charge transfer capability through the electrode surface. As shown in Figure 5a, Paper III, a marked reduction in peak currents was observed following the electrochemical

deposition of PmPD/AMP, indicating surface passivation by electrochemically inactive materials. However, upon treatment with a washing solution to form AMP-MIP, a partial recovery of the previously diminished peaks indicates the removal of the trapped template molecules, thus forming molecular cavities in the polymer and facilitating charge transfer at the electrode/solution interface.

Conversely, similar treatments on NIP, or the PmPD-modified RuO_2 electrode, caused no significant changes in the LSV voltammograms (Figure 5b, Paper III). This result supported, indirectly, that the current rise after treatment with the washing solution of PmPD/AMP was likely due to AMP removal. Thus, the imprinting of AMP in the PmPD film could be said to be successfully achieved.

3.3.4 Performance of AMP sensor

Limit of detection

From Figure 8d, Paper III, the response of the AMP sensor linearly increased with analyte concentrations up to 50 nM in pond water, resulting in LOD and LOQ values of 6 nM and 19 nM, respectively. This indicated the suitability of the sensor for analyzing AMP in environmental water samples, as AMP is found in surface water at approximately 46 nM and in wastewater effluents in the range of 7-121 nM [81], [242].

Selectivity

Two antibiotic candidates, AMO and doxycycline (DOX), were chosen to evaluate the sensor's ability to distinguish between different compounds (molecule structures are presented in Figure 7, Paper III). AMO shares structural similarity with the target molecule (AMP), as both belong to the aminopenicillin class, while DOX represents a structural distinct from tetracycline class. The results in Figure 8a-b, Paper III, demonstrated that the AMP sensor exhibits significantly higher response and RR for 10 µM of the target AMP compared to AMO and DOX, in both PBS and pond water.

Additionally, the sensor's performance was evaluated in pond water spiked with a low concentration (50 nM) of each antibiotic, mimicking real-world conditions as found for AMP in surface water and wastewater effluents. As shown in Figure 8c, Paper III, the AMP sensor demonstrated the highest response towards AMP compared to AMO and DOX. The RRs were also higher for AMP, underscoring the significance of forming an AMP imprinted cavities within the AMP-MIP layer that allows the discriminatory recognition of the target over other antibiotics.

To validate the reliability and accuracy of the sensor, recovery experiments were conducted using AMP solutions of varying concentrations in pond water (as detailed in Table 2, Paper III). The recoveries within the range of 98% to 114% confirms sensors' robust performance.

Conclusions

This thesis presents several novel contributions to the field of MIP-based electrochemical sensors for environmental monitoring. First, an AZO-selective MIP-based electrochemical sensor was developed, enabling rapid detection of AZO at environmentally relevant concentrations and representing a significant advancement in agricultural pollutant monitoring. Second, a class-selective MIP was synthesized, allowing the creation of an electrochemical sensor capable of detecting structurally similar compounds—particularly ML antibiotics—in a single measurement. Third, by combining a RuO_2 electrode with an AMP-selective MIP, a sensor was developed that enables reliable and accurate detection of AMP without the need for an external redox probe solution. More specifically, the following significant conclusions can be drawn from this study:

- The developed AZO-selective MIP exhibited strong selectivity when integrated with the electrode, enabling the construction of a sensor capable of rapid and accurate AZO detection. The sensor demonstrated a LOD of 3.6 nM and a LOQ of 11.8 nM in tap water. Given that AZO concentrations in lowland stream water can reach up to 73.6 nM, the sensor demonstrated the promising utility for cost-effective and routine monitoring of agricultural fungicide contamination.

- By targeting a MIP against a shared chemical structure common to a group of compounds, a class-selective material can be generated. In this study, selective recognition of ML antibiotics (ERY, CLA, and AZI) was achieved by employing APBA and mPD as functional monomers, leveraging the synergistic effects of covalent and noncovalent interactions. Specifically, SPE modified with the ML-selective MIP yielded the portable sensor element exhibiting appreciable recognition for macrolides, including ERY, CLA, and AZI, with low LOD (1–2 nM) and LOQ (4–5 nM) in tap water. Considering the low-cost and scalable SPE format, the finding offers strong potential for practical implementation in routine environmental monitoring of pharmaceutical pollutants.

- A MIP-based electrochemical sensor was developed for the reliable detection of AMP, employing RuO_2 as both the transducer and internal redox probe. Eliminating the need for an external redox solution enhanced detection reliability by reducing interference from external electroactive species. The sensor achieved a LOD of 6 nM in natural pond water, clearly demonstrating its potential for accurate analysis for antibiotic pollutants in environmental water.

- The combination of computational modelling and experimental studies enabled the rational selection of functional monomers, improving the performance of the sensors for their respective targets.

- All prepared sensors effectively distinguished target analytes from both structurally similar and dissimilar compounds across complex water matrices and achieving high recoveries between 93% and 119% in real water samples, confirming their robust and accurate performance, as well as suitability for environmental monitoring applications. The miniaturized

design of all sensors enables portable electrochemical detection of target contaminants, making them highly suitable for in-field environmental applications.

- This study demonstrates validated and effective strategies for developing MIP-based electrochemical sensors targeting environmental pollutants in aqueous media.

References

[1] *Pesticides use, pesticides trade and pesticides indicators*. FAO, 2022. doi: 10.4060/cc0918en.

[2] E. Y. Klein *et al.*, "Global increase and geographic convergence in antibiotic consumption between 2000 and 2015," *Proc. Natl. Acad. Sci. U.S.A.*, vol. 115, no. 15, Apr. 2018, doi: 10.1073/pnas.1717295115.

[3] A. Arif, "Water pollution and industries," *PAB*, vol. 9, no. 4, Dec. 2020, doi: 10.19045/bspab.2020.90237.

[4] Y. Liu *et al.*, "A review of water pollution arising from agriculture and mining activities in Central Asia: Facts, causes and effects," *Environmental Pollution*, vol. 291, p. 118209, Dec. 2021, doi: 10.1016/j.envpol.2021.118209.

[5] J. L. Wilkinson *et al.*, "Pharmaceutical pollution of the world's rivers," *Proc. Natl. Acad. Sci. U.S.A.*, vol. 119, no. 8, p. e2113947119, Feb. 2022, doi: 10.1073/pnas.2113947119.

[6] L. Liu, W. Wu, J. Zhang, P. Lv, L. Xu, and Y. Yan, "Progress of research on the toxicology of antibiotic pollution in aquatic organisms," *Acta Ecologica Sinica*, vol. 38, no. 1, pp. 36–41, Feb. 2018, doi: 10.1016/j.chnaes.2018.01.006.

[7] R. Qadri and M. A. Faiq, "Freshwater Pollution: Effects on Aquatic Life and Human Health," in *Fresh Water Pollution Dynamics and Remediation*, H. Qadri, R. A. Bhat, M. A. Mehmood, and G. H. Dar, Eds., Singapore: Springer Singapore, 2020, pp. 15–26. doi: 10.1007/978-981-13-8277-2_2.

[8] H. Ehalt Macedo, B. Lehner, J. A. Nicell, U. Khan, and E. Y. Klein, "Antibiotics in the global river system arising from human consumption," *PNAS Nexus*, vol. 4, no. 4, p. pgaf096, Mar. 2025, doi: 10.1093/pnasnexus/pgaf096.

[9] M. E. A. De Kraker, A. J. Stewardson, and S. Harbarth, "Will 10 Million People Die a Year due to Antimicrobial Resistance by 2050?," *PLoS Med*, vol. 13, no. 11, p. e1002184, Nov. 2016, doi: 10.1371/journal.pmed.1002184.

[10] C.-W. Huang, C. Lin, M. K. Nguyen, A. Hussain, X.-T. Bui, and H. H. Ngo, "A review of biosensor for environmental monitoring: principle, application, and corresponding achievement of sustainable development goals," *Bioengineered*, vol. 14, no. 1, pp. 58–80, Dec. 2023, doi: 10.1080/21655979.2022.2095089.

[11] A. Inobeme *et al.*, "Chemical Sensor Technologies for Sustainable Development: Recent Advances, Classification, and Environmental Monitoring," *Advanced Sensor Research*, vol. 3, no. 12, p. 2400066, Dec. 2024, doi: 10.1002/adsr.202400066.

[12] A. Kozitsina, T. Svalova, N. Malysheva, A. Okhokhonin, M. Vidrevich, and K. Brainina, "Sensors Based on Bio and Biomimetic Receptors in Medical Diagnostic, Environment, and Food Analysis," *Biosensors*, vol. 8, no. 2, p. 35, Apr. 2018, doi: 10.3390/bios8020035.

[13] C. W. Lee, J. M. Suh, and H. W. Jang, "Chemical Sensors Based on Two-Dimensional (2D) Materials for Selective Detection of Ions and Molecules in Liquid," *Front. Chem.*, vol. 7, p. 708, Nov. 2019, doi: 10.3389/fchem.2019.00708.

[14] J. J. BelBruno, "Molecularly Imprinted Polymers," *Chem. Rev.*, vol. 119, no. 1, pp. 94–119, Jan. 2019, doi: 10.1021/acs.chemrev.8b00171.

[15] P. Yáñez-Sedeño, S. Campuzano, and J. M. Pingarrón, "Electrochemical sensors based on magnetic molecularly imprinted polymers: A review," *Analytica Chimica Acta*, vol. 960, pp. 1–17, Apr. 2017, doi: 10.1016/j.aca.2017.01.003.

[16]   P. Lach *et al.*, "Self-reporting molecularly imprinted polymer with the covalently immobilized ferrocene redox probe for selective electrochemical sensing of p-synephrine," *Sensors and Actuators B: Chemical*, vol. 344, p. 130276, Oct. 2021, doi: 10.1016/j.snb.2021.130276.

[17]   G. Ozcelikay *et al.*, "Electrochemical MIP Sensor for Butyrylcholinesterase," *Polymers*, vol. 11, no. 12, p. 1970, Nov. 2019, doi: 10.3390/polym11121970.

[18]   A. Yarman and F. W. Scheller, "How Reliable Is the Electrochemical Readout of MIP Sensors?," *Sensors*, vol. 20, no. 9, p. 2677, May 2020, doi: 10.3390/s20092677.

[19]   P. Lach *et al.*, "Electroactive molecularly imprinted polymer nanoparticles for selective glyphosate determination," *Biosensors and Bioelectronics*, vol. 236, p. 115381, Sep. 2023, doi: 10.1016/j.bios.2023.115381.

[20]   A. Garcia-Cruz, O. S. Ahmad, K. Alanazi, E. Piletska, and S. A. Piletsky, "Generic sensor platform based on electro-responsive molecularly imprinted polymer nanoparticles (e-NanoMIPs)," *Microsyst Nanoeng*, vol. 6, no. 1, p. 83, Oct. 2020, doi: 10.1038/s41378-020-00193-3.

[21]   H. Li *et al.*, "RuO2/rGO heterostructures as mimic peroxidases for colorimetric detection of glucose," *Microchim Acta*, vol. 189, no. 7, p. 261, Jul. 2022, doi: 10.1007/s00604-022-05319-0.

[22]   N. Hodnik *et al.*, "New Insights into Corrosion of Ruthenium and Ruthenium Oxide Nanoparticles in Acidic Media," *J. Phys. Chem. C*, vol. 119, no. 18, pp. 10140–10147, May 2015, doi: 10.1021/acs.jpcc.5b01832.

[23]   D. Majumdar, T. Maiyalagan, and Z. Jiang, "Recent Progress in Ruthenium Oxide-Based Composites for Supercapacitor Applications," *ChemElectroChem*, vol. 6, no. 17, pp. 4343–4372, Sep. 2019, doi: 10.1002/celc.201900668.

[24]   N. Lenar, B. Paczosa-Bator, and R. Piech, "Optimization of Ruthenium Dioxide Solid Contact in Ion-Selective Electrodes," *Membranes*, vol. 10, no. 8, p. 182, Aug. 2020, doi: 10.3390/membranes10080182.

[25]   T. Roy, M. A. Salazar De Troya, M. A. Worsley, and V. A. Beck, "Topology optimization for the design of porous electrodes," *Struct Multidisc Optim*, vol. 65, no. 6, p. 171, Jun. 2022, doi: 10.1007/s00158-022-03249-2.

[26]   K. Uppuluri, M. Lazouskaya, D. Szwagierczak, K. Zaraska, and M. Tamm, "Fabrication, Potentiometric Characterization, and Application of Screen-Printed RuO2 pH Electrodes for Water Quality Testing," *Sensors*, vol. 21, no. 16, p. 5399, Aug. 2021, doi: 10.3390/s21165399.

[27]   J. W. Long, K. E. Swider, C. I. Merzbacher, and D. R. Rolison, "Voltammetric Characterization of Ruthenium Oxide-Based Aerogels and Other RuO$_2$ Solids: The Nature of Capacitance in Nanostructured Materials," *Langmuir*, vol. 15, no. 3, pp. 780–785, Feb. 1999, doi: 10.1021/la980785a.

[28]   S. Chalupczok, P. Kurzweil, H. Hartmann, and C. Schell, "The Redox Chemistry of Ruthenium Dioxide: A Cyclic Voltammetry Study—Review and Revision," *International Journal of Electrochemistry*, vol. 2018, pp. 1–15, 2018, doi: 10.1155/2018/1273768.

[29]   A. Srivastava and M. Singh, "Limitations and Challenges in the Practical Implementation of MIPs," in *Molecularly Imprinted Polymers as Artificial Antibodies for the Environmental Health*, S. Patra and M. Sillanpaa, Eds., Cham: Springer Nature Switzerland, 2024, pp. 389–412. doi: 10.1007/978-3-031-58995-9_14.

[30]   L. Chandra Voumik and T. Sultana, "Impact of urbanization, industrialization, electrification and renewable energy on the environment in BRICS: fresh evidence from novel CS-ARDL model," *Heliyon*, vol. 8, no. 11, p. e11457, Nov. 2022, doi: 10.1016/j.heliyon.2022.e11457.

[31]   L. Ma, Y. Zhang, S. Chen, L. Yu, and Y. Zhu, "Environmental effects and their causes of agricultural production: Evidence from the farming regions of China," *Ecological Indicators*, vol. 144, p. 109549, Nov. 2022, doi: 10.1016/j.ecolind.2022.109549.

[32]   K. Groh, C. Vom Berg, K. Schirmer, and A. Tlili, "Anthropogenic Chemicals As Underestimated Drivers of Biodiversity Loss: Scientific and Societal Implications," *Environ. Sci. Technol.*, vol. 56, no. 2, pp. 707–710, Jan. 2022, doi: 10.1021/acs.est.1c08399.

[33]   I. Manisalidis, E. Stavropoulou, A. Stavropoulos, and E. Bezirtzoglou, "Environmental and Health Impacts of Air Pollution: A Review," *Front. Public Health*, vol. 8, p. 14, Feb. 2020, doi: 10.3389/fpubh.2020.00014.

[34]   Y. Yang *et al.*, "Short-term and long-term exposures to fine particulate matter constituents and health: A systematic review and meta-analysis," *Environmental Pollution*, vol. 247, pp. 874–882, Apr. 2019, doi: 10.1016/j.envpol.2018.12.060.

[35]   J. F. Artiola, J. L. Walworth, S. A. Musil, and M. A. Crimmins, "Soil and Land Pollution," in *Environmental and Pollution Science*, Elsevier, 2019, pp. 219–235. doi: 10.1016/B978-0-12-814719-1.00014-8.

[36]   J. Singh, P. Yadav, A. K. Pal, and V. Mishra, "Water Pollutants: Origin and Status," in *Sensors in Water Pollutants Monitoring: Role of Material*, D. Pooja, P. Kumar, P. Singh, and S. Patil, Eds., in Advanced Functional Materials and Sensors., Singapore: Springer Singapore, 2020, pp. 5–20. doi: 10.1007/978-981-15-0671-0_2.

[37]   J. Liu, W. Feng, and F. Yang, "Sources, Risks, and Remediation Technologies of Pollutants in Aquatic Environments," *Water*, vol. 16, no. 11, p. 1532, May 2024, doi: 10.3390/w16111532.

[38]   L. Lin, H. Yang, and X. Xu, "Effects of Water Pollution on Human Health and Disease Heterogeneity: A Review," *Front. Environ. Sci.*, vol. 10, p. 880246, Jun. 2022, doi: 10.3389/fenvs.2022.880246.

[39]   M. S. Sankhla, "Water Contamination through Pesticide & Their Toxic Effect on Human Health," *IJRASET*, vol. 6, no. 1, pp. 967–970, Jan. 2018, doi: 10.22214/ijraset.2018.1146.

[40]   P. Amoatey and M. S. Baawain, "Effects of pollution on freshwater aquatic organisms," *Water Environment Research*, vol. 91, no. 10, pp. 1272–1287, Oct. 2019, doi: 10.1002/wer.1221.

[41]   A. Singh *et al.*, "Heavy Metal Contamination of Water and Their Toxic Effect on Living Organisms," in *The Toxicity of Environmental Pollutants*, D. Junqueira Dorta and D. Palma De Oliveira, Eds., IntechOpen, 2022. doi: 10.5772/intechopen.105075.

[42]   M. R. Silva, A. Lecus, C. Haehle, D. Garman, and S. Brunner, "Assessment of concentration and distribution of total mercury and polychlorinated biphenyls in Green Bay, Wisconsin, USA," *Environ Sci Pollut Res*, vol. 29, no. 9, pp. 13323–13332, Feb. 2022, doi: 10.1007/s11356-021-16417-6.

[43]   S. Bhojwani, K. Topolski, R. Mukherjee, D. Sengupta, and M. M. El-Halwagi, "Technology review and data analysis for cost assessment of water treatment systems," *Science of The Total Environment*, vol. 651, pp. 2749–2761, Feb. 2019, doi: 10.1016/j.scitotenv.2018.09.363.

[44]   S. Rodriguez-Mozaz *et al.*, "Antibiotic residues in final effluents of European wastewater treatment plants and their impact on the aquatic environment," *Environment International*, vol. 140, p. 105733, Jul. 2020, doi: 10.1016/j.envint.2020.105733.

[45]   I. Senta, S. Terzic, and M. Ahel, "Occurrence and fate of dissolved and particulate antimicrobials in municipal wastewater treatment," *Water Research*, vol. 47, *no. 2, pp. 705–714, Feb. 2013, doi: 10.1016/j.watres.2012.10.041.

[46]   P. A. Segura, M. François, C. Gagnon, and S. Sauvé, "Review of the Occurrence of Anti-infectives in Contaminated Wastewaters and Natural and Drinking Waters," *Environ Health Perspect*, vol. 117, no. 5, pp. 675–684, May 2009, doi: 10.1289/ehp.11776.

[47]   L. K. M. Chow, T. M. Ghaly, and M. R. Gillings, "A survey of sub-inhibitory concentrations of antibiotics in the environment," *Journal of Environmental Sciences*, vol. 99, pp. 21–27, Jan. 2021, doi: 10.1016/j.jes.2020.05.030.

[48]   J. P. Zubrod *et al.*, "Fungicides: An Overlooked Pesticide Class?," *Environ. Sci. Technol.*, vol. 53, no. 7, pp. 3347–3365, Apr. 2019, doi: 10.1021/acs.est.8b04392.

[49]   J. A. C. Barth *et al.*, "Mobility, Turnover and Storage of Pollutants in Soils, Sediments and Waters: Achievements and Results of the EU Project AquaTerra - A Review," in *Sustainable Agriculture*, E. Lichtfouse, M. Navarrete, P. Debaeke, S. Véronique, and C. Alberola, Eds., Dordrecht: Springer Netherlands, 2009, pp. 857–871. doi: 10.1007/978-90-481-2666-8_52.

[50]   A. C. Gerecke *et al.*, "Sources of pesticides in surface waters in Switzerland: pesticide load through waste water treatment plants—current situation and reduction potential," *Chemosphere*, vol. 48, no. 3, pp. 307–315, Jul. 2002, doi: 10.1016/S0045-6535(02)00080-2.

[51]   L. Maltby, T. C. M. Brock, and P. J. Van Den Brink, "Fungicide Risk Assessment for Aquatic Ecosystems: Importance of Interspecific Variation, Toxic Mode of Action, and Exposure Regime," *Environ. Sci. Technol.*, vol. 43, no. 19, pp. 7556–7563, Oct. 2009, doi: 10.1021/es901461c.

[52]   H. Tao, Z. Bao, C. Jin, W. Miao, Z. Fu, and Y. Jin, "Toxic effects and mechanisms of three commonly used fungicides on the human colon adenocarcinoma cell line Caco-2," *Environmental Pollution*, vol. 263, p. 114660, Aug. 2020, doi: 10.1016/j.envpol.2020.114660.

[53]   A. Çayır, M. Coşkun, and M. Coşkun, "Genotoxicity of commercial fungicide Cabrio Plus on human cell," *Cytotechnology*, vol. 68, no. 5, pp. 1697–1704, Oct. 2016, doi: 10.1007/s10616-015-9919-0.

[54]   M. K. Draskau and T. Svingen, "Azole Fungicides and Their Endocrine Disrupting Properties: Perspectives on Sex Hormone-Dependent Reproductive Development," *Front. Toxicol.*, vol. 4, p. 883254, Apr. 2022, doi: 10.3389/ftox.2022.883254.

[55]   M. Ye, J. Beach, J. Martin, and A. Senthilselvan, "Occupational Pesticide Exposures and Respiratory Health," *IJERPH*, vol. 10, no. 12, pp. 6442–6471, Nov. 2013, doi: 10.3390/ijerph10126442.

[56]   J. Liu and E. Schelar, "Pesticide Exposure and Child Neurodevelopment: Summary and Implications," *Workplace Health Saf*, vol. 60, no. 5, pp. 235–242, May 2012, doi: 10.3928/21650799-20120426-73.

[57] J. S. Ongono, R. Béranger, A. Baghdadli, and M. Mortamais, "Pesticides used in Europe and autism spectrum disorder risk: can novel exposure hypotheses be formulated beyond organophosphates, organochlorines, pyrethroids and carbamates? - A systematic review," *Environmental Research*, vol. 187, p. 109646, Aug. 2020, doi: 10.1016/j.envres.2020.109646.

[58] A. J. Leadbeater, "Plant Health Management: Fungicides and Antibiotics," in *Encyclopedia of Agriculture and Food Systems*, Elsevier, 2014, pp. 408–424. doi: 10.1016/B978-0-444-52512-3.00179-0.

[59] J. H. Kim, B. C. Campbell, N. Mahoney, K. L. Chan, R. J. Molyneux, and G. S. May, "Enhanced activity of strobilurin and fludioxonil by using berberine and phenolic compounds to target fungal antioxidative stress response," *Lett Appl Microbiol*, vol. 45, no. 2, pp. 134–141, Aug. 2007, doi: 10.1111/j.1472-765X.2007.02159.x.

[60] MMR, "Azoxystrobin Market: Global Industry Analysis And Forecast(2024-2030)." Accessed: Oct. 24, 2024. [Online]. Available: https://www.maximizemarketresearch.com/market-report/global-azoxystrobin-market/107455/

[61] N. Elfikrie, Y. B. Ho, S. Z. Zaidon, H. Juahir, and E. S. S. Tan, "Occurrence of pesticides in surface water, pesticides removal efficiency in drinking water treatment plant and potential health risk to consumers in Tengi River Basin, Malaysia," *Science of The Total Environment*, vol. 712, p. 136540, Apr. 2020, doi: 10.1016/j.scitotenv.2020.136540.

[62] I. Barnhoorn and C. Van Dyk, "The first report of selected herbicides and fungicides in water and fish from a highly utilized and polluted freshwater urban impoundment," *Environ Sci Pollut Res*, vol. 27, no. 26, pp. 33393–33398, Sep. 2020, doi: 10.1007/s11356-020-09930-7.

[63] T. Lu *et al.*, "The fungicide azoxystrobin promotes freshwater cyanobacterial dominance through altering competition," *Microbiome*, vol. 7, no. 1, p. 128, Dec. 2019, doi: 10.1186/s40168-019-0744-0.

[64] S. Echeverría-Sáenz, M. Spínola-Parallada, and A. C. Soto, "Pesticides Burden in Neotropical Rivers: Costa Rica as a Case Study," *Molecules*, vol. 26, no. 23, p. 7235, Nov. 2021, doi: 10.3390/molecules26237235.

[65] E. T. Rodrigues, I. Lopes, and M. Â. Pardal, "Occurrence, fate and effects of azoxystrobin in aquatic ecosystems: A review," *Environment International*, vol. 53, pp. 18–28, Mar. 2013, doi: 10.1016/j.envint.2012.12.005.

[66] F. Cao *et al.*, "Long-Term Exposure to Environmental Concentrations of Azoxystrobin Delays Sexual Development and Alters Reproduction in Zebrafish (*Danio rerio*)," *Environ. Sci. Technol.*, vol. 53, no. 3, pp. 1672–1679, Feb. 2019, doi: 10.1021/acs.est.8b05829.

[67] F. Cao, L. Zhu, H. Li, S. Yu, C. Wang, and L. Qiu, "Reproductive toxicity of azoxystrobin to adult zebrafish (Danio rerio)," *Environmental Pollution*, vol. 219, pp. 1109–1121, Dec. 2016, doi: 10.1016/j.envpol.2016.09.015.

[68] P. A. Olsvik, F. Kroglund, B. Finstad, and T. Kristensen, "Effects of the fungicide azoxystrobin on Atlantic salmon (Salmo salar L.) smolt," *Ecotoxicology and Environmental Safety*, vol. 73, no. 8, pp. 1852–1861, Nov. 2010, doi: 10.1016/j.ecoenv.2010.07.017.

[69] N. Singh *et al.*, "Metabolism of[14] C-azoxystrobin in water at different pH," *Journal of Environmental Science and Health, Part B*, vol. 45, no. 2, pp. 123–127, Jan. 2010, doi: 10.1080/03601230903471910.

[70]   M. Zhang *et al.*, "Metabolomic modulations in a freshwater microbial community exposed to the fungicide azoxystrobin," *Journal of Environmental Sciences*, vol. 97, pp. 102–109, Nov. 2020, doi: 10.1016/j.jes.2020.04.013.

[71]   C. Zhang *et al.*, "Ecotoxicology of strobilurin fungicides," *Science of The Total Environment*, vol. 742, p. 140611, Nov. 2020, doi: 10.1016/j.scitotenv.2020.140611.

[72]   K. Nguyen *et al.*, "Neurotoxicity assessment of QoI strobilurin fungicides azoxystrobin and trifloxystrobin in human SH-SY5Y neuroblastoma cells: Insights from lipidomics and mitochondrial bioenergetics," *NeuroToxicology*, vol. 91, pp. 290–304, Jul. 2022, doi: 10.1016/j.neuro.2022.06.002.

[73]   E. Djangalina, N. Altynova, N. Mit, and L. Djansugurova, "Complex approaches to assessing the pesticides risk on human health and environment," in *Pesticides in the Natural Environment*, Elsevier, 2022, pp. 163–198. doi: 10.1016/B978-0-323-90489-6.00007-0.

[74]   N. Berenzen, A. Lentzen-Godding, M. Probst, H. Schulz, R. Schulz, and M. Liess, "A comparison of predicted and measured levels of runoff-related pesticide concentrations in small lowland streams on a landscape level," *Chemosphere*, vol. 58, no. 5, pp. 683–691, Feb. 2005, doi: 10.1016/j.chemosphere.2004.05.009.

[75]   T. B. Minh *et al.*, "Antibiotics in the Hong Kong metropolitan area: Ubiquitous distribution and fate in Victoria Harbour," *Marine Pollution Bulletin*, vol. 58, no. 7, pp. 1052–1062, Jul. 2009, doi: 10.1016/j.marpolbul.2009.02.004.

[76]   R. Hirsch, T. Ternes, K. Haberer, and K.-L. Kratz, "Occurrence of antibiotics in the aquatic environment," *Science of The Total Environment*, vol. 225, no. 1–2, pp. 109–118, Jan. 1999, doi: 10.1016/S0048-9697(98)00337-4.

[77]   A. Göbel, A. Thomsen, C. S. McArdell, A. Joss, and W. Giger, "Occurrence and Sorption Behavior of Sulfonamides, Macrolides, and Trimethoprim in Activated Sludge Treatment," *Environ. Sci. Technol.*, vol. 39, no. 11, pp. 3981–3989, Jun. 2005, doi: 10.1021/es048550a.

[78]   E. Archer, B. Petrie, B. Kasprzyk-Hordern, and G. M. Wolfaardt, "The fate of pharmaceuticals and personal care products (PPCPs), endocrine disrupting contaminants (EDCs), metabolites and illicit drugs in a WWTW and environmental waters," *Chemosphere*, vol. 174, pp. 437–446, May 2017, doi: 10.1016/j.chemosphere.2017.01.101.

[79]   F. Mirzaie *et al.*, "Occurrence and distribution of azithromycin in wastewater treatment plants, seawater, and sediments of the northern part of the Persian Gulf around Bushehr port: A comparison with Pre-COVID 19 pandemic," *Chemosphere*, vol. 307, p. 135996, Nov. 2022, doi: 10.1016/j.chemosphere.2022.135996.

[80]   S. I. Abou-Elela and M. A. El-Khateeb, "Performance Evaluation of Activated Sludge Process for Treating Pharmaceutical Wastewater Contaminated With β-Lactam Antibiotics," *Journal of Industrial Pollution Control*, Dec. 2014, Accessed: Jun. 05, 2025. [Online]. Available: https://www.icontrolpollution.com/articles/performance-evaluation-of-activated-sludge-process-for-treating-pharmaceutical-wastewater-contaminated-with-lactam-antibiotics.php?aid=65344

[81]   P. Kulkarni *et al.*, "Antibiotic Concentrations Decrease during Wastewater Treatment but Persist at Low Levels in Reclaimed Water," *IJERPH*, vol. 14, no. 6, p. 668, Jun. 2017, doi: 10.3390/ijerph14060668.

[82]   A. Cassini *et al.*, "Attributable deaths and disability-adjusted life-years caused by infections with antibiotic-resistant bacteria in the EU and the European Economic Area in 2015: a population-level modelling analysis," *The Lancet Infectious Diseases*, vol. 19, no. 1, pp. 56–66, Jan. 2019, doi: 10.1016/S1473-3099(18)30605-4.

[83]   X. Zhou, G. J. P. Cuasquer, Z. Li, H. P. Mang, and Y. Lv, "Occurrence of typical antibiotics, representative antibiotic-resistant bacteria, and genes in fresh and stored source-separated human urine," *Environment International*, vol. 146, p. 106280, Jan. 2021, doi: 10.1016/j.envint.2020.106280.

[84]   T. Gangar and S. Patra, "Antibiotic persistence and its impact on the environment," *3 Biotech*, vol. 13, no. 12, p. 401, Dec. 2023, doi: 10.1007/s13205-023-03806-6.

[85]   M. Sharma, K. Kumar, and K. K. Dubey, "Disposal of unused antibiotics as household waste: A social driver of antimicrobial resistance," *Environmental Quality Mgmt*, vol. 30, no. 4, pp. 127–140, Jun. 2021, doi: 10.1002/tqem.21744.

[86]   L. Fang *et al.*, "A comprehensive and global evaluation of residual antibiotics in agricultural soils: Accumulation, potential ecological risks, and attenuation strategies," *Ecotoxicology and Environmental Safety*, vol. 262, p. 115175, Sep. 2023, doi: 10.1016/j.ecoenv.2023.115175.

[87]   A. Singh, S. G. Pratap, and A. Raj, "Occurrence and dissemination of antibiotics and antibiotic resistance in aquatic environment and its ecological implications: a review," *Environ Sci Pollut Res*, vol. 31, no. 35, pp. 47505–47529, Jul. 2024, doi: 10.1007/s11356-024-34355-x.

[88]   Y. Zeng *et al.*, "Occurrence and Risk Assessment of Antibiotics in Urban River–Wetland–Lake Systems in Southwest China," *Water*, vol. 16, no. 8, p. 1124, Apr. 2024, doi: 10.3390/w16081124.

[89]   U. Szymańska, M. Wiergowski, I. Sołtyszewski, J. Kuzemko, G. Wiergowska, and M. K. Woźniak, "Presence of antibiotics in the aquatic environment in Europe and their analytical monitoring: Recent trends and perspectives," *Microchemical Journal*, vol. 147, pp. 729–740, Jun. 2019, doi: 10.1016/j.microc.2019.04.003.

[90]   Z. Maghsodian *et al.*, "Occurrence and Distribution of Antibiotics in the Water, Sediment, and Biota of Freshwater and Marine Environments: A Review," *Antibiotics*, vol. 11, no. 11, p. 1461, Oct. 2022, doi: 10.3390/antibiotics11111461.

[91]   S. Arun, L. Xin, O. Gaonkar, B. Neppolian, G. Zhang, and P. Chakraborty, "Antibiotics in sewage treatment plants, receiving water bodies and groundwater of Chennai city and the suburb, South India: Occurrence, removal efficiencies, and risk assessment," *Science of The Total Environment*, vol. 851, p. 158195, Dec. 2022, doi: 10.1016/j.scitotenv.2022.158195.

[92]   M. Z. Akbari, Y. Xu, Z. Lu, and L. Peng, "Review of antibiotics treatment by advance oxidation processes," *Environmental Advances*, vol. 5, p. 100111, Oct. 2021, doi: 10.1016/j.envadv.2021.100111.

[93]   Z.-L. Li *et al.*, "Selective stress of antibiotics on microbial denitrification: Inhibitory effects, dynamics of microbial community structure and function," *Journal of Hazardous Materials*, vol. 405, p. 124366, Mar. 2021, doi: 10.1016/j.jhazmat.2020.124366.

[94]   B.-J. Ni *et al.*, "Ferrate effectively removes antibiotic resistance genes from wastewater through combined effect of microbial DNA damage and coagulation," *Water Research*, vol. 185, p. 116273, Oct. 2020, doi: 10.1016/j.watres.2020.116273.

[95] M. Cycoń, A. Mrozik, and Z. Piotrowska-Seget, "Antibiotics in the Soil Environment—Degradation and Their Impact on Microbial Activity and Diversity," *Front. Microbiol.*, vol. 10, p. 338, Mar. 2019, doi: 10.3389/fmicb.2019.00338.

[96] L. Sharma, G. Siedlewicz, and K. Pazdro, "The Toxic Effects of Antibiotics on Freshwater and Marine Photosynthetic Microorganisms: State of the Art," *Plants*, vol. 10, no. 3, p. 591, Mar. 2021, doi: 10.3390/plants10030591.

[97] M. Krupka, A. I. Piotrowicz-Cieślak, and D. J. Michalczyk, "Effects of antibiotics on the photosynthetic apparatus of plants," *Journal of Plant Interactions*, vol. 17, no. 1, pp. 96–104, Dec. 2022, doi: 10.1080/17429145.2021.2014579.

[98] C. Mu and W. Zhu, "Antibiotic effects on gut microbiota, metabolism, and beyond," *Appl Microbiol Biotechnol*, vol. 103, no. 23–24, pp. 9277–9285, Dec. 2019, doi: 10.1007/s00253-019-10165-x.

[99] C. J. L. Murray *et al.*, "Global burden of bacterial antimicrobial resistance in 2019: a systematic analysis," *The Lancet*, vol. 399, no. 10325, pp. 629–655, Feb. 2022, doi: 10.1016/S0140-6736(21)02724-0.

[100] World Bank Group, "By 2050, drug-resistant infections could cause global economic damage on par with 2008 financial crisis." Accessed: Oct. 22, 2024. [Online]. Available: https://www.worldbank.org/en/news/press-release/2016/09/18/by-2050-drug-resistant-infections-could-cause-global-economic-damage-on-par-with-2008-financial-crisis

[101] T. Golkar, M. Zieliński, and A. M. Berghuis, "Look and Outlook on Enzyme-Mediated Macrolide Resistance," *Front. Microbiol.*, vol. 9, p. 1942, Aug. 2018, doi: 10.3389/fmicb.2018.01942.

[102] M. S. Svetlov *et al.*, "Context-specific action of macrolide antibiotics on the eukaryotic ribosome," *Nat Commun*, vol. 12, no. 1, p. 2803, May 2021, doi: 10.1038/s41467-021-23068-1.

[103] L. Zhang, J. He, L. Bai, S. Ruan, T. Yang, and Y. Luo, "Ribosome-targeting antibacterial agents: Advances, challenges, and opportunities," *Medicinal Research Reviews*, vol. 41, no. 4, pp. 1855–1889, Jul. 2021, doi: 10.1002/med.21780.

[104] J. A. Kricker, C. P. Page, F. R. Gardarsson, O. Baldursson, T. Gudjonsson, and M. J. Parnham, "Nonantimicrobial Actions of Macrolides: Overview and Perspectives for Future Development," *Pharmacol Rev*, vol. 73, no. 4, pp. 1404–1433, Oct. 2021, doi: 10.1124/pharmrev.121.000300.

[105] V. De Jesus Gaffney, C. M. M. Almeida, A. Rodrigues, E. Ferreira, M. J. Benoliel, and V. V. Cardoso, "Occurrence of pharmaceuticals in a water supply system and related human health risk assessment," *Water Research*, vol. 72, pp. 199–208, Apr. 2015, doi: 10.1016/j.watres.2014.10.027.

[106] European Commission. Joint Research Centre., *Review of the 1st Watch List under the Water Framework Directive and recommendations for the 2nd Watch List.* LU: Publications Office, 2018. Accessed: Oct. 24, 2024. [Online]. Available: https://data.europa.eu/doi/10.2760/614367

[107] Y. Wu, C. Yang, and T. Tang, "Distribution of erythromycin in aquatic ecosystem: Microcosm study," *Huanjing Kexue Xuebao*, pp. 897–902, Mar. 2015, doi: 10.13671/j.hjkxxb.2014.0833.

[108] D. Vione, J. Feitosa-Felizzola, C. Minero, and S. Chiron, "Phototransformation of selected human-used macrolides in surface water: Kinetics, model predictions and degradation pathways," *Water Research*, vol. 43, no. 7, pp. 1959–1967, Apr. 2009, doi: 10.1016/j.watres.2009.01.027.

[109] S. A. E. M. Ibrahim, H. A. El-Bialy, and O. M. Gomaa, "Biodegradation of COVID19 antibiotic; azithromycin and its impact on soil microbial community in the presence of phenolic waste and with temperature variation," *World J Microbiol Biotechnol*, vol. 39, no. 6, p. 154, Jun. 2023, doi: 10.1007/s11274-023-03591-7.

[110] C. Fyfe, T. H. Grossman, K. Kerstein, and J. Sutcliffe, "Resistance to Macrolide Antibiotics in Public Health Pathogens," *Cold Spring Harb Perspect Med*, vol. 6, no. 10, p. a025395, Oct. 2016, doi: 10.1101/cshperspect.a025395.

[111] B. Bortone, C. Jackson, Y. Hsia, J. Bielicki, N. Magrini, and M. Sharland, "High global consumption of potentially inappropriate fixed dose combination antibiotics: Analysis of data from 75 countries," *PLoS ONE*, vol. 16, no. 1, p. e0241899, Jan. 2021, doi: 10.1371/journal.pone.0241899.

[112] F. Riu *et al.*, "Antibiotics and Carbohydrate-Containing Drugs Targeting Bacterial Cell Envelopes: An Overview," *Pharmaceuticals*, vol. 15, no. 8, p. 942, Jul. 2022, doi: 10.3390/ph15080942.

[113] S. M. Mitchell, J. L. Ullman, A. L. Teel, and R. J. Watts, "pH and temperature effects on the hydrolysis of three β-lactam antibiotics: Ampicillin, cefalotin and cefoxitin," *Science of The Total Environment*, vol. 466–467, pp. 547–555, Jan. 2014, doi: 10.1016/j.scitotenv.2013.06.027.

[114] J. Peris-Vicente *et al.*, "Liquid chromatography, a valuable tool in the determination of antibiotics in biological, food and environmental samples," *Microchemical Journal*, vol. 177, p. 107309, Jun. 2022, doi: 10.1016/j.microc.2022.107309.

[115] J. W. St. Geme and K. A. Rempe, "Haemophilus influenzae," in *Principles and Practice of Pediatric Infectious Diseases*, Elsevier, 2018, pp. 926-931.e3. doi: 10.1016/B978-0-323-40181-4.00172-9.

[116] X. Lai *et al.*, "Ultrasensitive high-performance liquid chromatography determination of tetracycline antibiotics and their 4-epimer derivatives based on dual effect of methanesulfonic acid," *J of Separation Science*, vol. 43, no. 2, pp. 398–405, Jan. 2020, doi: 10.1002/jssc.201900618.

[117] S. Polati, M. Bottaro, P. Frascarolo, F. Gosetti, V. Gianotti, and M. C. Gennaro, "HPLC-UV and HPLC-MSn multiresidue determination of amidosulfuron, azimsulfuron, nicosulfuron, rimsulfuron, thifensulfuron methyl, tribenuron methyl and azoxystrobin in surface waters," *Analytica Chimica Acta*, vol. 579, no. 2, pp. 146–151, Oct. 2006, doi: 10.1016/j.aca.2006.07.034.

[118] A. M. Filho, F. N. Dos Santos, and P. A. D. P. Pereira, "Development, validation and application of a method based on DI-SPME and GC–MS for determination of pesticides of different chemical groups in surface and groundwater samples," *Microchemical Journal*, vol. 96, no. 1, pp. 139–145, Sep. 2010, doi: 10.1016/j.microc.2010.02.018.

[119] T. Gallagher *et al.*, "Liquid Chromatography Mass Spectrometry Detection of Antibiotic Agents in Sputum from Persons with Cystic Fibrosis," *Antimicrob Agents Chemother*, vol. 65, no. 2, pp. e00927-20, Jan. 2021, doi: 10.1128/AAC.00927-20.

[120] V. Licul-Kucera, M. Ladányi, G. Hizsnyik, G. Záray, and V. G. Mihucz, "A filtration optimized on-line SPE–HPLC–MS/MS method for determination of three macrolide antibiotics dissolved and bound to suspended solids in surface water," *Microchemical Journal*, vol. 148, pp. 480–492, Jul. 2019, doi: 10.1016/j.microc.2019.05.015.

[121] S. Junger *et al.*, "Automated LC-MS/MS: Ready for the clinical routine Laboratory?," *Journal of Mass Spectrometry and Advances in the Clinical Lab*, vol. 30, pp. 1–9, Nov. 2023, doi: 10.1016/j.jmsacl.2023.07.001.

[122] ENVCO, "Wastewater Field Analysis." Accessed: Mar. 03, 2025. [Online]. Available: https://envcoglobal.com/catalog/water/wastewater/wastewater-field-analysis/

[123] ENVCO, "Eutech Cyberscan Series." Accessed: Mar. 03, 2025. [Online]. Available: https://envcoglobal.com/catalog/water/water-quality-handhelds/eutech-cyberscan-series/

[124] Libelium, "Water Quality IoT Solutions." Accessed: Mar. 03, 2025. [Online]. Available: https://www.libelium.com/iot-solutions/smart-water/

[125] H. Sohrabi *et al.*, "Recent advances on portable sensing and biosensing assays applied for detection of main chemical and biological pollutant agents in water samples: A critical review," *TrAC Trends in Analytical Chemistry*, vol. 143, p. 116344, Oct. 2021, doi: 10.1016/j.trac.2021.116344.

[126] X. Chen *et al.*, "An innovative hapten and monoclonal antibody-based immunoassay for determining tebuconazole residues in aqueous samples," *Food and Agricultural Immunology*, vol. 30, no. 1, pp. 677–691, Jan. 2019, doi: 10.1080/09540105.2019.1618793.

[127] G. Merola, E. Martini, M. Tomassetti, and L. Campanella, "New immunosensor for β-lactam antibiotics determination in river waste waters," *Sensors and Actuators B: Chemical*, vol. 199, pp. 301–313, Aug. 2014, doi: 10.1016/j.snb.2014.03.083.

[128] J. Cai *et al.*, "Magnetic DNA walker-engineered electrochemical sensor for highly sensitive detection of antibiotics," *Sensors and Actuators B: Chemical*, vol. 393, p. 134215, Oct. 2023, doi: 10.1016/j.snb.2023.134215.

[129] F. F. Talari, A. Bozorg, F. Faridbod, and M. Vossoughi, "A novel sensitive aptamer-based nanosensor using rGQDs and MWCNTs for rapid detection of diazinon pesticide," *Journal of Environmental Chemical Engineering*, vol. 9, no. 1, p. 104878, Feb. 2021, doi: 10.1016/j.jece.2020.104878.

[130] J. Lin *et al.*, "Simultaneous Quantification of Ampicillin and Kanamycin in Water Samples Based on Lateral Flow Aptasensor Strip with an Internal Line," *Molecules*, vol. 26, no. 13, p. 3806, Jun. 2021, doi: 10.3390/molecules26133806.

[131] Y. Luo *et al.*, "Detection methods for antibiotics in wastewater: a review," *Bioprocess Biosyst Eng*, vol. 47, no. 9, pp. 1433–1451, Sep. 2024, doi: 10.1007/s00449-024-03033-0.

[132] F. Mousseau, C. Féraudet Tarisse, S. Simon, T. Gacoin, A. Alexandrou, and C. I. Bouzigues, "Multititration: The New Method for Implementing Ultrasensitive and Quantitative Multiplexed In-Field Immunoassays Despite Cross-Reactivity?," *Anal. Chem.*, vol. 95, no. 36, pp. 13509–13518, Sep. 2023, doi: 10.1021/acs.analchem.3c01846.

[133] Y. Luo, M. Pehrsson, L. Langholm, M. Karsdal, A.-C. Bay-Jensen, and S. Sun, "Lot-to-Lot Variance in Immunoassays—Causes, Consequences, and Solutions," *Diagnostics*, vol. 13, no. 11, p. 1835, May 2023, doi: 10.3390/diagnostics13111835.

[134] V. Kumar and A. Mazumder, "Detection of Chemical Warfare Agents With Chemical Sensors," in *Encyclopedia of Sensors and Biosensors*, Elsevier, 2023, pp. 667–692. doi: 10.1016/B978-0-12-822548-6.00145-X.

[135] X. Chen *et al.*, "Highly Specific Antibiotic Detection on Water-Stable Black Phosphorus Field-Effect Transistors," *ACS Sens.*, vol. 8, no. 2, pp. 858–866, Feb. 2023, doi: 10.1021/acssensors.2c02562.

[136] Y. Zhang *et al.*, "Microfluidic sensors for the detection of emerging contaminants in water: A review," *Science of The Total Environment*, vol. 929, p. 172734, Jun. 2024, doi: 10.1016/j.scitotenv.2024.172734.

[137] A. Kling *et al.*, "Multianalyte Antibiotic Detection on an Electrochemical Microfluidic Platform," *Anal. Chem.*, vol. 88, no. 20, pp. 10036–10043, Oct. 2016, doi: 10.1021/acs.analchem.6b02294.

[138] F. Pena-Pereira *et al.*, "Miniaturized analytical methods for determination of environmental contaminants of emerging concern – A review," *Analytica Chimica Acta*, vol. 1158, p. 238108, May 2021, doi: 10.1016/j.aca.2020.11.040.

[139] G. Wulff, W. Vesper, R. Grobe-Einsler, and A. Sarhan, "Enzyme-analogue built polymers, 4. On the synthesis of polymers containing chiral cavities and their use for the resolution of racemates," *Makromol. Chem.*, vol. 178, no. 10, pp. 2799–2816, Oct. 1977, doi: 10.1002/macp.1977.021781004.

[140] K. Haupt, P. X. Medina Rangel, and B. T. S. Bui, "Molecularly Imprinted Polymers: Antibody Mimics for Bioimaging and Therapy," *Chem. Rev.*, vol. 120, no. 17, pp. 9554–9582, Sep. 2020, doi: 10.1021/acs.chemrev.0c00428.

[141] B. Fresco-Cala, A. D. Batista, and S. Cárdenas, "Molecularly Imprinted Polymer Micro- and Nano-Particles: A Review," *Molecules*, vol. 25, no. 20, p. 4740, Oct. 2020, doi: 10.3390/molecules25204740.

[142] J. W. Lowdon *et al.*, "MIPs for commercial application in low-cost sensors and assays – An overview of the current status quo," *Sensors and Actuators B: Chemical*, vol. 325, p. 128973, Dec. 2020, doi: 10.1016/j.snb.2020.128973.

[143] V. Ayerdurai, M. Cieplak, and W. Kutner, "Molecularly imprinted polymer-based electrochemical sensors for food contaminants determination," *TrAC Trends in Analytical Chemistry*, vol. 158, p. 116830, Jan. 2023, doi: 10.1016/j.trac.2022.116830.

[144] Y. Pan *et al.*, "Chemiluminescence sensors based on molecularly imprinted polymers for the determination of organophosphorus in milk," *Journal of Dairy Science*, vol. 105, no. 4, pp. 3019–3031, Apr. 2022, doi: 10.3168/jds.2021-21213.

[145] A. G. Ayankojo, J. Reut, V. B. C. Nguyen, R. Boroznjak, and V. Syritski, "Advances in Detection of Antibiotic Pollutants in Aqueous Media Using Molecular Imprinting Technique—A Review," *Biosensors*, vol. 12, no. 7, p. 441, Jun. 2022, doi: 10.3390/bios12070441.

[146] S. He *et al.*, "Advances of molecularly imprinted polymers (MIP) and the application in drug delivery," *European Polymer Journal*, vol. 143, p. 110179, Jan. 2021, doi: 10.1016/j.eurpolymj.2020.110179.

[147] A. G. Ayankojo, R. Boroznjak, J. Reut, A. Öpik, and V. Syritski, "Molecularly imprinted polymer based electrochemical sensor for quantitative detection of SARS-CoV-2 spike protein," *Sensors and Actuators B: Chemical*, vol. 353, p. 131160, Feb. 2022, doi: 10.1016/j.snb.2021.131160.

[148] T. Alizadeh and M. Akhoundian, "An ultra-sensitive and highly selective impedimetric sensor for vitamin D measurement based on a novel imprinted polymer synthesized utilizing template-derived functional monomer," *Analytica Chimica Acta*, vol. 1223, p. 340206, Aug. 2022, doi: 10.1016/j.aca.2022.340206.

[149] A. Herrera-Chacón, X. Cetó, and M. Del Valle, "Molecularly imprinted polymers - towards electrochemical sensors and electronic tongues," *Anal Bioanal Chem*, vol. 413, no. 24, pp. 6117–6140, Oct. 2021, doi: 10.1007/s00216-021-03313-8.

[150] X. Wu, "Synthetic Strategies for the Generation of Molecularly Imprinted Polymers," in *Molecularly Imprinted Polymers as Advanced Drug Delivery Systems*, Z. Liu, Y. Huang, and Y. Yang, Eds., Singapore: Springer Singapore, 2021, pp. 27–59. doi: 10.1007/978-981-16-0227-6_2.

[151] E. Yılmaz, B. Garipcan, H. Patra, and L. Uzun, "Molecular Imprinting Applications in Forensic Science," *Sensors*, vol. 17, no. 4, p. 691, Mar. 2017, doi: 10.3390/s17040691.

[152] A. Martín-Esteban, "Molecularly-imprinted polymers as a versatile, highly selective tool in sample preparation," *TrAC Trends in Analytical Chemistry*, vol. 45, pp. 169–181, Apr. 2013, doi: 10.1016/j.trac.2012.09.023.

[153] M. Gao *et al.*, "Recent Advances and Future Trends in the Detection of Contaminants by Molecularly Imprinted Polymers in Food Samples," *Front. Chem.*, vol. 8, p. 616326, Dec. 2020, doi: 10.3389/fchem.2020.616326.

[154] B.-C. Iacob, A. E. Bodoki, L. Oprean, and E. Bodoki, "Metal–Ligand Interactions in Molecular Imprinting," in *Ligand*, C. Saravanan and B. Biswas, Eds., InTech, 2018. doi: 10.5772/intechopen.73407.

[155] L. Wu and Y. Li, "Metal ion-mediated molecular-imprinting polymer for indirect recognition of formate, acetate and propionate," *Analytica Chimica Acta*, vol. 517, no. 1–2, pp. 145–151, Jul. 2004, doi: 10.1016/j.aca.2004.05.015.

[156] X. Shi, S. Song, A. Sun, J. Liu, D. Li, and J. Chen, "Characterisation and application of molecularly imprinted polymers for group-selective recognition of antibiotics in food samples," *Analyst*, vol. 137, no. 14, p. 3381, 2012, doi: 10.1039/c2an35213c.

[157] H. Surikumaran, S. Mohamad, N. Muhamad Sarih, and R. Muggundha Raoov, "β-Cyclodextrin based Molecular Imprinted Solid Phase Extraction for Class Selective Extraction of Priority Phenols in Water Samples," *Separation Science and Technology*, p. 150615133334007, Jun. 2015, doi: 10.1080/01496395.2015.1043016.

[158] E. N. Ndunda and B. Mizaikoff, "Molecularly imprinted polymers for the analysis and removal of polychlorinated aromatic compounds in the environment: a review," *Analyst*, vol. 141, no. 11, pp. 3141–3156, 2016, doi: 10.1039/C6AN00293E.

[159] A. G. Ayankojo, J. Reut, A. Öpik, A. Tretjakov, and V. Syritski, "Enhancing binding properties of imprinted polymers for the detection of small molecules," *Proc. Estonian Acad. Sci.*, vol. 67, no. 2, p. 138, 2018, doi: 10.3176/proc.2018.2.04.

[160] T. Sajini and B. Mathew, "A brief overview of molecularly imprinted polymers: Highlighting computational design, nano and photo-responsive imprinting," *Talanta Open*, vol. 4, p. 100072, Dec. 2021, doi: 10.1016/j.talo.2021.100072.

[161] I. A. Nicholls, B. C. G. Karlsson, G. D. Olsson, and A. M. Rosengren, "Computational Strategies for the Design and Study of Molecularly Imprinted Materials," *Ind. Eng. Chem. Res.*, vol. 52, no. 39, pp. 13900–13909, Oct. 2013, doi: 10.1021/ie3033119.

[162] T. Cowen, K. Karim, and S. Piletsky, "Computational approaches in the design of synthetic receptors – A review," *Analytica Chimica Acta*, vol. 936, pp. 62–74, Sep. 2016, doi: 10.1016/j.aca.2016.07.027.

[163]   R. J. Uzuriaga-Sánchez, S. Khan, A. Wong, G. Picasso, M. I. Pividori, and M. D. P. T. Sotomayor, "Magnetically separable polymer (Mag-MIP) for selective analysis of biotin in food samples," *Food Chemistry*, vol. 190, pp. 460–467, Jan. 2016, doi: 10.1016/j.foodchem.2015.05.129.

[164]   T. Pooventhiran *et al.*, "Detailed spectra, electronic properties, qualitative non-covalent interaction analysis, solvatochromism, docking and molecular dynamics simulations in different solvent atmosphere of cenobamate," *Struct Chem*, vol. 31, no. 6, pp. 2475–2485, Dec. 2020, doi: 10.1007/s11224-020-01607-8.

[165]   Y. Liu, F. Wang, T. Tan, and M. Lei, "Study of the properties of molecularly imprinted polymers by computational and conformational analysis," *Analytica Chimica Acta*, vol. 581, no. 1, pp. 137–146, Jan. 2007, doi: 10.1016/j.aca.2006.08.015.

[166]   K. Vollmayr-Lee, "Introduction to molecular dynamics simulations," *American Journal of Physics*, vol. 88, no. 5, pp. 401–422, May 2020, doi: 10.1119/10.0000654.

[167]   D. Pavel and J. Lagowski, "Computationally designed monomers and polymers for molecular imprinting of theophylline—part II," *Polymer*, vol. 46, no. 18, pp. 7543–7556, Aug. 2005, doi: 10.1016/j.polymer.2005.05.146.

[168]   D. Pavel, J. Lagowski, and C. J. Lepage, "Computationally designed monomers for molecular imprinting of chemical warfare agents – Part V," *Polymer*, vol. 47, no. 25, pp. 8389–8399, Nov. 2006, doi: 10.1016/j.polymer.2006.09.067.

[169]   N. Kumar, S. Saha, and G. N. Sastry, "Towards developing a criterion to characterize non-covalent bonds: a quantum mechanical study," *Phys. Chem. Chem. Phys.*, vol. 23, no. 14, pp. 8478–8488, 2021, doi: 10.1039/D0CP05689H.

[170]   P. Luliński, D. Maciejewska, M. Bamburowicz-Klimkowska, and M. Szutowski, "Dopamine-Imprinted Polymers: Template-Monomer Interactions, Analysis of Template Removal and Application to Solid Phase Extraction," *Molecules*, vol. 12, no. 11, pp. 2434–2449, Nov. 2007, doi: 10.3390/12112434.

[171]   W. Dong, M. Yan, M. Zhang, Z. Liu, and Y. Li, "A computational and experimental investigation of the interaction between the template molecule and the functional monomer used in the molecularly imprinted polymer," *Analytica Chimica Acta*, vol. 542, no. 2, pp. 186–192, Jun. 2005, doi: 10.1016/j.aca.2005.03.032.

[172]   P. S. Sharma, A. Pietrzyk-Le, F. D'Souza, and W. Kutner, "Electrochemically synthesized polymers in molecular imprinting for chemical sensing," *Anal Bioanal Chem*, vol. 402, no. 10, pp. 3177–3204, Apr. 2012, doi: 10.1007/s00216-011-5696-6.

[173]   M. C. Blanco-López, S. Gutiérrez-Fernández, M. J. Lobo-Castañón, A. J. Miranda-Ordieres & P. Tuñón-Blanco, "Electrochemical sensing with electrodes modified with molecularly imprinted polymer films," *Analytical and Bioanalytical Chemistry*, vol. 378, no. 8, pp. 1922–1928, Apr. 2004, doi: 10.1007/s00216-003-2330-2.

[174]   D. Zane, A. Raffaele, A. Curulli, G. B. Appetecchi, and S. Passerini, "Electrosynthesis of poly(o-phenylenediamine) in a room temperature ionic liquid," *Electrochemistry Communications*, vol. 9, no. 8, pp. 2037–2040, Aug. 2007, doi: 10.1016/j.elecom.2007.06.002.

[175]   G. Fomo, T. Waryo, U. Feleni, P. Baker, and E. Iwuoha, "Electrochemical Polymerization," in *Functional Polymers*, M. A. Jafar Mazumder, H. Sheardown, and A. Al-Ahmed, Eds., in Polymers and Polymeric Composites: A Reference Series. , Cham: Springer International Publishing, 2019, pp. 105–131. doi: 10.1007/978-3-319-95987-0_3.

[176] G. Appel, D. Schmeißer, J. Bauer, M. Bauer, H. J. Egelhaaf, and D. Oelkrug, "The formation of oligomers in the electrolyte upon polymerization of pyrrole," *Synthetic Metals*, vol. 99, no. 1, pp. 69–77, Jan. 1999, doi: 10.1016/S0379-6779(98)00200-8.

[177] R. D. Crapnell *et al.*, "Recent Advances in Electrosynthesized Molecularly Imprinted Polymer Sensing Platforms for Bioanalyte Detection," *Sensors*, vol. 19, no. 5, p. 1204, Mar. 2019, doi: 10.3390/s19051204.

[178] A. Pietrzyk, S. Suriyanarayanan, W. Kutner, R. Chitta, and F. D'Souza, "Selective Histamine Piezoelectric Chemosensor Using a Recognition Film of the Molecularly Imprinted Polymer of Bis(bithiophene) Derivatives," *Anal. Chem.*, vol. 81, no. 7, pp. 2633–2643, Apr. 2009, doi: 10.1021/ac8025652.

[179] A. Pietrzyk, S. Suriyanarayanan, W. Kutner, R. Chitta, M. E. Zandler, and F. D'Souza, "Molecularly imprinted polymer (MIP) based piezoelectric microgravimetry chemosensor for selective determination of adenine," *Biosensors and Bioelectronics*, vol. 25, no. 11, pp. 2522–2529, Jul. 2010, doi: 10.1016/j.bios.2010.04.015.

[180] P. Zahedi, M. Ziaee, M. Abdouss, A. Farazin, and B. Mizaikoff, "Biomacromolecule template-based molecularly imprinted polymers with an emphasis on their synthesis strategies: a review: Biomacromolecule Template-Based MIP," *Polym. Adv. Technol.*, vol. 27, no. 9, pp. 1124–1142, Sep. 2016, doi: 10.1002/pat.3754.

[181] M. D. L. Gonçalves, L. A. N. Truta, M. G. F. Sales, and F. T. C. Moreira, "Electrochemical Point-of Care (PoC) Determination of Interleukin-6 (IL-6) Using a Pyrrole (Py) Molecularly Imprinted Polymer (MIP) on a Carbon-Screen Printed Electrode (C-SPE)," *Analytical Letters*, vol. 54, no. 16, pp. 2611–2623, Nov. 2021, doi: 10.1080/00032719.2021.1879108.

[182] T.-X. Chu, V.-P. Vu, H.-T. Tran, T.-L. Tran, Q.-T. Tran, and T. Le Manh, "Molecularly Imprinted Polyaniline Nanowire-Based Electrochemical Biosensor for Chloramphenicol Detection: A Kinetic Study of Aniline Electropolymerization," *J. Electrochem. Soc.*, vol. 167, no. 2, p. 027527, Jan. 2020, doi: 10.1149/1945-7111/ab6a7e.

[183] Y. Pan *et al.*, "Developing a generally applicable electrochemical sensor for detecting macrolides in water with thiophene-based molecularly imprinted polymers," *Water Research*, vol. 205, p. 117670, Oct. 2021, doi: 10.1016/j.watres.2021.117670.

[184] B. Qader, M. Baron, I. Hussain, J. M. Sevilla, R. P. Johnson, and J. Gonzalez-Rodriguez, "Electrochemical determination of disulfoton using a molecularly imprinted poly-phenol polymer," *Electrochimica Acta*, vol. 295, pp. 333–339, Feb. 2019, doi: 10.1016/j.electacta.2018.10.127.

[185] A. Radi and M. Ragaa Abd-Ellatief, "Molecularly Imprinted Poly-o-phenylenediamine Electrochemical Sensor for Entacapone," *Electroanalysis*, vol. 33, no. 6, pp. 1578–1584, Jun. 2021, doi: 10.1002/elan.202100022.

[186] G. Kaniraja *et al.*, "Molecularly imprinted (3, 4-ethylenedioxythiophene) polymer based electrochemical non-enzymatic glucose sensor," *Organic Electronics*, vol. 138, p. 107181, Mar. 2025, doi: 10.1016/j.orgel.2024.107181.

[187] M. Karthikeyan, M. Dhinesh Kumar, G. Kaniraja, P. Ananthappan, V. Sivasamy Vasantha, and C. Karunakaran, "Gold nanoparticles enhanced molecularly imprinted poly(3-aminophenylboronic acid) sensor for myo-inositol detection," *Microchemical Journal*, vol. 189, p. 108536, Jun. 2023, doi: 10.1016/j.microc.2023.108536.

[188] Q. Wang *et al.*, "Recent advances in electrochemical sensors for antibiotics and their applications," *Chinese Chemical Letters*, vol. 32, no. 2, pp. 609–619, Feb. 2021, doi: 10.1016/j.cclet.2020.10.025.

[189] S. Rahman *et al.*, "Molecularly imprinted polymers (MIPs) combined with nanomaterials as electrochemical sensing applications for environmental pollutants," *Trends in Environmental Analytical Chemistry*, vol. 36, p. e00176, Dec. 2022, doi: 10.1016/j.teac.2022.e00176.

[190] P. S. Sharma, A. Garcia-Cruz, M. Cieplak, K. R. Noworyta, and W. Kutner, "'Gate effect' in molecularly imprinted polymers: the current state of understanding," *Current Opinion in Electrochemistry*, vol. 16, pp. 50–56, Aug. 2019, doi: 10.1016/j.coelec.2019.04.020.

[191] F. W. Scheller, X. Zhang, A. Yarman, U. Wollenberger, and R. E. Gyurcsányi, "Molecularly imprinted polymer-based electrochemical sensors for biopolymers," *Current Opinion in Electrochemistry*, vol. 14, pp. 53–59, Apr. 2019, doi: 10.1016/j.coelec.2018.12.005.

[192] D. Elfadil, A. Lamaoui, F. Della Pelle, A. Amine, and D. Compagnone, "Molecularly Imprinted Polymers Combined with Electrochemical Sensors for Food Contaminants Analysis," *Molecules*, vol. 26, no. 15, p. 4607, Jul. 2021, doi: 10.3390/molecules26154607.

[193] M. Pesavento, D. Merli, R. Biesuz, G. Alberti, S. Marchetti, and C. Milanese, "A MIP-based low-cost electrochemical sensor for 2-furaldehyde detection in beverages," *Analytica Chimica Acta*, vol. 1142, pp. 201–210, Jan. 2021, doi: 10.1016/j.aca.2020.10.059.

[194] Y. Yang *et al.*, "Magnetic molecularly imprinted electrochemical sensors: A review," *Analytica Chimica Acta*, vol. 1106, pp. 1–21, Apr. 2020, doi: 10.1016/j.aca.2020.01.044.

[195] S. Motia, B. Bouchikhi, and N. El Bari, "An electrochemical molecularly imprinted sensor based on chitosan capped with gold nanoparticles and its application for highly sensitive butylated hydroxyanisole analysis in foodstuff products," *Talanta*, vol. 223, p. 121689, Feb. 2021, doi: 10.1016/j.talanta.2020.121689.

[196] A. Kumar, P. K. Pathak, and B. B. Prasad, "Electrocatalytic Imprinted Polymer of N-Doped Hollow Carbon Nanosphere–Palladium Nanocomposite for Ultratrace Detection of Anticancer Drug 6-Mercaptopurine," *ACS Appl. Mater. Interfaces*, vol. 11, no. 17, pp. 16065–16074, May 2019, doi: 10.1021/acsami.9b02947.

[197] O. T. Vu *et al.*, "Highly Sensitive Molecularly Imprinted Polymer-Based Electrochemical Sensors Enhanced by Gold Nanoparticles for Norfloxacin Detection in Aquaculture Water," *ACS Omega*, vol. 8, no. 3, pp. 2887–2896, Jan. 2023, doi: 10.1021/acsomega.2c04414.

[198] S. Motia, I. A. Tudor, P. A. Ribeiro, M. Raposo, B. Bouchikhi, and N. El Bari, "Electrochemical sensor based on molecularly imprinted polymer for sensitive triclosan detection in wastewater and mineral water," *Science of The Total Environment*, vol. 664, pp. 647–658, May 2019, doi: 10.1016/j.scitotenv.2019.01.331.

[199] B. Feier, A. Blidar, A. Pusta, P. Carciuc, and C. Cristea, "Electrochemical Sensor Based on Molecularly Imprinted Polymer for the Detection of Cefalexin," *Biosensors*, vol. 9, no. 1, p. 31, Feb. 2019, doi: 10.3390/bios9010031.

[200] L. Wang, M. Pagett, and W. Zhang, "Molecularly imprinted polymer (MIP) based electrochemical sensors and their recent advances in health applications," *Sensors and Actuators Reports*, vol. 5, p. 100153, Jun. 2023, doi: 10.1016/j.snr.2023.100153.

[201] D. Wang *et al.*, "Selective detection of enrofloxacin in biological and environmental samples using a molecularly imprinted electrochemiluminescence sensor based on functionalized copper nanoclusters," *Talanta*, vol. 236, p. 122835, Jan. 2022, doi: 10.1016/j.talanta.2021.122835.

[202] A. Ghorbani, R. Ojani, M. R. Ganjali, and J. Raoof, "Direct voltammetric determination of carbendazim by utilizing a nanosized imprinted polymer/MWCNTs-modified electrode," *J IRAN CHEM SOC*, vol. 18, no. 11, pp. 3109–3118, Nov. 2021, doi: 10.1007/s13738-021-02255-3.

[203] H. Khosropour, M. Saboohi, M. Keramat, B. Rezaei, and A. A. Ensafi, "Electrochemical molecularly imprinted polymer sensor for ultrasensitive indoxacarb detection by tin disulfide quantum dots/carbon nitride/multiwalled carbon nanotubes as a nanocomposite," *Sensors and Actuators B: Chemical*, vol. 385, p. 133652, Jun. 2023, doi: 10.1016/j.snb.2023.133652.

[204] E. T. Rodrigues, M. Â. Pardal, C. Gante, J. Loureiro, and I. Lopes, "Determination and validation of an aquatic Maximum Acceptable Concentration-Environmental Quality Standard (MAC-EQS) value for the agricultural fungicide azoxystrobin," *Environmental Pollution*, vol. 221, pp. 150–158, Feb. 2017, doi: 10.1016/j.envpol.2016.11.058.

[205] A. G. Ayankojo, J. Reut, V. Ciocan, A. Öpik, and V. Syritski, "Molecularly imprinted polymer-based sensor for electrochemical detection of erythromycin," *Talanta*, vol. 209, p. 120502, Mar. 2020, doi: 10.1016/j.talanta.2019.120502.

[206] Yu. A. Yarkaeva, M. I. Nazyrov, D. A. Dymova, and V. N. Maistrenko, "A Voltammetric Sensor Based on a Chitosan, Graphitized Carbon Black, and Molecularly Imprinted Polyarylene Phthalide Composite for Clarithromycin Detection," *J Anal Chem*, vol. 79, no. 6, pp. 680–689, Jun. 2024, doi: 10.1134/S1061934824700059.

[207] X. Shi, X. Ren, N. Jing, and J. Zhang, "Electrochemical Determination of Ampicillin Based on an Electropolymerized Poly(o-Phenylenediamine)/Gold Nanoparticle/Single-Walled Carbon Nanotube Modified Glassy Carbon Electrode," *Analytical Letters*, vol. 53, no. 18, pp. 2854–2867, Dec. 2020, doi: 10.1080/00032719.2020.1759619.

[208] Y. Sun *et al.*, "ZrO$_2$ Nanofiber-Based Molecular Imprinted Electrochemical Sensor for Detection of Ampicillin," *J. Electrochem. Soc.*, vol. 171, no. 9, p. 096507, Sep. 2024, doi: 10.1149/1945-7111/ad7764.

[209] Z. Liu *et al.*, "Electrochemical assay of ampicillin using Fe3N-Co2N nanoarray coated with molecularly imprinted polymer," *Microchim Acta*, vol. 187, no. 8, p. 442, Aug. 2020, doi: 10.1007/s00604-020-04432-2.

[210] T. Tao, X. Wei, Z. Ye, B. Zong, Q. Li, and S. Mao, "Dual Recognition Strategy-Based Transistor Sensor Array for Ultrasensitive and Multi-Target Detection of Antibiotics," *Adv Funct Materials*, p. 2413485, Oct. 2024, doi: 10.1002/adfm.202413485.

[211] K. Hinrichs and K.-J. Eichhorn, Eds., *Ellipsometry of Functional Organic Surfaces and Films*, vol. 52. in Springer Series in Surface Sciences, vol. 52. Berlin, Heidelberg: Springer Berlin Heidelberg, 2014. doi: 10.1007/978-3-642-40128-2.

[212] A. Röseler and E. Korte, "Infrared Spectroscopic Ellipsometry," in *Handbook of Vibrational Spectroscopy*, 1st ed., J. M. Chalmers and P. R. Griffiths, Eds., Wiley, 2001. doi: 10.1002/0470027320.s2208.

[213] J. P.S. and D. S. Sutrave, "A Brief Study of Cyclic Voltammetry and Electrochemical Analysis," *IJCTR*, vol. 11, no. 9, pp. 77–88, 2018, doi: 10.20902/IJCTR.2018.110911.

[214] N. Elgrishi, K. J. Rountree, B. D. McCarthy, E. S. Rountree, T. T. Eisenhart, and J. L. Dempsey, "A Practical Beginner's Guide to Cyclic Voltammetry," *J. Chem. Educ.*, vol. 95, no. 2, pp. 197–206, Feb. 2018, doi: 10.1021/acs.jchemed.7b00361.

[215] E. P. Randviir and C. E. Banks, "Electrochemical impedance spectroscopy: an overview of bioanalytical applications," *Anal. Methods*, vol. 5, no. 5, p. 1098, 2013, doi: 10.1039/c3ay26476a.

[216] M. Ates, "Review study of electrochemical impedance spectroscopy and equivalent electrical circuits of conducting polymers on carbon surfaces," *Progress in Organic Coatings*, vol. 71, no. 1, pp. 1–10, May 2011, doi: 10.1016/j.porgcoat.2010.12.011.

[217] C. Baggiani, C. Giovannoli, L. Anfossi, C. Passini, P. Baravalle, and G. Giraudi, "A Connection between the Binding Properties of Imprinted and Nonimprinted Polymers: A Change of Perspective in Molecular Imprinting," *J. Am. Chem. Soc.*, vol. 134, no. 3, pp. 1513–1518, Jan. 2012, doi: 10.1021/ja205632t.

[218] C. Xiang, Q. Xie, J. Hu, and S. Yao, "Studies on electrochemical copolymerization of aniline with o-phenylenediamine and degradation of the resultant copolymers via electrochemical quartz crystal microbalance and scanning electrochemical microscope," *Synthetic Metals*, vol. 156, no. 5–6, pp. 444–453, Mar. 2006, doi: 10.1016/j.synthmet.2006.01.010.

[219] L. Chao *et al.*, "Short polyaniline nanorod prepared in the presence of *para* - phenylenediamine," *J of Applied Polymer Sci*, vol. 127, no. 3, pp. 1853–1862, Feb. 2013, doi: 10.1002/app.37920.

[220] J. Stejskal, "Polymers of phenylenediamines," *Progress in Polymer Science*, vol. 41, pp. 1–31, Feb. 2015, doi: 10.1016/j.progpolymsci.2014.10.007.

[221] R. Mazeikiene and A. Malinauskas, "Electrochemical copolymerization of aniline with m-phenylenediamine," *Synthetic Metals*, vol. 92, no. 3, pp. 259–263, Feb. 1998, doi: 10.1016/S0379-6779(98)80094-5.

[222] R. Mažeikienė, G. Niaura, and A. Malinauskas, "A comparative Raman spectroelectrochemical study of selected polyaniline derivatives in a pH-neutral solution," *Synthetic Metals*, vol. 160, no. 9–10, pp. 1060–1064, May 2010, doi: 10.1016/j.synthmet.2010.02.027.

[223] Q. Zhao *et al.*, "Dual functional monomer surface molecularly imprinted microspheres for polysaccharide recognition in aqueous solution," *Anal. Methods*, vol. 11, no. 21, pp. 2800–2808, 2019, doi: 10.1039/C9AY00132H.

[224] J. P. Sęk *et al.*, "Boronate-appended polymers with diol-functionalized ferrocene: an effective and selective method for voltammetric glucose sensing," *Dalton Trans.*, vol. 50, no. 3, pp. 880–889, 2021, doi: 10.1039/D0DT03776A.

[225] G. T. Williams, J. L. Kedge, and J. S. Fossey, "Molecular Boronic Acid-Based Saccharide Sensors," *ACS Sens.*, vol. 6, no. 4, pp. 1508–1528, Apr. 2021, doi: 10.1021/acssensors.1c00462.

[226] I.-A. Stoian *et al.*, "Biomimetic electrochemical sensor for the highly selective detection of azithromycin in biological samples," *Biosensors and Bioelectronics*, vol. 155, p. 112098, May 2020, doi: 10.1016/j.bios.2020.112098.

[227] Y. Chen *et al.*, "Ultralight aerogel based on molecular-modified poly(*m* -phenylenediamine) crosslinking with polyvinyl alcohol/graphene oxide for flow adsorption," *RSC Adv.*, vol. 9, no. 40, pp. 22950–22956, 2019, doi: 10.1039/C9RA04207E.

[228] A. K. M. Lutfor Rahman, "Study of the seasonal variations in Turag river water quality parameters," *Afr. J. Pure. Appl. Chem.*, vol. 6, no. 10, May 2012, doi: 10.5897/AJPAC12.023.

[229] A. D. C. MacColl, A. E. Nagar, and J. De Roij, "The evolutionary ecology of dwarfism in three-spined sticklebacks," *Journal of Animal Ecology*, vol. 82, no. 3, pp. 642–652, May 2013, doi: 10.1111/1365-2656.12028.

[230] A. G. Ayankojo, J. Reut, R. Boroznjak, A. Öpik, and V. Syritski, "Molecularly imprinted poly(meta-phenylenediamine) based QCM sensor for detecting Amoxicillin," *Sensors and Actuators B: Chemical*, vol. 258, pp. 766–774, Apr. 2018, doi: 10.1016/j.snb.2017.11.194.

[231] R. J. Umpleby, S. C. Baxter, Y. Chen, R. N. Shah, and K. D. Shimizu, "Characterization of Molecularly Imprinted Polymers with the Langmuir–Freundlich Isotherm," *Anal. Chem.*, vol. 73, no. 19, pp. 4584–4591, Oct. 2001, doi: 10.1021/ac0105686.

[232] A. Y. W. Lee, S. F. Lim, S. N. D. Chua, K. Sanaullah, R. Baini, and M. O. Abdullah, "Adsorption Equilibrium for Heavy Metal Divalent Ions (Cu^{2+} , Zn^{2+} , and Cd^{2+}) into Zirconium-Based Ferromagnetic Sorbent," *Advances in Materials Science and Engineering*, vol. 2017, pp. 1–13, 2017, doi: 10.1155/2017/1210673.

[233] M. G. Plaza, I. Durán, N. Querejeta, F. Rubiera, and C. Pevida, "Experimental and Simulation Study of Adsorption in Postcombustion Conditions Using a Microporous Biochar. 1. CO_2 and N_2 Adsorption," *Ind. Eng. Chem. Res.*, vol. 55, no. 11, pp. 3097–3112, Mar. 2016, doi: 10.1021/acs.iecr.5b04856.

[234] A. G. Ayankojo, J. Reut, A. Öpik, and V. Syritski, "Sulfamethizole-imprinted polymer on screen-printed electrodes: Towards the design of a portable environmental sensor," *Sensors and Actuators B: Chemical*, vol. 320, p. 128600, Oct. 2020, doi: 10.1016/j.snb.2020.128600.

[235] E. Sari, R. Üzek, M. Duman, and A. Denizli, "Fabrication of surface plasmon resonance nanosensor for the selective determination of erythromycin via molecular imprinted nanoparticles," *Talanta*, vol. 150, pp. 607–614, Apr. 2016, doi: 10.1016/j.talanta.2015.12.043.

[236] M. Okan and M. Duman, "Functional polymeric nanoparticle decorated microcantilever sensor for specific detection of erythromycin," *Sensors and Actuators B: Chemical*, vol. 256, pp. 325–333, Mar. 2018, doi: 10.1016/j.snb.2017.10.098.

[237] P. Rebelo, J. G. Pacheco, M. N. D. S. Cordeiro, A. Melo, and C. Delerue-Matos, "Azithromycin electrochemical detection using a molecularly imprinted polymer prepared on a disposable screen-printed electrode," *Anal. Methods*, vol. 12, no. 11, pp. 1486–1494, 2020, doi: 10.1039/C9AY02566A.

[238]   R. Cidu, F. Frau, and P. Tore, "Drinking water quality: Comparing inorganic components in bottled water and Italian tap water," *Journal of Food Composition and Analysis*, vol. 24, no. 2, pp. 184–193, Mar. 2011, doi: 10.1016/j.jfca.2010.08.005.

[239]   H. Zhang *et al.*, "Combined effects of seasonality and stagnation on tap water quality: Changes in chemical parameters, metabolic activity and co-existence in bacterial community," *Journal of Hazardous Materials*, vol. 403, p. 124018, Feb. 2021, doi: 10.1016/j.jhazmat.2020.124018.

[240]   C. Malitesta, E. Mazzotta, R. A. Picca, A. Poma, I. Chianella, and S. A. Piletsky, "MIP sensors – the electrochemical approach," *Anal Bioanal Chem*, vol. 402, no. 5, pp. 1827–1846, Feb. 2012, doi: 10.1007/s00216-011-5405-5.

[241]   G. Dutta, F. C. B. Fernandes, P. Estrela, D. Moschou, and P. R. Bueno, "Impact of surface roughness on the self-assembling of molecular films onto gold electrodes for label-free biosensing applications," *Electrochimica Acta*, vol. 378, p. 138137, May 2021, doi: 10.1016/j.electacta.2021.138137.

[242]   A. C. Faleye, A. A. Adegoke, K. Ramluckan, F. Bux, and T. A. Stenström, "Antibiotic Residue in the Aquatic Environment: Status in Africa," *Open Chemistry*, vol. 16, no. 1, pp. 890–903, Sep. 2018, doi: 10.1515/chem-2018-0099.

Acknowledgements

Summary

Molecularly Imprinted Polymer-modified Electrodes for Electrochemical Sensing of Emerging Aqueous Pollutants

Environmental pollutants released into the environment from healthcare and agricultural activities have exaggerated the situation of pollution and posed a significant threat to both public health and the balance of ecosystems. The spread of fungicides and antibiotics in water bodies causes toxicity and promotes the development of antibiotic-resistant bacterial strains, which affect human health by posing significant challenges to disease treatment. Therefore, the detection of these compounds in environmental water is crucial for safeguarding aquatic and human life.

For decades, conventional techniques such as high-performance liquid chromatography and mass spectrometry have been utilized to quantify such pollutants. However, they are usually associated with high cost, complex systems, or required skillful operators that are not suitable for routine pollutants monitoring. Even though biosensors and chemical sensors are developed for in-field environmental monitoring applications, they often accompanied by unstable natural receptors or limited selectivity, which can be improved using synthetic recognition elements.

Recent research thus has been focused on artificial molecular recognition material called molecularly imprinted polymer (MIP). MIPs are stable crosslinked polymer matrices containing engraved molecular recognition sites specific to the target analytes, which act as a synthetic recognition element when paired with electrochemical transducers, providing a portable sensors platform for accurate and rapid analysis. However, their practical implementation remains limited due to challenges in ensuring reliable performance when measuring real-world environmental samples. For instance, the design of MIP-based electrochemical sensing platform to detect AZO in complex water samples has not been previously reported. Additionally, the possibility of class-selective detection can further advantage the environmental monitoring since pollutants usually exist together in water samples. Furthermore, the performance of MIP-based electrochemical sensors usually replies to external redox probes which retain design complexity and potential interference with electroactive species. Hence, the development of an alternative strategy that enables direct signal generation while minimizing interference and simplifying sensor design would be highly beneficial.

This thesis aims to develop MIP-based electrochemical sensors for fast and reliable detection of both individual targets such as AZO and AMP, and broader pollutant classes such as the ML class of antibiotics.

To trace fungicide AZO amounts in water, the AZO-selective MIP was synthesized on a gold electrode to generate AZO-MIP based electrochemical sensor (AZO sensor). Aniline and m-phenylenediamine (mPD) were used as functional monomers, providing stronger binding energy to the AZO, as demonstrated by quantum chemical modeling results estimating the complex's energy.

ML antibiotic members, including erythromycin (ERY), clarithromycin, and azithromycin are commonly found in aqueous ecosystems according to EU surface water watch list of emerging pollutants. To detect them, class-selective MIP film was electrochemically deposited on the surface of gold electrode to form ML-MIP based electrochemical sensor (ML sensor). The MIP film was prepared by electrochemical polymerization of 3-aminophenylboronic acid (APBA) and mPD as dual-functional monomers in the presence of ERY as a template. By employing the reversible covalent interactions

between diols of macrolide and boronic acids of APBA as well as the noncovalent interactions between macrolide and mPD, a dual recognition involving the central macrocyclic lactone exclusive to all macrolides was successfully achieved, thus permitting the possible broad recognition of individual members of the class.

To overcome limitations associated with external redox probes, a single ruthenium oxide (RuO_2) electrode can serve a dual purpose—an electrochemical transducer and an internal redox probe—allowing direct signal measurement and eliminating the need for external probe solutions. Thus, poly(mPD) was deposited in the presence of AMP on a RuO_2 electrode to fabricate an AMP sensor for direct detection of AMP in pond water.

All the designed sensors in this thesis are characterized by electrochemical measurements, AZO and ML sensors were additionally characterized by ellipsometry method. Following optimizations of the pre-polymerization composition, polymerization parameters, and rebinding conditions, low limit of detections were achieved for AZO (3.6 nM), ML (1.1-1.7 nM), and AMP sensor (6.0 nM), demonstrated their capabilities to detect relevant concentration. Moreover, all sensors exhibited satisfactory selectivity and good recoveries (93-119%) for target analytes in tap or pond water samples, indicated their practical application in complex aqueous media. The presented approaches of preparing MIP-based electrochemical sensors hereby demonstrated their potential for selective and direct detection of fungicide and antibiotic contaminants in water at nM levels in which they naturally exist. The developed protocols offer a promising foundation for the reliable and effective design of portable analytical devices, suitable for routine in-field monitoring of emerging evironmental pollutants in aqueous media.

Lühikokkuvõte

Molekulaarselt jäljendatud polümeeriga modifitseeritud elektroodid esilekerkivate veesaasteainete elektrokeemiliseks tuvastamiseks

Tervishoiu- ja põllumajandustegevusest pärinevad keskkonnasaasteained on süvendanud keskkonnareostuse ulatust ning kujutavad tõsist ohtu nii rahvatervisele kui ka ökosüsteemide tasakaalule. Fungitsiidide ja antibiootikumide levik veekeskkonnas põhjustab toksilisi mõjusid veeökosüsteemidele ning antibiootikumide puhul soodustab ka resistentsust põhjustavate geenide levikut, mis mõjutab inimtervist, raskendades nakkushaiguste ravi. Seetõttu on nende ühendite usaldusväärne ja täpne tuvastamine keskkonnavees ülioluline nii veeökosüsteemide säilitamiseks kui ka rahvatervise kaitseks. Traditsiooniliselt on saasteainete kvantitatiivseks määramiseks kasutatud klassikalisi analüüsimeetodeid, nagu vedelikkromatograafia ja massispektromeetria. Kuigi need meetodid on väga täpsed ja tundlikud, kaasnevad nende rakendamisega märkimisväärsed kulud, keerukas seadmestik ning vajadus kõrge kvalifikatsiooniga personali järele, mis piirab nende sobivust rutiinseks keskkonnaseireks. Viimastel aastatel on keskkonnaseiresse integreeritud ka keemilisi ja bioloogilisi sensoreid, kuid nende laiemat kasutust takistavad sageli bioloogiliste retseptorite ebastabiilsus ja selektiivsuse puudulikkus. Neid kitsaskohti aitavad ületada sünteetilise tundliku elemendiga sensorid, mis pakuvad alternatiivina paremat stabiilsust ja sihtmärgipõhist tuvastust.

Viimaste aastate teadusuuringud on keskendunud tehislikele molekulaarse äratundmise materjalidele, eeskätt molekulaarselt jäljendatud polümeeridele (MIP, *molecularly imprinted polymers*). MIP-id on keemiliselt ja mehhaaniliselt stabiilsed võrkstruktuuriga polümeerid, mis sisaldavad sihtmolekulidele spetsiifilisi äratundmiskohti, nn "mälupesi". Need toimivad sünteetiliste retseptoritena, jäljendades bioloogiliste retseptorite selektiivsust. Integreerituna elektrokeemiliste muunduritega võimaldavad MIP-d luua miniatuurseid, kaasaskantavaid ja kuluefektiivseid sensorplatvorme kiireks ja täpseks analüüsiks. Kuigi MIP-põhiseid elektrokeemilisi andureid on ulatuslikult uuritud, on nende praktiline rakendamine saasteainete tuvastamiseks veekeskkonnas seni piiratud. Peamiseks takistuseks on raskused tagada mõõtmiste reprodutseeritavus ja tundlikkus keerukates reaalsetes proovides. Lisaks, puudub kirjanduses seni MIP-põhise elektrokeemilise sensorplatvormi väljatöötamine fungitsiidi asoksüstrobiini (AZO) tuvastamiseks. Samuti võib ühendiklassile selektiivne tuvastusvõime osutuda eriti kasulikuks keskkonnaseires, arvestades, et saasteained esinevad veeproovides sageli segudena. Enamasti viiakse MIP-põhiste elektrokeemiliste sensorite signaali mõõtmine läbi välise redoksindikaatori, näiteks heksatsüanoferriidi, juuresolekul. Sellisel juhul sõltub redoksreaktsioonist tingitud voolutugevus sellest, kui efektiivne on elektrilaengu ülekanne elektroodi ja lahuse piirpinnal. Sihtmolekulide seostumine MIP-iga avaldub tavaliselt voolutugevuse vähenemisena. Antud lähenemine lisab aga mõõtmisprotseduurile keerukust, võib põhjustada häiringuid elektroaktiivsete komponentide olemasolul ning annab ainult kaudse signaali, mis peegeldab mitte üksnes sihtmolekuli sidumist polümeeriga, vaid ka võimalikke muutusi polümeeri struktuuris interaktsiooni käigus. Seetõttu on oluline töötada välja alternatiivne lahendus, näiteks redoksindikaatori integreerimine elektroodimaterjali, et võimaldada otsest signaalimõõtmist, vähendada häiringuid ja lihtsustada mõõtmisprotseduuri.

Käesoleva doktoritöö eesmärk oli välja töötada MIP-põhised elektrokeemilised sensorid, mis võimaldavad kiirelt ja usaldusväärselt tuvastada nii individuaalseid

saasteaineid – nagu asoksüstrobiin (AZO) ja ampitsilliin (AMP) – kui ka laiemat saasteainete klassi, näiteks antibiootikumide makroliidide (ML) klassi.

Esmakordselt töötati välja AZO suhtes selektiivne MIP-põhine elektrokeemiline sensor (AZO-sensor), mis täidab olulise teadusliku ja praktilise lünga fungitsiidide tuvastamise valdkonnas. Funktsionaalsete monomeeridena kasutati aniliini (ANI) ja m-fenüleendiamiini (mPD), mis tagasid AZO molekulile parema sidumisenergia, nagu näitasid kvantkeemilise modelleerimise tulemused kompleksi energia hindamiseks.

Vastavalt ELi pinnavee jälgimisnimekirjale esilekerkivatest saateainestest esinevad makroliidid, sealhulgas erütromütsiin (ERY), klaritromütsiin (CLA) ja asitromütsiin (AZI), tavaliselt veekeskkondades. Selles töös töötati nende tuvastamiseks välja makroliidide klassile selektiivne MIP -põhine elektrokeemiline sensor (ML-sensor). MIP-kile valmistati kahe funktsionaalse monomeeri 3-aminofenüülboroonhappe (APBA) ja m-fenüleendiamiini (mPD) elektrokeemilise polümerisatsiooni teel ERY juuresolekul. Makroliididele ühise struktuurielemendi – makrotsüklilise laktooni – molekulaarne seondumiskoht moodustus polümeeris poolkovalentse (*semi-covalent*) jäljendamise meetodil, mis põhines pöörduvatel kovalentsetel interaktsioonidel makroliidi *cis*-dioolrühmade ja APBA boroonhapperühmade vahel ning mittekovalentsetel interaktsioonidel (peamiselt vesiniksidemed) ERY ja mPD vahel.

Välise redoksindikaatori kasutamise vajaduse kõrvaldamiseks töötati välja AMP-sensor, kus MIP polümeerikiht sünteesiti RuO_2 elektroodile, mis täitis samaaegselt redoksindikaatori ja elektrokeemilise muunduri rolli. Selline lähenemine välistas vajaduse täiendavate mõõtmisetappide järele ning võimaldas AMP otsest ja selektiivset tuvastamist tiigivees.

Kõiki selle doktoritöö raames välja töötatud sensoreid iseloomustati elektrokeemiliste mõõtmiste abil, nagu tsükliline voltammeetria (CVA) diferentsiaalne impulss voltammeetria (DPV), elektrokeemiline impedantsspektroskoopia (EIS). AZO- ja ML-sensoreid täiendavalt iseloomustati ka ellipsomeetrilise spektroskoopia (IRSE) meetodiga. Pärast polümerisatsiooni tingimuste ja analüüdi taassidumise parameetrite optimeerimist saavutati järgmised avastamispiirid: AZO-sensori puhul 3,6 nM, ML-sensori puhul 1,1–1,7 nM ning AMP-sensori puhul 6,0 nM, mis kinnitas nende võimekust tuvastada sihtanalüüti keskkonnale olulistes kontsentratsioonides. Lisaks näitasid kõik sensorid head selektiivsust ja rahuldavat analüütilist taastumist (93–119%) sihtanalüüdi määramisel kraani- ja tiigivee proovides, mis näitab nende praktilist rakendatavust keerukametes vesikeskkondades.

Doktoritöö uudsus seisneb selles, et esmakordselt on välja töötatud MIP-põhised elektrokeemilised sensorid fungitsiidi AZO ja makroliidide (ML) määramiseks veekeskkondades ning valmistatud sisseehitatud redoksindikaatoriga MIP-sensor RuO_2 elektroodil AMP tuvastamiseks. Esitatud lähenemisviisid MIP-põhiste elektrokeemiliste sensorite valmistamiseks tõestavad nende potentsiaali fungitsiidide ja antibiootikumide saasteainete selektiivseks ja otseseks määramiseks nanomolaarses kontsentratsioonivahemikus, milles neid looduslikult veekeskkonnas leidub. Väljatöötatud meetoditel on märkimisväärne potentsiaal usaldusväärsete ja tõhusate kaasaskantavate analüütiliste seadmete arendamiseks, mis võimaldavad keskkonnasaasteainete kohapealset rutiinset seiret vesikeskkonnas.

Appendix 1

PAPER I

V.B.C. Nguyen, J. Reut, J. Rappich, K. Hinrichs, V. Syritski, Molecularly Imprinted Polymer-Based Electrochemical Sensor for the Detection of Azoxystrobin in Aqueous Media, Polymers 16 (2024) 1394.

MDPI

Article

Molecularly Imprinted Polymer-Based Electrochemical Sensor for the Detection of Azoxystrobin in Aqueous Media

Vu Bao Chau Nguyen [1], Jekaterina Reut [1], Jörg Rappich [2], Karsten Hinrichs [3] and Vitali Syritski [1,*]

[1] Department of Materials and Environmental Technology, Tallinn University of Technology, Ehitajate tee 5, 19086 Tallinn, Estonia; vunguy@taltech.ee (V.B.C.N.)
[2] Young Investigator Group Nanoscale Solid-Liquid Interfaces, Helmholtz-Zentrum Berlin für Materialien und Energie GmbH, Schwarzschildstr. 8, 12489 Berlin, Germany; rappich@helmholtz-berlin.de
[3] Application Laboratories Berlin, Leibniz-Institut für Analytische Wissenschaften-ISAS-e.V., Schwarzschildstraße 8, 12489 Berlin, Germany; hinrichs@isas.de
* Correspondence: vitali.syritski@taltech.ee

Abstract: This work presents an electrochemical sensor detecting a fungicide-azoxystrobin (AZO) in aqueous environments. This AZO sensor utilizes a thin-film metal electrode (TFME) combined with an AZO-selective molecularly imprinted polymer (AZO–MIP). The AZO–MIP was directly generated on TFME through electrochemical polymerization from the solution containing two functional monomers: aniline (Ani) and m-phenylenediamine (mPD), and the template: AZO, which was afterwards removed to form AZO-selective cavities in the polymer matrix. The AZO–MIP preparation was characterized by electrochemical and ellipsometry measurements. Optimization of the synthesis parameters, including the charge density applied during electrodeposition, the monomer-to-template ratio, was performed to enhance the sensor's performance. The results demonstrated that the AZO sensor achieved a low limit of detection (LOD) of 3.6 nM and a limit of quantification (LOQ) of 11.8 nM in tap water, indicating its sensitivity in a complex aqueous environment. The sensor also exhibited satisfactory selectivity for AZO in both ultrapure and tap-water samples and achieved a good recovery (94–119%) for the target analyte. This study highlights the potential of MIP-based electrochemical sensors for the rapid and accurate detection of fungicide contaminants in water, contributing to the advancement of analytical tools for water-quality monitoring and risk assessment.

Keywords: molecularly imprinted polymer; environmental pollutant; fungicide; azoxystrobin; electrochemical sensor

1. Introduction

The presence of various organic pollutants in environmental water poses significant risks to both human and environmental health. Agrochemicals, namely fungicides, have garnered significant interest among these pollutants. This is because they are essential for ensuring food security, which leads to an increase in their preventive use. However, this rise in consumption comes with a significant level of toxicity to a broad range of organisms and aquatic biota [1]. Azoxystrobin (AZO), a common fungicide used in agriculture, belongs to the strobilurin class and is renowned for its broad-spectrum effectiveness against a wide range of fungal pathogens [2]. It functions by suppressing the respiratory chain in fungi, therefore impeding their growth and reproduction [3].

According to a recent report from Maximize Market Research, the global AZO market exhibited a substantial growth trajectory, escalating from USD 0.91 billion in 2021 to a remarkable projection of USD 1.93 billion by 2029 [4]. This remarkable surge in AZO usage has triggered profound concerns about its environmental impact, particularly concerning potential waterbody contamination [5]. For instance, the presence of AZO contamination has been detected in freshwater ecosystems in South Africa and China, alongside other organic pollutants [6,7]. One major concern associated with AZO is its significant threat

to aquatic ecosystems due to its highly toxic nature. According to the European Food Safety Authority, AZO can rapidly eradicate up to 50% of aquatic organisms within a short period, even at concentrations as low as 1 mgL^{-1} [8]. This alarming toxicity level is a cause for concern, especially when considering its adverse effects on fishes, particularly those where exposure to the pollutant can cause them to suffer from various health issues, including physiological disruptions, reduced growth rates, reproductive disorders, and even mortality [9–12]. Studies have demonstrated that AZO causes oxidative stress and apoptosis in aquatic species, impacting their mitochondrial respiration. [11]. Moreover, prolonged exposure to AZO could disturb the fragile equilibrium of aquatic ecosystems. For example, AZO concentrations in the range of 0.2–0.5 mgL^{-1} significantly reduce the growth of eukaryotic algae in freshwater [13], and they can harm aquatic plants by inhibiting antioxidant enzymes and causing DNA damage [14].

Furthermore, the potential risks of AZO exposure extend to human health by contaminating water supplies. Extended exposure to AZO has been associated with suppression of mitochondrial oxidative respiration and changes in neuronal cell lipid abundance [15]. Also, genotoxic activity risk has been identified, showing varying effects with short-term and long-term exposure, depending on age groups [16].

Conventional analytical techniques, including high-performance liquid chromatography (HPLC) [17,18] and gas chromatography-mass spectrometry (GC-MS) [19] have been widely used for analyzing azoxystrobin. However, these techniques often require expensive equipment and skilled personnel, rendering them impractical for quick on-site evaluations. Given the widespread use and persistence of AZO in water bodies, the development of simple and commercially feasible sensing technologies to detect AZO becomes imperative to assess and mitigate the associated risks.

In designing chemo/biosensors, molecular imprinting technique stands out as an indispensable means of generating the state-of-the-art recognition elements called molecularly imprinted polymers (MIPs). MIPs, crosslinked polymer matrices with engraved molecular recognition sites specific for the target analyte [20], have distinguished themselves as versatile biomimetic receptors in analytical chemistry, offering promising alternatives to biological receptors for sensitive and selective target analyte detection [21]. MIPs integrated with various sensor transducers have been extensively studied for the detection of numerous environmental pollutants [22,23]. Electrochemical sensors, in particular, have garnered significant interest. They offer real-time monitoring of analytes, simplicity in handling, and sufficient sensitivity at a reduced cost. Additionally, their compatibility with microfluidic systems, large-scale fabrication, and multiplexing technologies makes them an ideal starting point for realizing low-cost and portable sensing platforms suitable for the in-field detection and quantification of environmental contaminants [24,25].

Despite the potential of MIP-based electrochemical sensors, their development for AZO detection in water remains limited. To the best of our knowledge, the synthesis of MIPs tailored for AZO recognition and their subsequent application in electrochemical sensing platforms have not been previously reported.

This work aims to address this knowledge gap by developing a MIP-based electrochemical sensor for the sensitive and selective detection of AZO in aqueous media. Two functional monomers, namely, aniline (Ani) and meta-phenylenediamine (mPD), were selected among other electropolymerizable monomers through computer modelling. This involved estimating the geometric optimization using Universal Force Field (UFF) and the binding energies using density functional theory (DFT)–based quantum chemical calculation. The successful implementation of this AZO–MIP-based sensor (AZO sensor) will provide a valuable tool for the rapid on-site monitoring of AZO in water, facilitating early detection and mitigation of potential risks associated with its presence.

2. Materials and Methods

2.1. Chemicals and Materials

All used chemicals, except acetic acid supplied by Lach-ner, were purchased from Sigma, St. Louis, MO, USA. The chemicals were received and stored under standard conditions. The aqueous solutions were prepared with ultrapure water (Direct-Q 3 UV Water Purification system, resistivity 18.2 MΩ cm at 25 °C, Merck KGaA, Darmstadt, Germany). The polymer synthesis was conducted in phosphate buffered saline (PBS) (0.01 M, pH 7.4) containing 20% of acetonitrile. Analyte solutions were meticulously prepared using ultrapure as well as tap water. All electrochemical measurements were conducted in a 0.3 M KCl solution containing 4 mM redox probe $K_3[Fe(CN)_6]/K_4[Fe(CN)_6]$. Thin-film metal electrodes (TFME) were obtained from MicruX Technologies, Gijón, Spain, and consisted of a 1 mm diameter circular (approximately 0.785 mm^2) gold working electrode (WE), a gold reference electrode (RE), and a gold counter electrode (CE). To perform all electrochemical measurements, TFME were connected to an electrochemical workstation (Reference 600, Gamry Instruments, Warminster, PA, USA). The potentials associated with the TFME activation process were referenced against the Ag/AgCl/3 M KCl external reference electrode, while all other potentials were referenced against the RE of TFME.

2.2. Functional Monomer Selection

To select the suitable functional monomer, electropolymerizable monomers including 2-methyl-4-nitroaniline (2M4N), 3-aminothiophenol (3ATP), aniline (Ani), meta-phenylenediamine (mPD), pyrazole (PRZ), and pyrrole (PYR) were selected. The binding energy between each monomer and AZO was estimated with a 1:1 ratio. The initial structures of their pre-polymerization complexes were prepared and subjected to geometric optimization using Avogadro 1.2.0 software, employing the Universal Force Field (UFF) for energy minimization. Subsequently, binding energies were computed utilising density functional theory (DFT) method at B3LYP/6-31+G level, employing Gaussian '09 software packages.

2.3. Sensor Preparation

The AZO sensor was prepared by the electrodeposition of an AZO–MIP film on the WE surface of gold TFME. Prior to electrodeposition, the WE and RE of TFME were activated by cycling the potential between 0.5 and 1.55 V in a 0.05 M sulfuric acid solution, with a scan rate of 100 mV/s, for a minimum of 10 cycles. Subsequently, they were rinsed with ultrapure water and dried under a nitrogen atmosphere.

Co-polymer of Ani and mPD film containing AZO, denoted as poly(Ani-co-mPD)/AZO, was synthesized at the constant current of 0.3 μA in a setup where the electrodes of TFME were exposed to a PBS with 20% of acetonitrile containing Ani, mPD and AZO, at the determined optimal concentrations. Molecular imprints of AZO were generated within poly(Ani-co-mPD)/AZO by immersing the modified electrode in a 5% acetic acid solution on vortex for 30 min, followed by ultrapure water for 30 min to remove AZO, resulting in AZO–MIP formation.

To ensure the coexistence of Ani and mPD in the poly(Ani-co-mPD), and to evaluate the efficiency of the removal process using a 5% acetic acid solution, a custom build dry-air purged IR spectroscopic ellipsometer externally attached to a FT-IR spectrometer (Vertex 70, Bruker, Billerica, MA, USA) was employed. The tanΨ measurements were taken in the mid infrared spectral range at incidence angles of 70° and 80°. Additional information regarding the configuration and procedure can be found at [26,27].

The sensor preparation stages were characterized by cyclic voltammetry (CV) and electrochemical impedance spectroscopy (EIS) in a 0.3 M KCl solution containing 4 mM redox probe $K_3[Fe(CN)_6]/K_4[Fe(CN)_6]$. CV was performed by cycling the potential between −0.2 and 0.2 V at a scan rate of 50 mV/s while EIS measurements were carried out at an alternating potential with an amplitude 10 mV and a frequency range of 0.1 Hz to 10 kHz.

2.4. Evaluation of Sensor Performance

The sensor senses the changes in charge transfer between AZO–MIP-modified WE of TFME and redox probe ions ($[Fe(CN)_6]^{3-}$/$[Fe(CN)_6]^{4-}$) before and after incubation in a sample solution containing the target analyte, AZO. Following incubation of the sensor in a sample solution, AZO binds AZO–MIP and hinders the charge transfer to WE of TFME.

Differential pulse voltammetry (DPV) was used to measure this effect and conducted in a 0.3 M KCl solution containing 4 mM redox probe ($K_3[Fe(CN)_6]$/$K_4[Fe(CN)_6]$) at a potential range of 0 to 0.4 V, pulse amplitude of 35 mV, a pulse width of 0.04 s, a sample period of 0.5 s and a step potential of 7 mV (the optimization details of DPV parameters in Section S1).

Thus, the concentration-dependent sensor response, I_n, can be represented as a normalized-suppression of the DPV current peak as follows:

$$I_n = (I_0 - I)/I_0 \tag{1}$$

where I_0 and I are the current peak values measured by DPV after incubation in ultrapure water without and with the target analyte, respectively.

All analyte solutions were prepared in ultrapure as well as tap water except otherwise stated in which case the pH was adjusted to the desired value using drops of 1 M HCl or 1 M NaOH.

The limits of detection (LOD) and quantification (LOQ) were determined from the linear regression of the sensor's response to low concentrations of the analyte in PBS, using Equations (2) and (3), as follows:

$$LOD = 3SD/b \tag{2}$$

$$LOQ = 10SD/b \tag{3}$$

where SD and b are the standard deviation of the residual and the slope of the regression line, respectively.

The selectivity of the AZO sensor was evaluated by comparing the sensor's response upon rebinding of AZO and other interfering fungicides, including pyraclostrobin (PRC), kresoxim-methyl (KSX) at the same concentrations in ultrapure water. Similar experiments were conducted in tap water spiked with the desired analyte concentrations. For this purpose, tap-water samples were collected from the water-supply line of Tallinn University of Technology and used without further treatment.

3. Results and Discussion

3.1. Functional Monomers Selection

The choice of functional monomer is a critical factor in achieving the optimal performance of a MIP. The effectiveness of MIPs primarily depends on the strength of the interaction between the template molecule and the functional monomer [28]. This interaction facilitates the formation of molecular memory within the MIP by considering both the shape and arrangement of functional groups in the template molecule. The following electropolymerizable monomers with functional groups capable of engaging in hydrogen bonds with AZO's oxygen atoms were examined: 2M4N, 3ATP, Ani, mPD, PRZ, and PYR (Figure 1). A computational modelling was utilized to compare the binding energies between the monomers and AZO to identify a more stable complex (Table S1). As can be seen, Ani showed the highest binding energies with AZO, signifying its potential to form robust non-covalent interactions (hydrogen bonding) with the template. However, Ani possesses only one amino group, which is capable of hydrogen bonding with AZO and is also involved in the formation of the polymer chain during polymerization. This could potentially compromise the recognition capabilities of the resulting MIP. To address this concern, mPD was introduced as a co-monomer to ensure the hydrogen bonding with AZO, which, along with the contribution of π-π interactions between AZO and both monomers, resulted in enhanced selectivity and stability of the polymer structure. The

feasibility of the formation of a co-polymer of Ani and mPD during electrochemical poly-merization has been successfully demonstrated in previous studies [29,30]. Additionally, it was found that phenylenediamines can act as branching or crosslinking sites when they undergo copolymerization with Ani [31–33]. Hence, by incorporating mPD into the func-tional monomer mixture, it was expected that a more stable MIP structure with enhanced molecular recognition capabilities would be achieved.
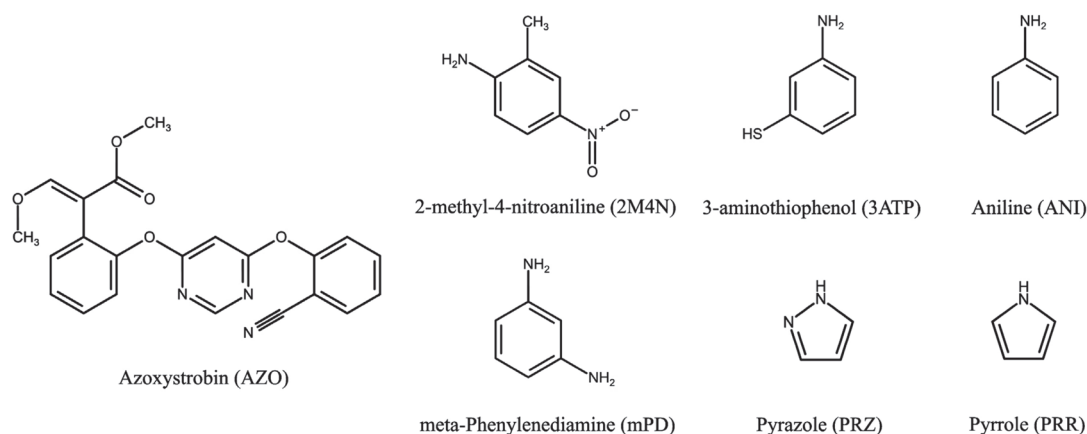
Figure 1. Structural formula of Azoxystrobin (AZO) and electropolymerizable monomers examined as potential functional monomers for AZO–MIP synthesis.

Furthermore, it should be noted that the possible non-covalent interactions between AZO and monomers, mPD and Ani, include, in addition to hydrogen bonding, π-π interac-tions between the aromatic moieties present in the studied molecules. These interactions can contribute significantly to the strength of non-covalent interaction in the prepoly-merization complex as well as in the resulting MIP. Therefore, the composition of the polymerization solution including the use of single or dual monomers as well as the ratio of monomers to the template was optimized experimentally (see Section 3.2 and Figure S5a in Supplementary Information).

3.2. Synthesis and Characterization of AZO–MIP Film

In electrochemical MIP synthesis, it is essential to preserve the structural integrity of the template molecules during electropolymerization at an applied potential. Therefore, a preliminary test was conducted to confirm that the AZO remained unoxidized at the electrodeposition potential of the selected monomer.

CV measurements (Figure S2) were performed to determine the appropriate electro-chemical potential for synthesis of the co-polymer poly(Ani-co-mPD) while preventing the undesired oxidation of AZO. The CV scans revealed that Ani undergoes oxidation at approx-imately 300 mV, while mPD oxidizes at around 250 mV. Remarkably, the proximity of Ani's oxidation potential to that of mPD, suggesting the feasibility of generating a co-polymer using these two monomers due to the potential combination of their electrochemically generated radical cations, enabling the propagation of chain growth. Consequently, it is expected that the oxidation of both monomers in their solution mixture will occur at a potential higher than 300 mV.

In this study, the galvanostatic method was employed for AZO–MIP film synthesis. This method was chosen for its ability to precisely control polymerization through current regulation, enhancing the reproducibility and uniformity of the resulting AZO–MIP films. The current was adjusted to attain the required electrodeposition potential of above 300 mV. By adjusting the time of the galvanostatic process, the polymer film thickness can be precisely controlled, providing tunability in the final MIP film efficiency.

The electrochemical polymerization in this study was performed under neutral pH conditions. In these conditions, Ani molecules easily undergo oxidation, resulting in the formation of a stable non-conductive emeraldine base [33–35]. Furthermore, the poly(m-phenylenediamine), or poly(mPD), film synthesized under neutral pH conditions exhibits excellent stability coupled with imprinting capability, making it an ideal choice for MIP layer formation [36–38].

The electrodeposited thin co-polymer film was characterized using IRSE (Figure 2a). The spectra of polyaniline (poly(Ani)) and poly(mPD) electrodeposited under similar conditions as those of the poly(Ani-co-mPD) film, were presented for comparison. Examining the region of 1400–1700 cm^{-1} of spectra, several characteristic bands can be clearly distinguished. Specifically, the absorption bands in poly(Ani) spectrum at 1498 and 1515 cm^{-1} are attributed to benzenoid (aromatic) ring stretching, while the band at 1595 cm^{-1} with a shoulder at 1570 cm^{-1} is attributed to C=C stretching in a quinoid ring. This may indicate the partially oxidized (emeraldine) form of poly(Ani) [39]. However, in the spectrum of poly(mPD), only one broad absorption band near 1630 cm^{-1} is present, which can be attributed to the stretching mode of quinoid imine [40,41] as well as to the C=C stretching vibration in a phenazine-like segment [40,42]. The spectrum of poly(Ani-co-mPD) now displays the characteristic bands of both poly(Ani) (red arrows) and poly(mPD) (blue arrow) at wavenumbers of 1498, 1515, and 1630 cm^{-1}, with a shoulder at 1600 cm^{-1}. This suggests that the synthesized co-polymer structure differs from the corresponding homopolymers structures and obviously contains the aromatic rings in combination with quinoid rings as well as phenazine-like segments.
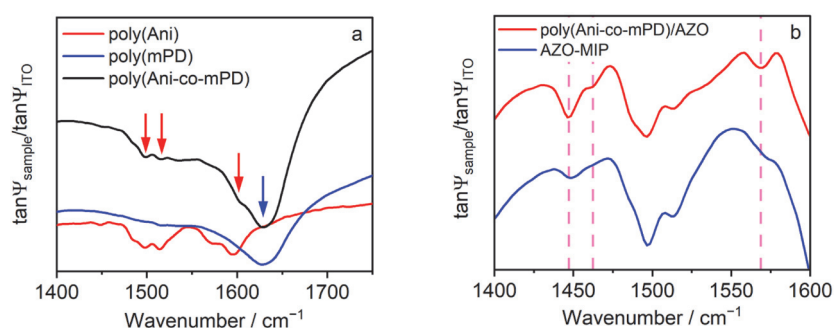
Figure 2. (**a**) Referenced IRSE spectra of poly(Ani), poly(mPD), and poly(Ani-co-mPD) films on ITO; and (**b**) referenced IRSE spectra of poly(Ani-co-mPD)/AZO films on ITO before washing (solid red line) and after washing (solid blue line). Vertical dashed lines show varied responses post-washing process, including disappearance or attenuation.

To prepare AZO–MIP, the polymer film synthesized in the presence of AZO (poly(Ani-co-mPD)/AZO) was treated with 5% acetic acid to remove AZO from the polymer matrix. To confirm the removal of AZO, the film before and after the treatment was evaluated using IRSE (Figure 2b). As can be seen, there are changes in the frequency positions in the range 1400–1600 cm^{-1}. Specifically, the peak at 1447 cm^{-1} was attenuated, and peaks at 1463 and 1569 cm^{-1} vanished after washing. Since these peak positions are close to those of AZO (Figure S3), it can be concluded that the AZO present in the poly(Ani-co-mPD)/AZO was removed after treatment in an acetic acid solution, presumably resulting in the formation of the AZO–MIP film.

In addition, the formation of AZO–MIP on the Au WE was evaluated by electrochemical techniques, including CV and EIS. These measurements helped to establish a connection between each stage of modification by monitoring alterations in charge transfer between the redox pair in solution and on the Au WE surface. CV analysis indicated a reduction in both anodic and cathodic current peaks following poly(Ani-co-mPD)/AZO electrodeposition (Figure S4a), signifying the development of a non-conductive film hindering charge

transfer at the electrode–solution interface. The observed recovery of current peaks after acetic acid treatment suggested improved permeability of the polymer layer due to the formation of imprinted cavities of AZO–MIP. Similar trends were observed in the EIS spectra (Figure S4b), where the semicircle diameter representing charge transfer resistance, Rct, increased after polymer film electrodeposition (Table S2), and then decreased after subsequent treatment with acetic acid to form AZO–MIP. The selective adsorption of AZO by AZO–MIP resulted in changes observed in both the CVs and the EIS spectra.

The advantage of poly(Ani-co-mPD) over the homopolymers poly(Ani) or poly(mPD) for AZO–MIP formation was unequivocally demonstrated by comparing the response signals of the sensors equipped with corresponding MIPs for AZO detection (Figure S5a). As shown, the sensor with the MIP synthesized from the co-polymer exhibits a superior response compared to the sensors with the MIPs prepared from poly(Ani) or poly(mPD). In addition, the MIP-based sensor synthesized using co-monomers also shows better performance in comparison with its reference non-imprinted polymer (NIP)-based sensor (Figure S5b), indicating the effectiveness of molecular imprinting.

3.2.1. Effect of Thickness

To determine the optimal polymer thickness of the AZO–MIP, at which the sensor produces the highest response towards AZO, the WE of TFME was modified with poly(Ani-co-mPD)/AZO films of various thicknesses generated by passing different charge densities, ranging from 3 to 6 mC/cm^2. As can be seen, the sensor equipped with AZO–MIP formed from film generated by 5 mC/cm^2 demonstrates the highest response and was consequently selected as optimal for further study (Figure 3a).
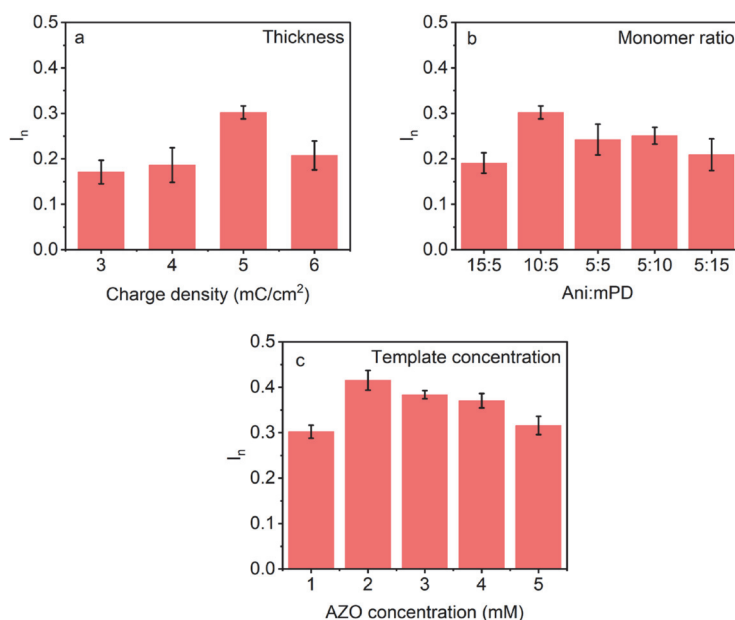
Figure 3. Optimization of AZO–MIP preparation. Responses of the sensors equipped with various AZO–MIPs after incubation in 10 μM AZO in ultrapure water. AZO–MIPs were prepared using different: (**a**) charge densities; (**b**) Ani:mPD ratios; and (**c**) AZO concentrations at constant Ani:mPD ratio of 10:5.

3.2.2. Effect of the Monomer to Template Ratio

The recognition capabilities of an MIP can be influenced by the template:monomer ratio used to build the MIP [36]. A high amount of monomer may reduce binding selectivity

due to increased non-specific binding, while a low amount of monomer may decrease the number of binding sites in the formed polymer due to insufficient interactions with the template [43]. Therefore, the optimal Ani:mPD and AZO:Ani-co-mPD molar ratios were determined. As can be seen, the sensor equipped with AZO–MIP prepared from the synthesis solution containing 10 mM of Ani and 5 mM of mPD exhibits the most favorable response towards AZO (Figure 3b). Furthermore, by keeping these concentrations in the synthesis solution constant and varying the concentrations of AZO from 1 to 5 mM, it was determined that the presence of 2 mM of AZO resulted in the highest responsiveness of the AZO sensor (Figure 3c). Thus, the optimal concentration ratio of AZO:Ani:mPD in the synthesis solution was determined to be 2:10:5 mM and was used for further experimental investigations.

3.3. Performance of AZO Sensor

3.3.1. Effect of pH

The influence of the pH of the analyzed solution on the sensor's response was studied to ensure accurate and reliable detection of AZO in real-world aqueous environments. The responses of AZO sensor were evaluated upon incubation in 10 μM AZO aqueous solution at pH values ranging from 5 to 8, aligning with the natural pH levels found in environmental water [44–47]. Hydrolysis and decomposition of AZO molecules can occur at lower pH values, while higher pH values may cause degradation due to nucleophilic substitution reactions [48]. The data presented in Figure 4a demonstrated an ascending trend in sensor response with increasing pH until 7, followed by a subsequent lowering of the signal.
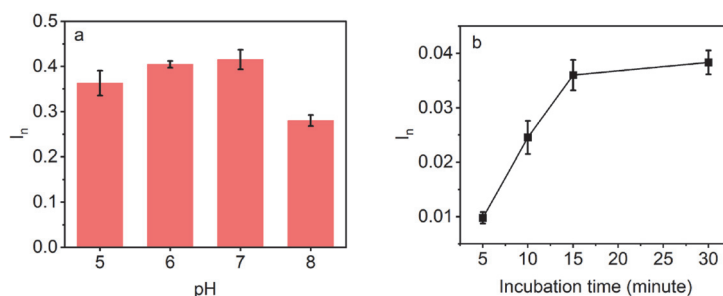
Figure 4. (**a**) Responses of AZO sensor upon incubation in 10 μM AZO solution in ultrapure water of different pH values; and (**b**) effects of incubation times on the DPV responses of AZO sensor after rebinding in 50 nM AZO solution in ultrapure water.

3.3.2. Effect of Incubation Time

A rapid response time is a desirable characteristic for chemical sensors in environmental monitoring. In this study, the total time required to obtain the detection result includes the electrochemical DPV measurements, which take a maximum of 5 min, and sensor incubation in an analyte solution to allow for its rebinding on MIP, which may require a longer amount of time. Hence, the optimal incubation time for the AZO sensor was experimentally determined by measuring the sensor's responses upon incubating in the 50 nM AZO solution for various durations, including 5, 10, 15, and 30 min (Figure 4b). The findings indicate that the sensor's response substantially increases as the incubation time is prolonged up to 15 min. Beyond this point, any further increase is marginal. Considering the response signal values and the plateau effect observed beyond 15 min, this incubation time was deemed sufficient to achieve optimal analyte binding to the AZO–MIP.

3.3.3. Sensitivity Study

The purpose of the sensitivity study was to evaluate the performance of the AZO sensor in detecting low analyte concentrations and to determine LOD and LOQ. As shown in Figure 5, the response of the AZO sensor exhibited a quasi-linear increase in response

signal with rising analyte concentrations in the range of 6–50 nM. In the case of AZO spiked into ultrapure water (Figure 5a), the sensor could detect it with LOD and LOQ of 2.0 nM and 6.7 nM, respectively. However, when the sensor was tested in AZO solutions prepared in tap water (Figure 5b), its responses exhibited higher variations, as indicated by an elevated standard deviation, and subsequently raised the LOD and LOQ values of 3.6 nM and 11.8 nM, respectively. This could be attributed to tap water, which predominantly contains multiple dissolved ions, minerals, and other compounds [49–51], thereby leading to an increased background signal and noise. Nevertheless, AZO concentrations in the lowland stream water were found to be as high as 73.6 nM [52], indicating the practical utility of the AZO sensor for the analysis of environmental water.
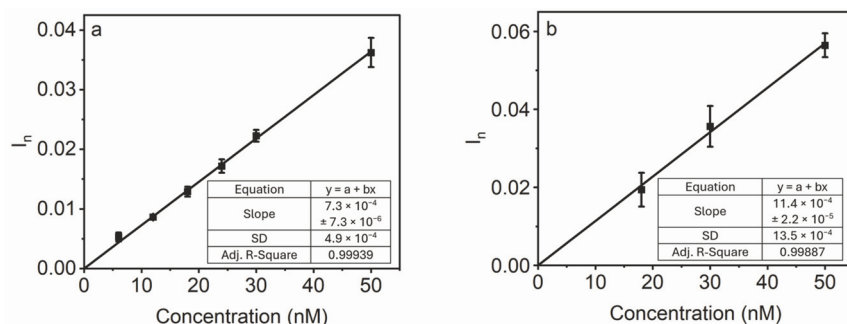
Figure 5. Performance of the AZO sensor at low analyte concentrations (6–50 nM) in: (**a**) ultrapure water; and (**b**) tap water. The solid line is a linear regression fit. The error bars represent standard deviation of three measurements carried out by three independent AZO sensors.

3.3.4. Selectivity Study

Two fungicides, kresoxim-methyl (KSX) and pyraclostrobin (PRC), which belong to the same group of strobilurin fungicides as AZO, were chosen for evaluating the sensor's ability to distinguish between different compounds (refer to Figure S6 for detailed structures). Despite their structural similarities, the AZO sensor exhibits a stronger response to the target compound (AZO) compared to the other tested fungicides (KSX and PRC) (Figure 6). In general, the signal caused by the AZO presence was approximately two and four times higher than the signals generated by PRC and KSX, respectively (Table S3). Hence, the AZO sensor is capable of discriminating between AZO and other molecules in the tap-water matrix.
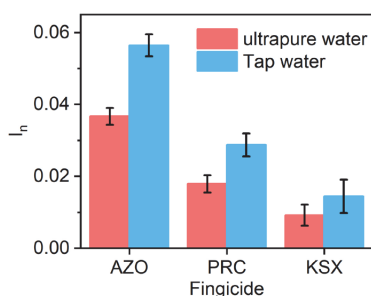
Figure 6. Responses of the AZO sensor after incubating in a 50 nM concentration of each different fungicide (AZO, PRC, and KSX) in ultrapure and tap water.

To validate the accuracy of the sensor's measurements and assess its practical utility, a series of recovery experiments were conducted using AZO solutions of varying concentrations in tap-water (as detailed in Table 1). The sensor showed good recoveries within the range of 94% to 119%, confirming its robust performance.

Table 1. Recoveries of the AZO sensor in tap-water samples.

Spiked AZO (nM)	Found AZO (nM)	Recovery (%)
15 ± 0.1	18 ± 1	119 ± 6
30 ± 0.2	29 ± 1	95 ± 4
50 ± 0.4	47 ± 3	94 ± 7

4. Conclusions

This report showcases the successful development of an electrochemical sensor with a robust MIP-based sensing element for detecting the fungicide AZO in water. The sensor combines the selectivity of AZO–MIP with the low-cost and compact TFME. To enhance the selectivity of AZO–MIP, it was synthesized by co-polymerization of two functional monomers, Ani and mPD. Following optimization, the sensor exhibited appreciable recognition of AZO and was capable of detecting low levels of analyte with an LOD value of 3.6 nM and an LOQ value of 11.8 nM in tap water. Importantly, the sensor showcased good selectivity, effectively distinguishing AZO from similar fungicide compounds (PRC and KSX) both in ultrapure and tap-water samples. Additionally, the sensor demonstrated a good recovery, ranging from 94% to 119% in tap-water samples. Considering that AZO concentrations can be found in the lowland stream water that are as high as 73.6 nM, the practical utility of the AZO sensor for the cost-effective on-site detection of AZO in environmental water is evident.

Supplementary Materials: The following supporting information can be downloaded at: https://www.mdpi.com/article/10.3390/polym16101394/s1, Figure S1: The influence of DPV parameters: step size (a), pulse time (b) and pulse size (c) on the oxidation peak current of AZO sensor recorded in 0.3 M KCl solution containing 4 mM $K_3[Fe(CN)_6]/K_4[Fe(CN)_6]$. Each DPV underwent an individual baseline; Figure S2: A fragment of the first cycle of the cyclic voltammogram recorded on Au TFME in PBS at the presence of 5 mM Ani, 5 mM mPD, or mixture of 5 mM mPD and 5 mM Ani (see color codes on the graphs) at a scan rate of 100 mV/s; Figure S3: Attenuated total reflection (ATR) absorbance of AZO powder; Figure S4: CVs (a) and EIS (b) characterization of bare gold, poly(Ani-co-mPD)/AZO, AZOMIP and AZO on AZOMIP that are prepared on Au TFME. The measurements were performed in 0.3 M KCl solution containing 4 mM $K_3[Fe(CN)_6]/K_4[Fe(CN)_6]$; Figure S5: (a) Responses of AZO sensor based on AZO–MIPs formed from the different polymers upon incubation in 50 nM AZO solution in ultrapure water. (b) Responses of sensors modified with AZOMIP and NIP layers formed from poly(Ani-co-mPD); Figure S6: Structures of fungicides used for selectivity study; Scheme S1: AZO structure with highlighted oxygen atoms; Scheme S2: A schematic representation of possible binding interaction between Ani and mPD monomers with template AZO; Table S1: Binding energies (kcal/mol) of interactions between the functional monomers and AZO at O5 site as calculated by Gaussian'09 software; Table S2: Hydrogen bond binding energy of mPD and Ani towards different oxygen atoms of AZO as calculated by Gaussian'09 software; Table S3: Charge transfer resistance (Rct) values obtained from fitting EIS spectra to a Randles equivalent circuit consisting of a solution resistance (Rs), a constant phase element (CPE), a charge transfer resistance (Rct), and a Warburg impedance (Wd); Table S4: Selectivity coefficient (k) for rebinding of the fungicides to AZO sensor as calculated by Equation (SE1). References [53,54] are cited in the Supplementary Materials.

Author Contributions: Conceptualization, V.S. and J.R. (Jekaterina Reut); methodology, V.B.C.N., J.R. (Jekaterina Reut) and V.S.; validation, V.B.C.N., J.R. (Jekaterina Reut) and V.S.; formal analysis, V.B.C.N.; investigation, V.B.C.N., V.S., J.R. (Jörg Rappich) and K.H.; resources, V.S.; data curation, V.S.; writing—original draft preparation, V.B.C.N.; writing—review and editing, V.B.C.N., J.R. (Jekaterina Reut), V.S., J.R. (Jörg Rappich) and K.H.; visualization, V.S. and V.B.C.N.; supervision, V.S.; project administration, V.S.; funding acquisition, V.S. All authors have read and agreed to the published version of the manuscript.

References

1. Gikas, G.D.; Parlakidis, P.; Mavropoulos, T.; Vryzas, Z. Particularities of Fungicides and Factors Affecting Their Fate and Removal Efficacy: A Review. *Sustainability* **2022**, *14*, 4056. [CrossRef]
2. Leadbeater, A.J. Plant Health Management: Fungicides and Antibiotics. In *Encyclopedia of Agriculture and Food Systems*; Elsevier: Amsterdam, The Netherlands, 2014; pp. 408–424. ISBN 978-0-08-093139-5.
3. Kim, J.H.; Campbell, B.C.; Mahoney, N.; Chan, K.L.; Molyneux, R.J.; May, G.S. Enhanced activity of strobilurin and fludioxonil by using berberine and phenolic compounds to target fungal antioxidative stress response. *Lett. Appl. Microbiol.* **2007**, *45*, 134–141. [CrossRef] [PubMed]
4. Azoxystrobin Market: Global Industry Analysis And Forecast (2022–2029). 2023. Available online: https://www.maximizemarketresearch.com/market-report/global-azoxystrobin-market/107455/ (accessed on 19 October 2023).
5. Wu, P.; Wu, W.Z.; Han, Z.H.; Yang, H. Desorption and mobilization of three strobilurin fungicides in three types of soil. *Environ. Monit. Assess.* **2016**, *188*, 363. [CrossRef]
6. Barnhoorn, I.; Van Dyk, C. The first report of selected herbicides and fungicides in water and fish from a highly utilized and polluted freshwater urban impoundment. *Environ. Sci. Pollut. Res.* **2020**, *27*, 33393–33398. [CrossRef] [PubMed]
7. Lu, T.; Zhang, Q.; Lavoie, M.; Zhu, Y.; Ye, Y.; Yang, J.; Paerl, H.W.; Qian, H.; Zhu, Y.-G. The fungicide azoxystrobin promotes freshwater cyanobacterial dominance through altering competition. *Microbiome* **2019**, *7*, 128. [CrossRef]
8. European Food Safety Authority. Conclusion on the peer review of the pesticide risk assessment of the active substance azoxystrobin. *EFSA J.* **2010**, *8*, 1542.
9. Cao, F.; Martyniuk, C.J.; Wu, P.; Zhao, F.; Pang, S.; Wang, C.; Qiu, L. Long-Term Exposure to Environmental Concentrations of Azoxystrobin Delays Sexual Development and Alters Reproduction in Zebrafish (*Danio rerio*). *Environ. Sci. Technol.* **2019**, *53*, 1672–1679. [CrossRef] [PubMed]
10. Cao, F.; Zhu, L.; Li, H.; Yu, S.; Wang, C.; Qiu, L. Reproductive toxicity of azoxystrobin to adult zebrafish (*Danio rerio*). *Environ. Pollut.* **2016**, *219*, 1109–1121. [CrossRef] [PubMed]
11. Olsvik, P.A.; Kroglund, F.; Finstad, B.; Kristensen, T. Effects of the fungicide azoxystrobin on Atlantic salmon (*Salmo salar* L.) smolt. *Ecotoxicol. Environ. Saf.* **2010**, *73*, 1852–1861. [CrossRef] [PubMed]
12. Rodrigues, E.T.; Lopes, I.; Pardal, M.Â. Occurrence, fate and effects of azoxystrobin in aquatic ecosystems: A review. *Environ. Int.* **2013**, *53*, 18–28. [CrossRef] [PubMed]
13. Zhang, M.; Liu, W.; Qu, Q.; Ke, M.; Zhang, Z.; Zhou, Z.; Lu, T.; Qian, H. Metabolomic modulations in a freshwater microbial community exposed to the fungicide azoxystrobin. *J. Environ. Sci.* **2020**, *97*, 102–109. [CrossRef] [PubMed]
14. Zhang, C.; Zhou, T.; Xu, Y.; Du, Z.; Li, B.; Wang, J.; Wang, J.; Zhu, L. Ecotoxicology of strobilurin fungicides. *Sci. Total Environ.* **2020**, *742*, 140611. [CrossRef]
15. Nguyen, K.; Sanchez, C.L.; Brammer-Robbins, E.; Pena-Delgado, C.; Kroyter, N.; El Ahmadie, N.; Watkins, J.M.; Aristizabal-Henao, J.J.; Bowden, J.A.; Souders, C.L.; et al. Neurotoxicity assessment of QoI strobilurin fungicides azoxystrobin and trifloxystrobin in human SH-SY5Y neuroblastoma cells: Insights from lipidomics and mitochondrial bioenergetics. *NeuroToxicology* **2022**, *91*, 290–304. [CrossRef] [PubMed]
16. Djangalina, E.; Altynova, N.; Mit, N.; Djansugurova, L. Complex approaches to assessing the pesticides risk on human health and environment. In *Pesticides in the Natural Environment*; Elsevier: Amsterdam, The Netherlands, 2022; pp. 163–198. ISBN 978-0-323-90489-6.
17. Polati, S.; Bottaro, M.; Frascarolo, P.; Gosetti, F.; Gianotti, V.; Gennaro, M.C. HPLC-UV and HPLC-MSn multiresidue determination of amidosulfuron, azimsulfuron, nicosulfuron, rimsulfuron, thifensulfuron methyl, tribenuron methyl and azoxystrobin in surface waters. *Anal. Chim. Acta* **2006**, *579*, 146–151. [CrossRef]
18. Hernández, F.; Portolés, T.; Ibáñez, M.; Bustos-López, M.C.; Díaz, R.; Botero-Coy, A.M.; Fuentes, C.L.; Peñuela, G. Use of time-of-flight mass spectrometry for large screening of organic pollutants in surface waters and soils from a rice production area in Colombia. *Sci. Total Environ.* **2012**, *439*, 249–259. [CrossRef] [PubMed]
19. Filho, A.M.; Dos Santos, F.N.; Pereira, P.A.D.P. Development, validation and application of a method based on DI-SPME and GC–MS for determination of pesticides of different chemical groups in surface and groundwater samples. *Microchem. J.* **2010**, *96*, 139–145. [CrossRef]

20. Vasapollo, G.; Sole, R.D.; Mergola, L.; Lazzoi, M.R.; Scardino, A.; Scorrano, S.; Mele, G. Molecularly Imprinted Polymers: Present and Future Prospective. *Int. J. Mol. Sci.* **2011**, *12*, 5908–5945. [CrossRef]

21. Herrera-Chacón, A.; Cetó, X.; Del Valle, M. Molecularly imprinted polymers—Towards electrochemical sensors and electronic tongues. *Anal. Bioanal. Chem.* **2021**, *413*, 6117–6140. [CrossRef]

22. Ayankojo, A.G.; Reut, J.; Nguyen, V.B.C.; Boroznjak, R.; Syritski, V. Advances in Detection of Antibiotic Pollutants in Aqueous Media Using Molecular Imprinting Technique—A Review. *Biosensors* **2022**, *12*, 441. [CrossRef] [PubMed]

23. Rebelo, P.; Costa-Rama, E.; Seguro, I.; Pacheco, J.G.; Nouws, H.P.A.; Cordeiro, M.N.D.S.; Delerue-Matos, C. Molecularly imprinted polymer-based electrochemical sensors for environmental analysis. *Biosens. Bioelectron.* **2021**, *172*, 112719. [CrossRef] [PubMed]

24. Kanoun, O.; Lazarević-Pašti, T.; Pašti, I.; Nasraoui, S.; Talbi, M.; Brahem, A.; Adiraju, A.; Sheremet, E.; Rodriguez, R.D.; Ben Ali, M.; et al. A Review of Nanocomposite-Modified Electrochemical Sensors for Water Quality Monitoring. *Sensors* **2021**, *21*, 4131. [CrossRef] [PubMed]

25. Umapathi, R.; Ghoreishian, S.M.; Sonwal, S.; Rani, G.M.; Huh, Y.S. Portable electrochemical sensing methodologies for on-site detection of pesticide residues in fruits and vegetables. *Coord. Chem. Rev.* **2022**, *453*, 214305. [CrossRef]

26. Hinrichs, K.; Eichhorn, K.-J. (Eds.) *Ellipsometry of Functional Organic Surfaces and Films*; Springer Series in Surface Sciences; Springer: Berlin/Heidelberg, Germany, 2014; Volume 52, ISBN 978-3-642-40127-5.

27. Röseler, A.; Korte, E. Infrared Spectroscopic Ellipsometry. In *Handbook of Vibrational Spectroscopy*; Chalmers, J.M., Griffiths, P.R., Eds.; Wiley: Hoboken, NJ, USA, 2001; ISBN 978-0-471-98847-2.

28. Ayankojo, A.G.; Reut, J.; Öpik, A.; Tretjakov, A.; Syritski, V. Enhancing binding properties of imprinted polymers for the detection of small molecules. *Proc. Est. Acad. Sci.* **2018**, *67*, 138. [CrossRef]

29. Mazeikiene, R.; Malinauskas, A. Electrochemical copolymerization of aniline with m-phenylenediamine. *Synth. Met.* **1998**, *92*, 259–263. [CrossRef]

30. Mažeikienė, R.; Niaura, G.; Malinauskas, A. A comparative Raman spectroelectrochemical study of selected polyaniline derivatives in a pH-neutral solution. *Synth. Met.* **2010**, *160*, 1060–1064. [CrossRef]

31. Chao, L.; Ho, K.; Shen, S.; Pu, H.; Hsieh, T.; Kuo, C.; Tseng, B. Short polyaniline nanorod prepared in the presence of *para*-phenylenediamine. *J. Appl. Polym. Sci.* **2013**, *127*, 1853–1862. [CrossRef]

32. Xiang, C.; Xie, Q.; Hu, J.; Yao, S. Studies on electrochemical copolymerization of aniline with o-phenylenediamine and degradation of the resultant copolymers via electrochemical quartz crystal microbalance and scanning electrochemical microscope. *Synth. Met.* **2006**, *156*, 444–453. [CrossRef]

33. Stejskal, J. Polymers of phenylenediamines. *Prog. Polym. Sci.* **2015**, *41*, 1–31. [CrossRef]

34. Stejskal, J.; Trchová, M. Aniline oligomers versus polyaniline. *Polym. Int.* **2012**, *61*, 240–251. [CrossRef]

35. Vishnu, N.; Kumar, A.S.; Pillai, K.C. Unusual neutral pH assisted electrochemical polymerization of aniline on a MWCNT modified electrode and its enhanced electro-analytical features. *Analyst* **2013**, *138*, 6296. [CrossRef] [PubMed]

36. Nguyen, V.B.C.; Ayankojo, A.G.; Reut, J.; Rappich, J.; Furchner, A.; Hinrichs, K.; Syritski, V. Molecularly imprinted co-polymer for class-selective electrochemical detection of macrolide antibiotics in aqueous media. *Sens. Actuators B Chem.* **2023**, *374*, 132768. [CrossRef]

37. Ayankojo, A.G.; Boroznjak, R.; Reut, J.; Tuvikene, J.; Timmusk, T.; Syritski, V. Electrochemical sensor based on molecularly imprinted polymer for rapid quantitative detection of brain-derived neurotrophic factor. *Sens. Actuators B Chem.* **2023**, *397*, 134656. [CrossRef]

38. Ayankojo, A.G.; Reut, J.; Ciocan, V.; Öpik, A.; Syritski, V. Molecularly imprinted polymer-based sensor for electrochemical detection of erythromycin. *Talanta* **2020**, *209*, 120502. [CrossRef] [PubMed]

39. Boyer, M.-I.; Quillard, S.; Rebourt, E.; Louarn, G.; Buisson, J.P.; Monkman, A.; Lefrant, S. Vibrational Analysis of Polyaniline: A Model Compound Approach. *J. Phys. Chem. B* **1998**, *102*, 7382–7392. [CrossRef]

40. Li, X.-G.; Huang, M.-R.; Duan, W.; Yang, Y.-L. Novel Multifunctional Polymers from Aromatic Diamines by Oxidative Polymer-izations. *Chem. Rev.* **2002**, *102*, 2925–3030. [CrossRef]

41. Zhang, L.; Chai, L.; Liu, J.; Wang, H.; Yu, W.; Sang, P. pH Manipulation: A Facile Method for Lowering Oxidation State and Keeping Good Yield of Poly (*m*-phenylenediamine) and Its Powerful Ag$^+$ Adsorption Ability. *Langmuir* **2011**, *27*, 13729–13738. [CrossRef]

42. Li, X.; Duan, W.; Huang, M.; Yang, Y. Preparation and characterization of soluble terpolymers from *m*-phenylenediamine, *o*-anisidine, and 2,3-xylidine. *J. Polym. Sci. A Polym. Chem.* **2001**, *39*, 3989–4000. [CrossRef]

43. Liu, J.; Chang, H.; Zhao, W.; Liang, D.; Tang, S.; Jin, R. Theoretical design and preparation of molecularly imprinted polymers of formaldehyde and acrylamide. *J. Polym. Res.* **2021**, *28*, 433. [CrossRef]

44. Ram, A.; Tiwari, S.K.; Pandey, H.K.; Chaurasia, A.K.; Singh, S.; Singh, Y.V. Groundwater quality assessment using water quality index (WQI) under GIS framework. *Appl. Water Sci.* **2021**, *11*, 46. [CrossRef]

45. Hassan Omer, N. Water Quality Parameters. In *Water Quality—Science, Assessments and Policy*; Summers, K., Ed.; IntechOpen: London, UK, 2020; ISBN 978-1-78985-577-7.

46. Mattson, M.D. Acid lakes and rivers. In *Environmental Geology*; Encyclopedia of Earth Science; Kluwer Academic Publishers: Dordrecht, The Netherlands, 1999; pp. 6–9. ISBN 978-0-412-74050-3.

47. Senapathi, V.; Chung, S.Y.; Lee, S.; Park, N. Assessment of river water quality via environmentric multivariate statistical tools and water quality index: A case study of Nakdong River Basin, Korea. *Carpathian J. Earth Environ. Sci.* **2014**, *9*, 125–132.

48. Specifications FAO. *FAO Specifications and Evaluations for Agricultural Pesticides*; Food and Agriculture Organization of the United Nations (FAO): Rome, Italy, 2023.
49. Dinelli, E.; Lima, A.; Albanese, S.; Birke, M.; Cicchella, D.; Giaccio, L.; Valera, P.; De Vivo, B. Major and trace elements in tap water from Italy. *J. Geochem. Explor.* **2012**, *112*, 54–75. [CrossRef]
50. Han, Z.; An, W.; Yang, M.; Zhang, Y. Assessing the impact of source water on tap water bacterial communities in 46 drinking water supply systems in China. *Water Res.* **2020**, *172*, 115469. [CrossRef] [PubMed]
51. Azoulay, A.; Garzon, P.; Eisenberg, M.J. Comparison of the mineral content of tap water and bottled waters. *J. Gen. Intern. Med.* **2001**, *16*, 168–175. [CrossRef] [PubMed]
52. Berenzen, N.; Lentzen-Godding, A.; Probst, M.; Schulz, H.; Schulz, R.; Liess, M. A comparison of predicted and measured levels of runoff-related pesticide concentrations in small lowland streams on a landscape level. *Chemosphere* **2005**, *58*, 683–691. [CrossRef] [PubMed]
53. Madej, M.; Kochana, J.; Baś, B. Determination of viloxazine by differential pulse voltammetry with boron-doped diamond electrode. *Monatsh Chem.* **2019**, *150*, 1655–1665. [CrossRef]
54. Gharous, M.; Bounab, L.; Pereira, F.J.; Choukairi, M.; López, R.; Aller, A.J. Electrochemical Kinetics and Detection of Paracetamol by Stevensite-Modified Carbon Paste Electrode in Biological Fluids and Pharmaceutical Formulations. *Int. J. Mol. Sci.* **2023**, *24*, 11269. [CrossRef] [PubMed]

Appendix 2

Molecularly imprinted co-polymer for class-selective electrochemical detection of macrolide antibiotics in aqueous media

Vu Bao Chau Nguyen [a], Akinrinade George Ayankojo [a], Jekaterina Reut [a], Jörg Rappich [b], Andreas Furchner [c], Karsten Hinrichs [d], Vitali Syritski [a,*]

[a] *Department of Materials and Environmental Technology, Tallinn University of Technology, Ehitajate tee 5, 19086 Tallinn, Estonia*
[b] *Helmholtz-Zentrum Berlin für Materialien und Energie GmbH, Institut für Silizium-Photovoltaik, Kekuléstr. 5, 12489 Berlin, Germany*
[c] *Helmholtz-Zentrum Berlin für Materialien und Energie GmbH, Division Energy and Information, Schwarzschildstraße 8, 12489 Berlin, Germany*
[d] *Leibniz-Institut für Analytische Wissenschaften - ISAS - e.V., Department Berlin, Schwarzschildstraße 8, 12489 Berlin, Germany*

ABSTRACT

This work demonstrates the determination of macrolide antibiotics in aqueous environments using a screen-printed electrode (SPE) combined with a molecularly imprinted polymer (MIP) prepared from dual functional monomers. By employing the reversible covalent interactions between diols of macrolide and boronic acids of 3-aminophenylboronic acid (APBA) as well as the noncovalent interactions between macrolide and m-phenyl-enediamine (mPD), a dual recognition involving the central macrocyclic lactone exclusive to all macrolides was successfully achieved, thus permitting the possible broad recognition of individual members of the class. The prepared macrolide MIP (mMIP) was characterised by electrochemical and ellipsometric measurements. Following optimization, the sensor demonstrated about four times better recognition for macrolides, including erythromycin (Ery), clarithromycin (Cla), and azithromycin (Azi), than its non-imprinted reference. In addition, low analytical limits were achieved (LOD 1.1–1.6 nM and LOQ 3.8–5.3 nM). Moreover, an excellent selectivity was displayed towards the macrolides in both buffer and tap water samples, and a good recovery (93–108%) of the analytes was achieved. The analytical approach described herein could be further developed as a portable sensing device capable of on-site monitoring of macrolides in environmental water.

1. Introduction

Water pollution is a well-known global challenge that threatens human and animal health. Although it is estimated that most people have access to safe drinking water, increasing reports about the presence of harmful contaminants in tap water samples from different parts of the world make water pollution more alarming [1]. This situation is worsened by the increasing usage and escape of antibiotic molecules into the aqueous environment, culminating in the prevalence of antibiotic resistance [2–4]. Antibiotics have become one of the most frequently prescribed medicines in the last few decades. Between 2000 and 2015, global antibiotic consumption climbed by 65%, and antimicrobial resistance is predicted to cause about 10 million deaths per year by 2050 [5,6]. Also, the European Antimicrobial Resistance Surveillance Network (EARS-Net) data estimate that EU/EEA countries' healthcare systems spend about USD PPP 1.5 billion each year treating more than 670,000 infections caused by antibiotic-resistant bacteria.

Unfortunately, it is reported that approximately 33,000 deaths annually are due to these infections [7,8].

Many reports demonstrate that most antibiotics that reach the municipal wastewater treatment plants are incompletely eliminated during the treatment process and are consequently released into the environment [9–11]. Moreover, trace amounts of antibiotics in drinking water have also been reported [12,13]. Among the antibiotics commonly found in aqueous ecosystems, macrolides including erythromycin (Ery), clarithromycin (Cla), and azithromycin (Azi) are identified, hence their continual inclusion in the EU surface water watch list of emerging pollutants [14]. This is due to their wide usage in human and veterinary medicines [15]. Also, a growing number of reports demonstrate that certain bacterial strains develop genetic mutations after exposure to macrolides, albeit at a low concentration [16].

For decades, traditional methods such as high-performance liquid chromatography [17], atomic absorption spectroscopy [18], mass spectrometry [19], enzyme-linked immunosorbent assay [20], and

biosensors [21], etc. were commonly used for detecting antibiotics from environmental water. However, these techniques require expensive instrumentation, well-trained operators, and the use of unstable natural receptors (e.g., in biosensors). Moreover, since the analysis of macrolides in water presents significant challenges due to their existence at very low concentrations, portable and highly sensitive sensor devices that can outperform traditional analytical methods are still in high demand [22,23].

Molecularly imprinted polymers (MIPs) are functional materials with target-driven molecular recognition capable of mimicking biological receptors in discriminating between molecules but outperforming them in environmental stability and preparation cost [24]. MIPs have been shown as prospective materials for many analytical applications, including selective separation, purification, and chemical sensors [25]. Acting as a synthetic recognition element, MIP combined with an inexpensive and disposable sensor chip such as a screen-printed electrode (SPE) represents a potential for constructing a portable electrochemical sensor platform for rapid and accurate in-situ environmental analysis [26,27]. Thus, numerous publications detailing the integration of MIPs with SPEs have been reported for a wide variety of antibiotics [28–30]. Similarly, several research papers have illustrated the use of MIP-based sensors for the determination of a single individual member of macrolide antibiotics, especially Ery, Cla, and Azi [31–33]. Notwithstanding, fabricating a single sensor device capable of antibiotic class recognition could be more beneficial for daily routine macrolide monitoring in environmental water [31]. However, such sensors which could be formulated either by an array of MIPs or by carefully selecting a template or surrogate molecule that would induce the generation of binding cavities possessing a high affinity for all class members [34,35], are scarcely presented. In our previous research, the noncovalent imprinting strategy where hydrogen bonds were formed between Ery and a computationally-assisted selected functional monomer, mPD, was intended to fabricate MIP-based sensors for macrolide determination [31]. Although the sensor shows an excellent performance towards Ery, it failed in analysing other macrolides, including Cla and Azi, despite their close structural similarity.

To overcome this limitation, the fabrication of a class-selective MIP capable of recognizing a group of closely related compounds rather than one constituent becomes imperative. Such an approach was first reported for detecting amphenicol antibiotics in food samples [36]. It has also been reported that applying a single template to synthesise class-selective MIP helped maximise time efficiency and save costs by reducing the number of required templates in the preparation stage compared to the multi-template synthesis approach [37]. In environmental waters, all antibiotic pollutants, including macrolides, coexist at varying concentrations; thus, the possibility of a class-selective detection would be of great significance to environmental monitoring.

This study aims to prepare macrolide-selective MIP (mMIP) on a disposable electrochemical sensor platform – SPE – that would be capable of determining Ery, Cla, and Azi as representative macrolide antibiotics in tap water. To ensure a macrolide class selective detection, we adopt a dual molecular recognition using a combination of covalent and noncovalent interactions with Ery, a selected macrolide template molecule.

2. Experimental

2.1. Chemicals and materials

All used chemicals, besides acetic acid given by Lach-ner, were purchased from Sigma. The chemicals were received and stored under standard conditions. The aqueous solutions were dissolved completely with ultrapure water (resistivity 18.2 MΩ cm at 25 °C, Merck KGaA, Darmstadt, Germany). The synthesis and analyte solutions were prepared in phosphate-buffered saline (PBS) (0.01 M, pH 7.4). All electrochemical measurements were conducted in a 1 M KCl solution containing 4 mM redox probe $K_3[Fe(CN)_6]/K_4[Fe(CN)_6]$. SPEs were ordered from BVT technologies, a.s. in the Czech Republic and included a 1 mm diameter circular gold working electrode (Au WE), a gold counter electrode, and silver coated by AgCl as the reference electrode to which all potentials were quoted. To perform all electrochemical measurements, SPEs were connected to an electrochemical workstation (Reference 600, Gamry Instruments, USA).

2.2. Sensor preparation

The mMIP sensor was prepared by the electrodeposition of an mMIP film on the Au WE surface of SPE. Prior to the electrodeposition, the Au WE of the SPE was activated in 0.1 M sulfuric acid solution, cycling the potential between 0.1 and 1.15 V at a scan rate of 100 mV/s for 15 cycles, followed by washing in ultrapure water and drying under a nitrogen atmosphere. Co-polymer of mPD and APBA, poly(mPD-co-APBA), was synthesised at the constant potential of 0.5 V (see Section 3.2) in a set-up where the electrodes of the SPE were exposed to a PBS containing the monomers, mPD and APBA, at the determined optimal concentrations. Similarly, the poly(mPD-co-APBA) film containing Ery, poly(mPD-co-APBA)-Ery, was synthesised under the same condition but including Ery in the pre-polymerization solution. Molecular imprints of Ery were generated within poly(mPD-co-APBA)-Ery by immersing the modified electrode in a 5% acetic acid solution for 30 min to remove Ery, resulting in mMIP formation. Poly(mPD-co-APBA) was similarly treated to generate a reference of non-imprinted polymer (NIP) film.

To ensure equal thickness between mMIP and NIP films, the charges passed through the working electrode during electrosynthesis were correlated to the thickness determined by spectroscopic ellipsometry (SE 850, Sentech Instruments GmbH, Berlin, Germany) from Ψ and Δ measurements between 370 and 800 nm at incidence angles of 50°, 60° and 70°. Further details of the set-up and method can be found in [38].

The sensor preparation stages were characterised by cyclic voltammetry (CV) and electrochemical impedance spectroscopy (EIS) in a 1 M KCl solution containing 4 mM redox probe $K_3[Fe(CN)_6]/K_4[Fe(CN)_6]$. CV was achieved by cycling the potential between 0 and 0.5 V at a scan rate of 50 mV/s, while EIS measurement was performed at an alternating potential with an amplitude 10 mV and frequency range of 0.1–100 kHz.

2.3. Evaluation of sensor performance

The performance of the sensor was studied by electrochemical analysis using differential pulse voltammetry (DPV) in a 1 M KCl solution containing 4 mM redox probe ($K_3[Fe(CN)_6]/K_4[Fe(CN)_6]$) at a potential range of 0–0.4 V, pulse amplitude of 25 mV, a pulse width of 0.1 s, a sample period of 0.5 s and a step potential of 5 mV. The sensor monitors the changes in charge transfer between Au WE of the SPE and redox probe ions ($[Fe(CN)_6]^{3-}/[Fe(CN)_6]^{4-}$) via the imprinting cavities created within the polymer. Following sensor incubation for 15 min in PBS-containing analyte solution, the charge transfer would be greatly hindered by the analyte molecules bound to the imprinted cavities of mMIP, thereby resulting in a concentration-dependent suppression of the DPV current peak. This suppression is defined as the sensor response and expressed as follows:

$$I_n = (I_0 - I)/I_0 \qquad (1)$$

where I_0 and I are the current peak values measured by DPV after incubation in PBS without and with the target analyte, respectively. All analyte solutions were prepared in PBS (pH 7.4) except otherwise stated, in which case the pH was adjusted to the desired value using drops of either 1 M HCl or 1 M NaOH.

The limits of detection (LOD) and quantification (LOQ) were determined from the linear regression of the sensor's response to low concentrations of the analyte in PBS, using Eqs. (2) and (3):

$$LOD = 3 \bullet SD/b \qquad (2)$$

$$LOQ = 10 \bullet SD/b \qquad (3)$$

where *SD* and *b* are the standard deviation of the residual and the slope of the regression line, respectively.

The selectivity of the sensor was evaluated by comparing the sensor's response upon rebinding of macrolides and other interfering antibiotics, including ciprofloxacin (Cipro), sulfamethizole (SMZ), and amoxicillin (AMO), at the same concentrations. Similar experiments were conducted in tap water spiked with the desired analyte concentrations. For this purpose, tap water samples were collected from Tallinn University of Technology water supply line and used without further treatment.

3. Results and discussion

3.1. Rational design of the class-selective mMIP

The recognition properties of mMIP are highly dependent on the chemical interactions formed between the target molecule and the functional monomers at the pre-polymerization stage that are subsequently memorised and retained by the formed polymer [39]. The double recognition approach used in this work is achieved by combining covalent and noncovalent strategies. The covalent strategy aims at forming a reversible interaction between the 1,2-diols moiety of the macrocyclic lactone unique to all macrolide antibiotics and the boronic

acid group of functional monomers such as APBA. This interaction is well known and has been employed in preparing several sensors for various analytes [40–44]. Herein, this reversible covalent interaction was confirmed between Ery and APBA by nuclear magnetic resonance spectroscopic measurements carried out in solutions of individual molecules as well as their mixture (see section S1). In addition, the non-covalent strategy adopts the previously established hydrogen bonds between Ery and mPD as complementary recognition centres to further enhance macrolide selective recognition [31]. The scheme showcasing the chemical interactions between macrolide (e.g Ery) and the monomers (APBA and mPD) is depicted in Fig. S1.

3.2. Synthesis and characterization of class-selective mMIP

The co-polymerization of the selected functional monomers, mPD and APBA, in the presence of Ery was initiated electrochemically. To determine the electrochemical potential for the synthesis of the co-polymer poly(mPD-co-APBA), while at the same time avoiding unwanted oxidation of the template molecules during electro-polymerization, CV measurements were carried out (Fig. 1a). The CV scans show that the oxidation of mPD and APBA start at a potential of about 0.2 V and 0.4 V, respectively. The close oxidation potentials of mPD and APBA make it plausible to generate a co-polymer with the two monomers since their electrochemically generated radical cations could
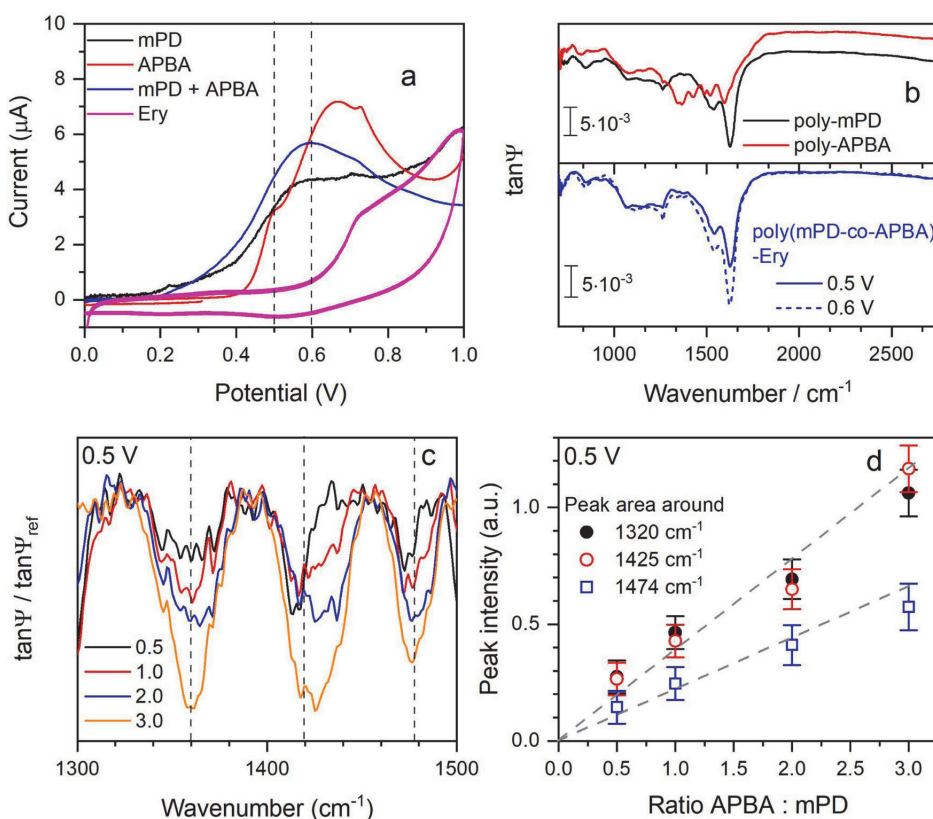
Fig. 1. (a) Cyclic voltammetry of the gold electrode recorded at a scan rate of 100 mV/s in the presence of 5 mM mPD, 5 mM APBA, mixture of 5 mM mPD and 5 mM APBA or 5 mM Ery. (b) IRSE spectra of poly-mPD and poly-APBA layer (top) and co-polymer poly(mPD-co-APBA) polymerised at 0.5 V and 0.6 V (bottom, baseline corrected to visualise the difference). (c) IRSE spectra of poly(mPD-co-APBA) polymerised at 0.5 V from the different molar ratio of APBA to mPD. (d) Calibration graph of integrated IRSE peak intensities vs. APBA:mPD ratio. (c) and (d) were obtained after normalisation to poly-mPD spectra and baseline corrected for a better visualisation of the bands evolution with increasing amount of APBA in the electrolyte.

combine to propagate the chain growth [45]. Thus, the oxidation of both monomers in their solution mixture at a potential starting from 0.4 V is expected. However, since at 0.6 V, the onset of Ery oxidation already appears (Fig. 1a), the electropolymerization potential of the co-polymer should be selected in the range of 0.4 – 0.6 V. Nevertheless, for the rational choice of electrodeposition potential, possible changes in the vibrational signatures between polymer films synthesised using either 0.5 or 0.6 V were analysed by IRSE. As observed in Fig. 1b, both layers show no pronounced differences, but rather a slight increase in the thickness of the film synthesised at 0.6 V was observed. Therefore, to

ensure the formation of poly(mPD-co-APBA)-Ery without interfering with the possible oxidation of Ery molecules, electrodeposition of the co-polymer film was carried out using a constant potential of 0.5 V. Furthermore, the tan Ψ spectra of poly-mPD and poly-APBA are similar with a slight difference in the spectral range between 1300 and 1500 cm^{-1} as can be seen in Fig. 1b (top) [46,47]. Therefore, we focus on the IRSE measurements within this spectral range to confirm poly (mPD-co-APBA) formation while using solutions containing different molar ratios of APBA and mPD for the electropolymerization process. The spectra in Fig. 1c shows 3 APBA-related absorption bands at about
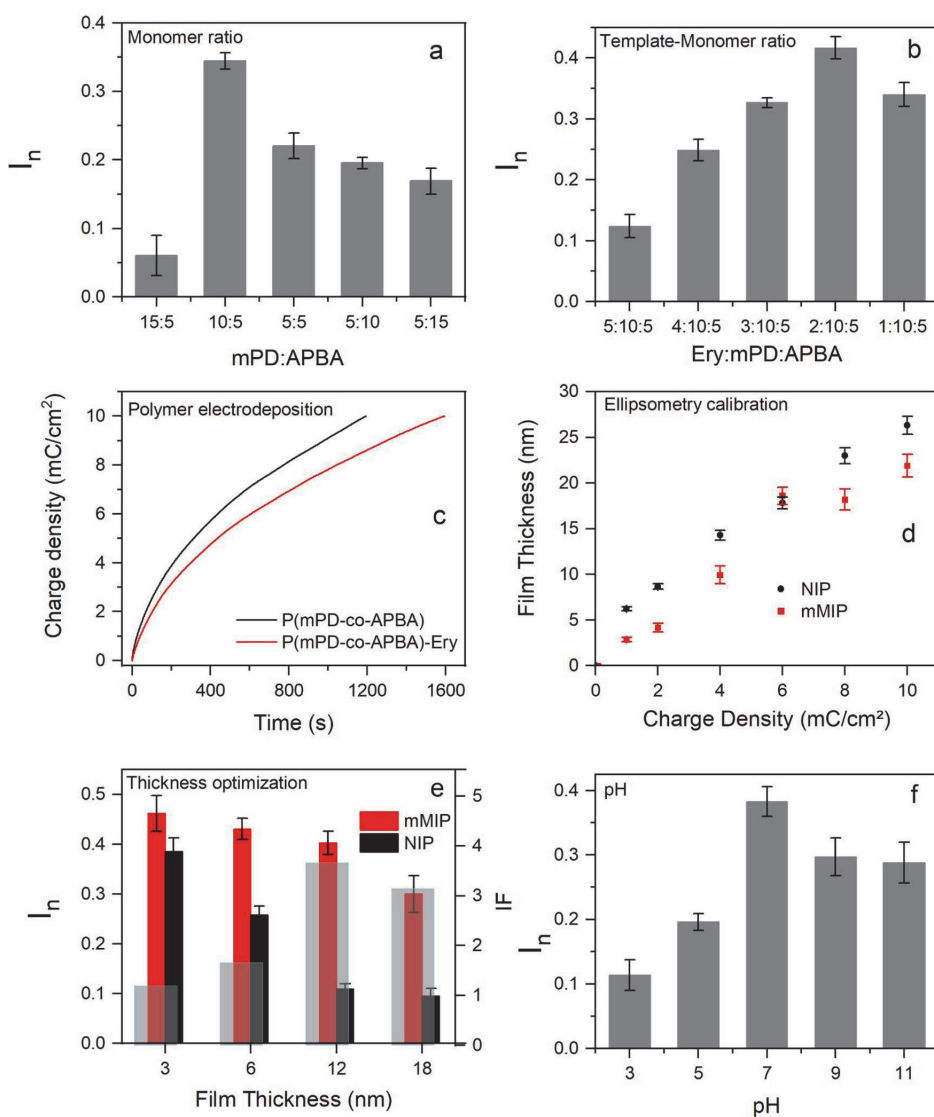

Fig. 2. Optimization of mMIP preparation. Responses of mMIP-modified SPE upon incubation in 40 μM Ery solution in PBS, MIPs were prepared using: (a) different mPD: APBA ratios, (b) different Ery concentrations while keeping mPD and APBA concentrations at 10 and 5 mM, respectively. (c) Charge-time dependences of poly (mPD-co-APBA) and poly(mPD-co-APBA)-Ery electrodeposition on Au of the SPE until the charge density reaches 10 mC/cm². (d) Calibration graph obtained from spectroscopic ellipsometry measurements correlating the thickness of mMIP and NIP films to the amount of charge used during electrodeposition. (e) mMIP and NIP based sensors' responses upon rebinding of 40 μM Ery solution in PBS. (f) Responses of mMIP-based sensor upon incubation in 40 μM Ery solution in PBS of different pH values.

1320 cm^{-1}, 1425 cm^{-1}, and 1475 cm^{-1} that increase in intensity with the increasing amount of APBA in the solution. Moreover, the integrated IRSE peak intensities plotted as a function of the APBA:mPD ratio (Fig. 1d) demonstrate a linear increase of the amount of poly-APBA incorporated in the co-polymer with increasing APBA:mPD ratio.

To monitor mMIP formation on the sensor surface, CV and EIS measurements were performed to associate each modification stage with the observed changes in charge transfer between the redox pair and the Au WE surface. Following electrodeposition of poly(mPD-co-APBA)-Ery, the anodic and cathodic current peaks of CV suffer significant depression (Fig. S3a), indicating the formation of a non-conducting film that obstructs charge transfer at the electrode/solution interface. However, after acetic acid treatment, a substantial recovery of the peaks was observed, suggesting the increased permeability of the polymer layer to the redox probe ions via the imprinted cavities formed after the removal of entrapped Ery molecules from the polymer; hence, mMIP formation. Similar behaviour is observed in EIS spectra (Fig. S3b) where the semi-circle diameter, which corresponds to the charge transfer resistance (R_{ct}) greatly increased after electrodeposition (Table S1), followed by a subsequent decrease after treatment in acetic acid to form mMIP. Furthermore, to confirm the formation of Ery-induced imprints in the polymer, the preparation of the reference sensor (NIP) was subjected to similar CV and EIS measurements. It was noted that while poly(mPD-APBA) formation resulted in similar depression of CV current peaks and increase in EIS R_{ct}, treatment with acetic acid yielded much less changes in the measured parameters thus validating the suggestion that the removal of Ery from poly(mPD-co-APBA)-Ery film resulted in the observed increase in charge transfer via the imprinted cavities created in the polymer. Moreover, after the adsorption of 1.6 µM Ery on mMIP a much more significant change is observed in both CV voltammogram and EIS R_{ct} value on the mMIP as compared to the NIP (see Table S1), indicating an enhanced adsorption of the target on the mMIP based sensor. Furthermore, scanning electron microscopic analyses revealed morphological differences between the bare and polymer film modified electrodes as well as between mMIP and NIP (See section S3).

3.2.1. Effect of the monomer to template ratio

The MIP-based sensor's performance could be affected by the molar ratio of template to monomers used during the imprinting stage. Thus, to enhance mMIP performance, we optimised first the molar ratio of mPD to APBA and then the molar ratio of template to monomers. As shown in Fig. 2a, mMIP prepared with 10 mM mPD and 5 mM APBA exhibited the highest sensor response. To achieve the optimal concentration ratio of template to monomers, the sensor's response following incubation in PBS containing an increasing concentration of Ery (1 – 5 mM) and a fixed amount of mPD and APBA, 10 and 5 mM, respectively, were studied. Fig. 2b indicates an increasing response with decreasing Ery concentration from 5 to 2 mM, followed by a decline with a lower concentration. These results further established that a too high ratio of functional monomers to templates is not beneficial for molecular imprinting. Moreover, it has been demonstrated that such arrangement usually leads to an increase in non-specific interactions, whereas too low ratios result in fewer complexation events because of insufficient chemical interactions with the template [48]. Thus, the optimal molar concentration ratio of Ery:mPD:APBA required to prepare an mMIP-based sensor for macrolide determination was derived as 2:10:5 mM and was used in further experiments.

3.2.2. Effect of mMIP thickness

The thickness of a MIP layer is critical to the performance of a MIP-based sensor and is also significant in ensuring its reproducibility and accurate analysis. Thus, to synthesise a mMIP with an optimal thickness, poly(mPD-co-APBA)-Ery was electrodeposited by passing a required amount of electrical charge to the working electrode of the SPE. Notwithstanding, an accurate evaluation of MIP performance, especially on a label-free sensor platform, demands a reference polymeric material

– a non-imprinted polymer (NIP) – prepared using the same protocol as the MIP but in the absence of the template [29]. Accordingly, a NIP consisting of poly(mPD-co-APBA) was electrodeposited using the same charge density as for the mMIP. As seen in Fig. 2c, the growth rate for both films was sharp at the initial stage of electrosynthesis but gradually slowed down until a charge density of 10 mC/cm^2 was reached (100% current efficiency is assumed). The higher growth rate of poly (mPD-co-APBA) as compared to poly(mPD-co-APBA)-Ery is evident, indicating that the presence of Ery, an electrochemically inactive molecule, in the pre-polymerization solution slightly affects the growth of poly(mPD-co-APBA)-Ery by slowing down the oxidation of the monomers and the conductivity of the growing polymer chain. Thus more charges would be applied for mMIP to generate the same polymer thickness as the NIP. Therefore, to ensure an objective similarity in mMIP and NIP thicknesses, spectroscopic ellipsometry measurements were performed that calibrate the polymer thicknesses with respect to the amount of the electrical charge passing through the electrode [49]. The ellipsometric Ψ and Δ data were evaluated in SpectraRay 3 (Sentech) using an optical layer model of air/film/gold. We performed a multi-sample fit on the spectra of all mMIP (NIP) samples, which minimises the correlations between thicknesses and dielectric function of the polymer films, thus resulting in robust calibration curves even for thin films. Fig. 2d shows the thickness vs. charge density calibration plot for mMIP and NIP films deposited by applying charge densities ranging from 1 to 10 mC/cm^2. As seen, the thicknesses of mMIP and NIP films increase rather linearly with the applied charge; hence, their objective similarity could be obtained by using the charge densities that correspond to the same film thickness on the calibration graph (Table S2). Thus, to derive an optimal thickness for mMIP-based sensor preparation, the responses induced by 40 µM concentration of Ery on different thickness of mMIP- and NIP-based sensors were compared (Fig. 2e). As observed, the mMIP and NIP responses decrease with increasing thickness from 3 to 18 nm. However, at a thickness of 12 nm, the best performance of the mMIP relative to the NIP (Table S1) was achieved, as estimated from their relative response values, i.e., $I_n(mMIP)/I_n(NIP)$ where $I_n(mMIP)$ and $I_n(NIP)$ are the responses obtained from mMIP and NIP sensors respectively. Thus, for an accurate analysis of mMIP performance, a charge density of 5.0 mC/cm^2 and 3.7 mC/cm^2 were adopted for preparing mMIP and NIP films, respectively.

3.2.3. Effect of pH

The rebinding of a macrolide antibiotic to the prepared mMIP is expected to proceed through hydrogen bonding as well as the reversible covalent interaction between 1,2-diols moieties of macrolide and boronic acid groups of mMIP. It is known that the latter is pH-dependent; namely, the boronate ester linkage formation is favoured at pH> 7 and is cleaved under acidic conditions [50]. Thus, the effect of the pH of analyte solution on macrolide recognition by the mMIP sensor was studied. For this purpose, the sensor was incubated in aqueous solution containing 40 µM Ery at different pH values (3−11), and their responses were measured (Fig. 2f). The sensor response increased with increasing pH achieving its maximal value at pH 7 and then slightly decreased. The increase in sensor response from pH 3–7 can be explained based on the consideration of the influence of pH on the interaction between boronic acid and diols. At a low pH the interaction is less likely to occur, resulting in lower binding of Ery to the mMIP and consequently lower sensor response, whereas the interaction becomes more favourable with increasing pH hence, the sensor response becomes more significant due to an enhanced binding of the analyte on the mMIP modified sensor.

Although a further increase in response with pH above 7 could be generally expected for the interaction involving a boronic acid and diol, the substantial amount of noncovalent interactions involved in the molecular recognition of mMIP is assumed to have contributed to the slight decrease in sensor response at pH> 7. Moreover, a previous report has advised against the generalisation of the binding constants of

boronic acid and diols and that each situation should be examined on a case-by-case experimental study [51]. In addition, a previous report has indicated that the rebinding of macrolide i.e azithromycin on a MIP-based sensor could be achieved at a pH of 7 [50]. Thus, the solution with a pH of around 7 can be considered optimal for macrolide analysis with the prepared mMIP sensor. Fortunately, a pH value close to 7 is even more beneficial for this research since environmental water usually exists at the pH ranging from 6.5 to 8.5 [52,53].

3.3. Evaluation of sensor performance

3.3.1. Rebinding study

To evaluate the performance of the sensor towards macrolides recognition, its response to three representative members of the class, including Ery, Cla, and Azi were studied. These three antibiotics are included in the EU watch list of environmental pollutants [14]; hence, their detection is crucial. After incubation in increasing concentration of each analyte, the sensor's responses were recorded and plotted as adsorption isotherms (Fig. 3(a-c)). As seen, the sensor showed similar adsorption profiles to the three macrolides, and the Langmuir–Freundlich (LF) model provides accurate fits to the experimental data (see section S5 for details) indicating a heterogeneous character of the binding sites created within the polymer layer [54].

We estimated the rebinding performance of mMIP-modified sensors relative to NIP by comparing their responses at saturation (I_{max}). The mMIP-based sensor signalled about a 4-fold higher response (3.8, 3.5 and 4.4 for Ery, Cla and Azi, respectively) than the NIP-based reference (Tables S3–S5). Since the NIP differs from the mMIP only in the exclusion of Ery during polymerization, such a significant difference in their responses could mainly arise from the pre-formed binding cavities created within the mMIP that ultimately defined its enhanced analyte recognition.

Additionally, the sensor's performance at a low analyte concentration range was studied by recording the sensor's response to sub-nanomolar concentrations of each macrolide. As shown in Fig. 3d, the response increases linearly with the analyte concentrations up to about 20 nM. The parameters obtained from the linear regression of their responses (Table S6) are utilised in computing the limits of detection (LOD) and quantification (LOQ) using Eqs. (2) and (3), respectively. As seen, the LOD and LOQ are within the range of ca. 1–2 nM and 4–5 nM, respectively, indicating a significant improvement over previously reported MIP-based electroanalytical sensors (Table S7) for macrolide antibiotic detection.

3.3.2. Selectivity study

Three antibiotic candidates, including amoxicillin (AMO), ciprofloxacin (Cipro), and sulfamethizole (SMZ) (See Fig. S6 for detailed structures) belong to different antibiotic classes such as penicillins, fluoroquinolones, and sulfonamides, respectively, which were chosen to test the sensor's selectivity. These choices stem from their broad prescription and the possibility of being used in place of, or in combination with, macrolides, thus suggesting their coexistence with the targets in the same environment.

Fig. 4 shows the response induced by individual antibiotics at a concentration of 40 μM. Clearly, the mMIP-based sensor demonstrates much higher responses towards the three macrolides (Ery, Clari, and Azi) than other molecules (Cipro, Amo, SMZ). Although the NIP also shows higher responses towards macrolides than interferents, the
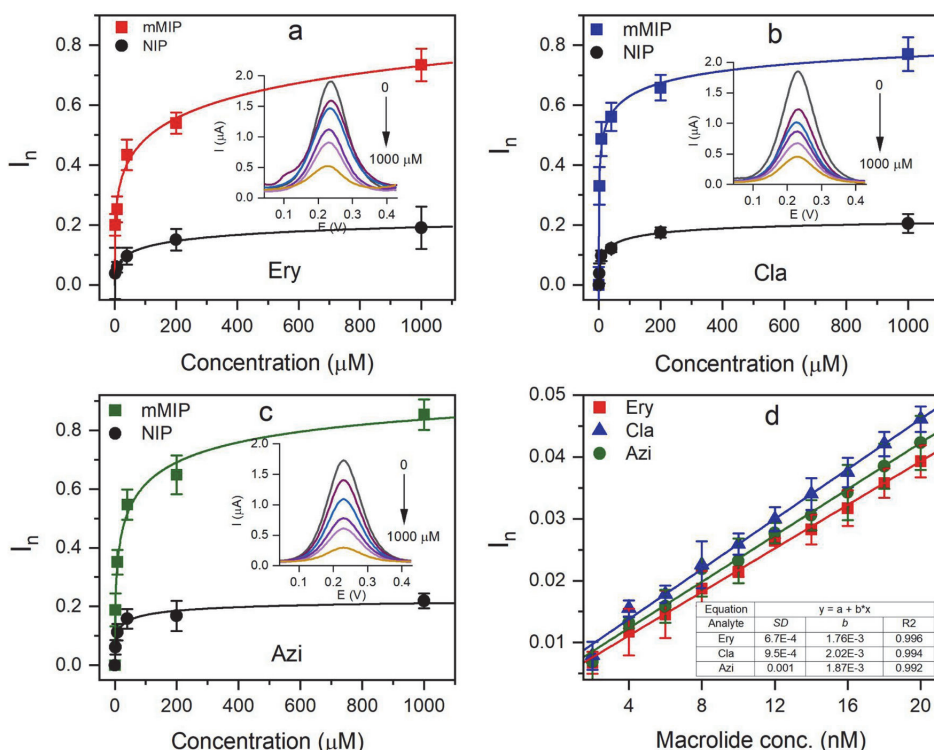

Fig. 3. (a-c) Adsorption isotherms of mMIP- and NIP-based sensors towards increasing Ery, Cla and Azi concentrations (1.6, 8, 40, 200 and 1000 μM). Solid lines represent fits to Langmuir–Freundlich (LF) isotherm and insets are the DPV voltammograms induced on mMIP-based sensors; (d) Performance of mMIP/SPE sensor at low analyte concentration (2–20 nM). The solid lines are linear regression fits.
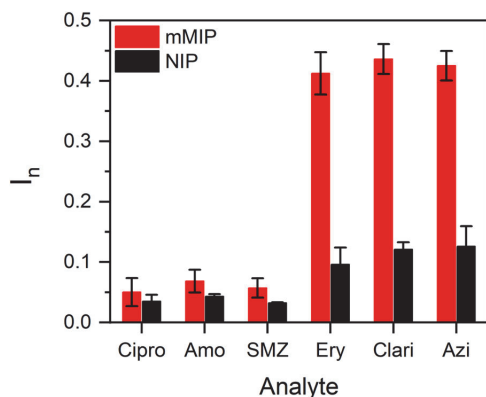
Fig. 4. mMIP- and NIP-based sensor responses obtained upon incubating in 40 μM concentration of individual antibiotics (Cipro, AMO, SMZ, Azi, Clari, and Ery) in PBS.

responses are about four times lower than those on mMIP. Moreover, the responses of both mMIP- and NIP-based sensors towards Cipro, Amo, and SMZ are either comparable or are less significantly different. To further quantify the selective properties, the selectivity coefficient *k*, was calculated (See Table S8). The mMIP based sensor preferably binds macrolides as compared to other antibiotics giving selectivity coefficient of an average of 3. These observations reveal that the imprints created within mMIP confer selectivity towards macrolides. Hence, the sensor's response could be less impeded by the presence of other antibiotics.

Tap water contains mainly dissolved ions such as bicarbonate, sulphate, fluoride, calcium, and various minerals such as sodium, potassium, manganese as well as trace amounts of other compounds that meet the drinking water quality standards [55,56]. Thus, tap water can be considered a sufficiently complex matrix for the selectivity study and was therefore spiked with the required amount of each analyte to prepare the sample solutions. Fig. 5a indicates that the sensor clearly distinguishes between the recognition of macrolides and other molecules. Whereas increasing concentrations of interfering analytes do not yield a significant increase in response, the rising amount of each macrolide induced a corresponding growth in the sensor's response. Thus, the sensor's selective property is preserved even in tap water, and the presence of other molecules, notwithstanding the concentration, may not appreciably affect the performance of the sensor in the intended media.

Moreover, we considered it interesting to study the sensor's response following exposure to an aqueous solution containing a mixture of macrolides. Thus, tap water spiked with an equimolar mixture of Ery, Clari, and Azi (0.013, 0.07 or 0.33 μM) amounting to a total concentration of either 0.04, 0.21 or 1 μM respectively were prepared, and the induced responses were analysed. As shown in Fig. 5b, the responses generated by the mixtures are comparable with those caused by individual macrolides at the same concentration (differences range from 3% to 10%). This observation more likely suggests that the sensor selectively recognizes the parent macrocyclic lactone central to all macrolides, thereby crediting the significance of the imprinting strategy.

Additionally, the recoveries of the analytes were examined in tap water fortified with different concentrations of each macrolide. As presented in Table S9, the analytes show good recoveries ranging from 93% to 108%, thus indicating the sensor's adaptability for use in the intended media.

4. Conclusions

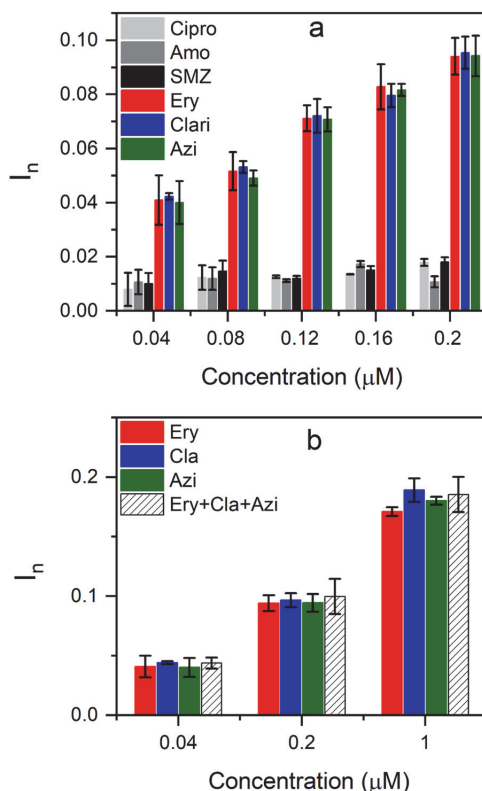This work demonstrates the use of an electrochemical sensor

Fig. 5. Responses of mMIP-based sensors upon incubation in tap water containing (a) increasing concentrations (0.04 – 0.2 μM) of different analytes cipro, Amo, SMZ, Ery, Cla, Azi and (b) 0.04, 0.2 and 1 μM concentrations of macrolides and their equimolar mixture. The solution mixtures were prepared in a way to obtain the required final macrolide molar concentrations.

modified with a class-selective MIP as the recognition element for determining macrolide antibiotics in aqueous solution. By selecting APBA and mPD as functional monomers, selective macrolide recognition is achieved by the synergistic effects of covalent and noncovalent interactions. Following careful optimization, the sensor exhibits appreciable recognition for macrolides, including Ery, Cla, and Azi, with low limits of detection (LOD is 1 – 2 nM) and quantification (LOQ is 4 – 5 nM). Importantly, the sensor demonstrated an impressive selectivity towards macrolides against interfering antibiotic compounds in buffer and tap water samples. Additionally, the sensor has excellent recovery from 93% to 108% in tap water, demonstrating its practical utility in the intended media. Thus, the described analytical approach could be further developed as a portable sensing device capable of on-site monitoring of macrolides in environmental water. However, to detect macrolides from other environmental water samples such as waste water from sewage treatment plants, where the highest concentration of azithromycin was found to be about 598 ng/L (or 0.8 nM) [9], the sensitivity of the sensor would need to be improved. This could be achieved, for example, by increasing the surface area of the mMIP layer using nanostructures, e.g., nanoparticles, nanospheres, or mesoporous structures [57–59].

CRediT authorship contribution statement

Vu Bao Chau Nguyen: Formal analysis, Investigation, Writing –

Declaration of Competing Interest

The authors declare that they have no known competing financial interests or personal relationships that could have appeared to influence the work reported in this paper.

Data availability

Data will be made available on request.

Acknowledgement

Appendix A. Supporting information

Supplementary data associated with this article can be found in the online version at doi:10.1016/j.snb.2022.132768.

References

[1] M. Kumar, P. Borah, P. Devi, Chapter 3 - Priority and emerging pollutants in water, in: P. Devi, P. Singh, S.K. Kansal (Eds.), Inorg. Pollut. Water, Elsevier, 2020, pp. 33–49, https://doi.org/10.1016/B978-0-12-818965-8.00003-2.

[2] S.A. Kraemer, A. Ramachandran, G.G. Perron, Antibiotic pollution in the environment: from microbial ecology to public policy, Microorganisms 7 (2019) 180, https://doi.org/10.3390/microorganisms7060180.

[3] A. Karkman, K. Pärnänen, D.G.J. Larsson, Fecal pollution can explain antibiotic resistance gene abundances in anthropogenically impacted environments, Nat. Commun. 10 (2019) 80, https://doi.org/10.1038/s41467-018-07992-3.

[4] M. Amarasiri, D. Sano, S. Suzuki, Understanding human health risks caused by antibiotic resistant bacteria (ARB) and antibiotic resistance genes (ARG) in water environments: Current knowledge and questions to be answered, Crit. Rev. Environ. Sci. Technol. 50 (2020) 2016–2059, https://doi.org/10.1080/10643389.2019.1692611.

[5] M.E.A. de Kraker, A.J. Stewardson, S. Harbarth, Will 10 million people die a year due to antimicrobial resistance by 2050, e1002184–e1002184, PLoS Med 13 (2016), https://doi.org/10.1371/journal.pmed.1002184.

[6] E.Y. Klein, T.P. Van Boeckel, E.M. Martinez, S. Gandra, S.A. Levin, H. Goossens, R. Laxminarayan, Global increase and geographic convergence in antibiotic consumption between 2000 and 2015, Proc. Natl. Acad. Sci. 115 (2018), E3463, https://doi.org/10.1073/pnas.1717295115.

[7] A. Cassini, L.D. Högberg, D. Plachouras, A. Quattrocchi, A. Hoxha, G.S. Simonsen, M. Colomb-Cotinat, M.E. Kretzschmar, B. Devleesschauwer, M. Cecchini, D. A. Ouakrim, T.C. Oliveira, M.J. Struelens, C. Suetens, D.L. Monnet, R. Strauss, K. Mertens, T. Struyf, B. Catry, K. Latour, I.N. Ivanov, E.G. Dobreva, A. Tambic Andraševic, S. Soprek, A. Budimir, N. Paphitou, H. Žemličková, S. Schytte Olsen, U. Wolff Sönksen, P. Märtin, M. Ivanova, O. Lyytikäinen, J. Jalava, B. Coignard, T. Eckmanns, M. Abu Sin, S. Haller, G.L. Daikos, A. Gikas, S. Tsiodras, F. Kontopidou, Á. Tóth, Á. Hajdu, Ó. Guólaugsson, K.G. Kristinsson, S. Murchan, K. Burns, P. Pezzotti, C. Gagliotti, U. Dumpis, A. Liuimiene, M. Perrin, M.A. Borg, S. C. de Greeff, J.C. Monen, M.B. Koek, P. Elstrøm, D. Zabicka, A. Deptula, W. Hryniewicz, M. Caniça, P.J. Nogueira, P.A. Fernandes, V. Manageiro, G.

A. Popescu, R.I. Serban, E. Schréterová, S. Litvová, M. Štefkovicová, J. Kolman, I. Klavs, A. Korošec, B. Aracil, A. Asensio, M. Pérez-Vázquez, H. Billström, S. Larsson, J.S. Reilly, A. Johnson, S. Hopkins, Attributable deaths and disability-adjusted life-years caused by infections with antibiotic-resistant bacteria in the EU and the European Economic Area in 2015: a population-level modelling analysis, Lancet Infect. Dis. 19 (2019) 56–66, https://doi.org/10.1016/S1473-3099(18)30605-4.

[8] OECD, Stemming the Superbug Tide: Just A Few Dollars More, Organisation for Economic Co-operation and Development, Paris, 2018. https://doi.org/10.1787/9789264307599-en (accessed September 6, 2022).

[9] S. Rodriguez-Mozaz, I. Vaz-Moreira, S. Varela Della Giustina, M. Llorca, D. Barceló, S. Schubert, T.U. Berendonk, I. Michael-Kordatou, D. Fatta-Kassinos, J.L. Martinez, C. Elpers, I. Henriques, T. Jaeger, T. Schwartz, E. Paulshus, K. O'Sullivan, K.M. M. Pärnänen, M. Virta, T.T. Do, F. Walsh, C.M. Manaia, Antibiotic residues in final effluents of European wastewater treatment plants and their impact on the aquatic environment, Environ. Int. 140 (2020), 105733, https://doi.org/10.1016/j.envint.2020.105733.

[10] I. Senta, S. Terzic, M. Ahel, Occurrence and fate of dissolved and particulate antimicrobials in municipal wastewater treatment, Water Res 47 (2013) 705–714, https://doi.org/10.1016/j.watres.2012.10.041.

[11] P.A. Segura, M. François, C. Gagnon, S. Sauvé, Review of the Occurrence of Anti-infectives in Contaminated Wastewaters and Natural and Drinking Waters, Environ. Health Perspect. 117 (2009) 675–684, https://doi.org/10.1289/ehp.11776.

[12] V. de Jesus Gaffney, C.M.M. Almeida, A. Rodrigues, E. Ferreira, M.J. Benoliel, V. V. Cardoso, Occurrence of pharmaceuticals in a water supply system and related human health risk assessment, Occur. Fate Remov. Assess. Emerg. Contam Water Water Cycle Wastewater Drink. Water 72 (2015) 199–208, https://doi.org/10.1016/j.watres.2014.10.027.

[13] T. Meng, W. Cheng, T. Wan, M. Wang, J. Ren, Y. Li, C. Huang, Occurrence of antibiotics in rural drinking water and related human health risk assessment, Environ. Technol. 42 (2021) 671–681, https://doi.org/10.1080/09593330.2019.1642390.

[14] European Commission, Joint Research Centre, D. Napierska, I. Sanseverino, R. Loos, D. Marinov, T. Lettieri, Review of the 1st Watch List under the Water Framework Directive and recommendations for the 2nd Watch List, Publications Office, 2018. https://doi.org/10.2760/614367.

[15] T. Golkar, M. Zieliński, A.M. Berghuis, Look and outlook on enzyme-mediated macrolide resistance, Front. Microbiol. 9 (2018) 1942, https://doi.org/10.3389/fmicb.2018.01942.

[16] C. Fyfe, T.H. Grossman, K. Kerstein, J. Sutcliffe, Resistance to macrolide antibiotics in public health pathogens, Cold Spring Harb. Perspect. Med. 6 (2016), a025395, https://doi.org/10.1101/cshperspect.a025395.

[17] X. Lai, J. Liu, X. Xu, J. Li, B. Zhang, L. Wei, H. Cai, X. Cheng, Ultrasensitive high-performance liquid chromatography determination of tetracycline antibiotics and their 4-epimer derivatives based on dual effect of methanesulfonic acid, J. Sep. Sci. 43 (2019), https://doi.org/10.1002/jssc.201900618.

[18] I. Ketikidis, C.N. Banti, N. Kourkoumelis, C.G. Tsiafoulis, C. Papachristodoulou, A. G. Kalampounias, S.K. Hadjikakou, Conjugation of Penicillin-G with Silver(I) Ions Expands Its Antimicrobial Activity against Gram Negative Bacteria, Antibiotics 9 (2020), https://doi.org/10.3390/antibiotics9010025.

[19] T. Gallagher, S. Riedel, J. Kapcia, L.J. Caverly, L. Carmody, L.M. Kalikin, J. Lu, J. Phan, M. Gargus, M. Kagawa, S.W. Leemans, J.A. Rothman, F. Grun, J.J. LiPuma, K.L. Whiteson, Liquid Chromatography Mass Spectrometry Detection of Antibiotic Agents in Sputum from Persons with Cystic Fibrosis, e00927-20, Antimicrob. Agents Chemother. 65 (2021), https://doi.org/10.1128/AAC.00927-20.

[20] X. Wang, J. Li, D. Jian, Y. Zhang, Y. Shan, S. Wang, F. Liu, Paper-based antibiotic sensor (PAS) relying on colorimetric indirect competitive enzyme-linked immunosorbent assay for quantitative tetracycline and chloramphenicol detection, Sens. Actuators B Chem. 329 (2020), 129173, https://doi.org/10.1016/j.snb.2020.129173.

[21] A.R. Cardoso, L.P.T. Carneiro, G. Cabral-Miranda, M.F. Bachmann, M.G.F. Sales, Employing machinery for antibiotic detection: Using DNA gyrase for ciprofloxacin detection, Chem. Eng. J. 409 (2021), 128135, https://doi.org/10.1016/j.cej.2020.128135.

[22] M. Gama, C.B.G. Bottoli, Molecularly imprinted polymers for bioanalytical sample preparation, J. Chromatogr. B 1043 (2016), https://doi.org/10.1016/j.jchromb.2016.09.045.

[23] O.S. Ahmad, T.S. Bedwell, C. Esen, A. Garcia-Cruz, S.A. Piletsky, Molecularly Imprinted Polymers in Electrochemical and Optical Sensors, Trends Biotechnol. 37 (2019) 294–309, https://doi.org/10.1016/j.tibtech.2018.08.009.

[24] K. Haupt, P.X. Medina Rangel, B.T.S. Bui, Molecularly imprinted polymers: antibody mimics for bioimaging and therapy, Chem. Rev. 120 (2020) 9554–9582, https://doi.org/10.1021/acs.chemrev.0c00428.

[25] J.W. Lowdon, H. Diliën, P. Singla, M. Peeters, T.J. Cleij, B. van Grinsven, K. Eersels, MIPs for commercial application in low-cost sensors and assays – An overview of the current status quo, Sens. Actuators B Chem. 325 (2020), 128973, https://doi.org/10.1016/j.snb.2020.128973.

[26] Z. Taleat, A. Khoshroo, M. Mazloum-Ardakani, Screen-printed electrodes for biosensing: a review (2008–2013), Microchim. Acta 181 (2014) 865–891, https://doi.org/10.1007/s00604-014-1181-1.

[27] E. Costa-Rama, M.T. Fernández-Abedul, Paper-based screen-printed electrodes: a new generation of low-cost electroanalytical platforms, Biosensors 11 (2021), https://doi.org/10.3390/bios11020051.

[28] A.G. Ayankojo, J. Reut, V.B.C. Nguyen, R. Boroznjak, V. Syritski, Advances in detection of antibiotic pollutants in aqueous media using molecular imprinting

technique—a review, Biosensors 12 (2022) 441, https://doi.org/10.3390/bios12070441.

[29] A.G. Ayankojo, J. Reut, A. Öpik, V. Syritski, Sulfamethizole-imprinted polymer on screen-printed electrodes: Towards the design of a portable environmental sensor, Sens. Actuators B Chem. 320 (2020), 128600, https://doi.org/10.1016/j.snb.2020.128600.

[30] A.P.M. Tavares, M.H. de Sá, M.G.F. Sales, Innovative screen-printed electrodes on cork composite substrates applied to sulfadiazine electrochemical sensing, J. Electroanal. Chem. 880 (2021), 114922, https://doi.org/10.1016/j.jelechem.2020.114922.

[31] A.G. Ayankojo, J. Reut, V. Ciocan, A. Öpik, V. Syritski, Molecularly imprinted polymer-based sensor for electrochemical detection of erythromycin, Talanta 209 (2020), 120502, https://doi.org/10.1016/j.talanta.2019.120502.

[32] M.A. Abu-Dalo, N.S. Nassory, N.I. Abdulla, I.R. Al-Mheidat, Azithromycin-molecularly imprinted polymer based on PVC membrane for Azithromycin determination in drugs using coated graphite electrode, J. Electroanal. Chem. 751 (2015) 75–79, https://doi.org/10.1016/j.jelechem.2015.05.030.

[33] S. Mahmoudi, H. Rashedi, F. Faridbod, A molecularly imprinted polymer (MIP)-based biomimetic potentiometric sensing device for the analysis of clarithromycin, Anal. Bioanal. Electrochem. 10 (2018) 1654–1667.

[34] S. Wang, Y. She, S. Hong, X. Du, M. Yan, Y. Wang, Y. Qi, M. Wang, W. Jiang, J. Wang, Dual-template imprinted polymers for class-selective solid-phase extraction of seventeen triazine herbicides and metabolites in agro-products, J. Hazard. Mater. 367 (2018), https://doi.org/10.1016/j.jhazmat.2018.12.089.

[35] D. Tan, C. Han, Z. Yu, X. Sun, J. Chen, X. Dhanjai, D. Shao, Wang, Dummy molecularly imprinted polymers for class-selective extraction of amphetamine-type stimulants from alcoholic and nonalcoholic beverages, J. Chromatogr. A. 1663 (2022), 462759, https://doi.org/10.1016/j.chroma.2021.462759.

[36] X. Shi, S. Song, A. Sun, J. Liu, D. Li, J. Chen, Characterisation and application of molecularly imprinted polymers for group-selective recognition of molecules in food samples, Analyst 137 (2012) 3381, https://doi.org/10.1039/c2an35213c.

[37] E.N. Ndunda, B. Mizaikoff, Molecularly imprinted polymers for the analysis and removal of polychlorinated aromatic compounds in the environment: a review, Analyst 141 (2016) 3141–3156, https://doi.org/10.1039/C6AN00293E.

[38] K. Hinrichs, K.-J. Eichhorn (Eds.), Ellipsometry of Functional Organic Surfaces and Films, Springer Berlin Heidelberg, Berlin, Heidelberg, 2014, https://doi.org/10.1007/978-3-642-40128-2.

[39] A.G. Ayankojo, J. Reut, A. Öpik, A. Tretjakov, V. Syritski, Enhancing binding properties of imprinted polymers for the detection of small molecules, Proc. Est. Acad. Sci. 67 (2018) 138–146, https://doi.org/10.3176/proc.2018.2.04.

[40] F. Liu, X. Kan, Dual-analyte electrochemical sensor for fructose and alizarin red S specifically sensitive detection based on indicator displacement assay, Electrochim. Acta 319 (2019) 286–292, https://doi.org/10.1016/j.electacta.2019.07.001.

[41] G.T. Williams, J.L. Kedge, J.S. Fossey, Molecular boronic acid-based saccharide sensors, ACS Sens 6 (2021) 1508–1528, https://doi.org/10.1021/acssensors.1c00462.

[42] J.P. Sęk, S. Kaczmarczyk, K. Guńka, A. Kowalczyk, K.M. Borys, A. Kasprzak, A. M. Nowicka, Boronate-appended polymers with diol-functionalized ferrocene: an effective and selective method for voltammetric glucose sensing, Dalton Trans. 50 (2021) 880–889, https://doi.org/10.1039/D0DT03776A.

[43] Q. Zhao, H. Zhao, W. Huang, X. Yang, L. Yao, J. Liu, J. Li, J. Wang, Dual functional monomer surface molecularly imprinted microspheres for polysaccharide recognition in aqueous solution, Anal. Methods 11 (2019) 2800–2808, https://doi.org/10.1039/C9AY00132H.

[44] A.G. Ayankojo, R. Boroznjak, J. Reut, A. Öpik, V. Syritski, Molecularly imprinted polymer based electrochemical sensor for quantitative detection of SARS-CoV-2 spike protein, Sens. Actuators B Chem. 353 (2022), 131160, https://doi.org/10.1016/j.snb.2021.131160.

[45] H. Sarıarslan, E. Karaca, M. Şahin, N.Ö. Pekmez, Electrochemical synthesis and corrosion protection of poly(3-aminophenylboronic acid-co-pyrrole) on mild steel, RSC Adv. 10 (2020) 38548–38560, https://doi.org/10.1039/D0RA07311C.

[46] J.A. Faniran, H.F. Shurvell, Infrared spectra of phenylboronic acid (normal and deuterated) and diphenyl phenylboronate, Can. J. Chem. 46 (1968) 2089–2095, https://doi.org/10.1139/v68-341.

[47] X. Liu, X. Hu, Z. Xie, P. Chen, X. Sun, J. Yan, S. Zhou, In situ bifunctionalized carbon dots with boronic acid and amino groups for ultrasensitive dopamine detection, Anal. Methods 8 (2016) 3236–3241, https://doi.org/10.1039/C6AY00142D.

[48] K. Pratama, M. Manik, D. Rahayu, A. Nur Hasanah, Effect of the Molecularly Imprinted Polymer Component Ratio on Analytical Performance, Chem. Pharm. Bull. (Tokyo). 68 (2020) 1013–1024, https://doi.org/10.1248/cpb.c20-00551.

[49] A.G. Ayankojo, A. Tretjakov, J. Reut, R. Boroznjak, A. Öpik, J. Rappich, A. Furchner, K. Hinrichs, V. Syritski, Molecularly imprinted polymer integrated with a surface acoustic wave technique for detection of sulfamethizole, Anal. Chem. 88 (2016) 1476–1484.

[50] I.-A. Stoian, B.-C. Iacob, C.-L. Dudaş, L. Barbu-Tudoran, D. Bogdan, I.O. Marian, E. Bodoki, R. Oprean, Biomimetic electrochemical sensor for the highly selective detection of azithromycin in biological samples, Biosens. Bioelectron. 155 (2020), 112098, https://doi.org/10.1016/j.bios.2020.112098.

[51] G. Springsteen, B. Wang, A detailed examination of boronic acid–diol complexation, Tetrahedron 58 (2002) 5291–5300, https://doi.org/10.1016/S0040-4020(02)00489-1.

[52] A.K.M. Rahman, Study of the seasonal variations in Turag river water quality parameters, Afr. J. Pure Appl. Chem. 6 (2012), https://doi.org/10.5897/AJPAC12.023.

[53] V. Senapathi, S.Y. Chung, S. Lee, N. Park, Assessment of river water quality via environmentric multivariate statistical tools and water quality index: A case study of Nakdong River Basin, Korea, Carpathian J. Earth Environ. Sci. 9 (2014).

[54] R.J. Umpleby, S.C. Baxter, A.M. Rampey, G.T. Rushton, Y. Chen, K.D. Shimizu, Characterization of the heterogeneous binding site affinity distributions in molecularly imprinted polymers, Mol. Impr. Polym. Sep. Sci. 804 (2004) 141–149, https://doi.org/10.1016/j.jchromb.2004.01.064.

[55] R. Cidu, F. Frau, P. Tore, Drinking water quality: Comparing inorganic components in bottled water and Italian tap water, J. Food Compos. Anal. 24 (2011) 184–193, https://doi.org/10.1016/j.jfca.2010.08.005.

[56] H. Zhang, L. Xu, T. Huang, M. Yan, K. Liu, Y. Miao, H. He, N. Li, S. Raju, T. Cao, Combined effects of seasonality and stagnation on tap water quality: Changes in chemical parameters, metabolic activity and co-existence in bacterial community, J. Hazard. Mater. (2020), https://doi.org/10.1016/j.jhazmat.2020.124018.

[57] S. Motia, B. Bouchikhi, N. El Bari, An electrochemical molecularly imprinted sensor based on chitosan capped with gold nanoparticles and its application for highly sensitive butylated hydroxyanisole analysis in foodstuff products, Talanta 223 (2021), 121689, https://doi.org/10.1016/j.talanta.2020.121689.

[58] A. Kumar, P.K. Pathak, B.B. Prasad, Electrocatalytic Imprinted Polymer of N-Doped Hollow Carbon Nanosphere–Palladium Nanocomposite for Ultratrace Detection of Anticancer Drug 6-Mercaptopurine, ACS Appl. Mater. Interfaces 11 (2019) 16065–16074, https://doi.org/10.1021/acsami.9b02947.

[59] A.G. Ayankojo, J. Reut, A. Öpik, A. Furchner, V. Syritski, Hybrid molecularly imprinted polymer for amoxicillin detection, Biosens. Bioelectron. 118 (2018) 102–107, https://doi.org/10.1016/j.bios.2018.07.042.

Vu Bao Chau Nguyen received his first MSc in Biomedical Engineering from Ho Chi Minh University of Technology (Vietnam) in 2017. He received the second MSc in Materials Science from Tallinn University of Technology (Estonia) in 2021. Currently he is a full-time Ph.D. student in the Department of Materials and Environmental Technology at Tallinn University of Technology and his research focuses on synthesizing molecularly imprinted polymers (MIPs) having selectivity towards environmental pollutants and their integration with portable sensor platforms to develop cost-effective aquatic monitoring devices.

Akinrinade George Ayankojo is a research scientist at the Department of Materials and Environmental Technology in TalTech. He received his PhD (2018) in chemical and materials technology from TalTech and his MSc from the same department. His research interest includes the development of molecularly imprinted polymer-based sensors for small and large molecules of analytical interest.

Jekaterina Reut is currently a research scientist at the Department of Materials and Environmental Technology in TalTech. She received her PhD (2004) in the field of electrically conducting polymers from TalTech. Her research interest is in the area of the design and synthesis of molecularly imprinted polymers for biosensing applications.

Jörg Rappich received his PhD in Chemistry at the Free University of Berlin in 1989. Currently he is research scientist at the institute of Silizium-Photovoltaik at the Helmholtz-Zentrum Berlin für Materialien and Energie GmbH (HZB). His research interests include electrochemical surface functionalization of metals, semiconductors and carbon material by small molecules and thin polymeric layers. Furthermore, he's fascinated by in-situ investigations during electrochemical processing.

Andreas Furchner received his PhD in Physics at the Technische Universät Berlin in 2014. His research is on the study of thin films and functionalized surfaces by polarized infrared spectroscopy, including IR laser ellipsometry, IR Mueller-matrix polarimetry, in situ IR ellipsometry, hyperspectral amplitude–phase imaging, quantitative thin film analysis, and optical modeling of complex sample systems. Currently, he is working at Helmholtz-Zentrum Berlin für Materialien and Energie GmbH, focusing on the investigation of catalytically active thin films via infrared ellipsometry and polarimetry.

Karsten Hinrichs received his PhD from the TU Berlin, Germany in 1999 and he holds a habilitation degree in Physical Chemistry of the TU Dresden. Since 2012 he is a member of the Graduate School of Analytical Sciences at HU Berlin. In 2018 he was editor of the Springer Nature book "Ellipsometry of functional surfaces and thin films" (2nd edition). Currently he works at ISAS e.V. Topical research of him and his team focuses on structure-spectra correlations of functional thin films and the method development of infrared laser-based polarimetry.

Vitali Syritski received his PhD in Chemistry at Tallinn University of Technology in 2004. Currently he is a lead research scientist and the head of the Laboratory of Biofunctional Materials in the Department of Materials and Environmental Technology at TalTech. His present research interests include molecularly imprinted technology and electrochemical analysis. In particular, he has focused on development of chemical and biosensors for accurate and fast detection of disease biomarkers and environmental contaminants.

Appendix 3

PAPER III

V.B.C. Nguyen, J. Reut, A.G. Ayankojo, V. Syritski, Direct Electrochemical Sensing of Ampicillin in Aqueous Media by a Ruthenium Oxide Electrode Decorated with a Molecularly Imprinted Polymer, Talanta 287 (2025) 127580.

Direct electrochemical sensing of ampicillin in aqueous media by a ruthenium oxide electrode decorated with a molecularly imprinted polymer

Vu Bao Chau Nguyen [ID], Jekaterina Reut, Akinrinade George Ayankojo, Vitali Syritski [*] [ID]

Department of Materials and Environmental Technology, Tallinn University of Technology, Ehitajate tee 5, 19086, Tallinn, Estonia

ARTICLE INFO

ABSTRACT

Ampicillin (AMP) ranks third among the top ten most frequently sold antibiotic combinations globally, raising concerns due to its extensive use. Improper disposal practices in agriculture, aquaculture, and healthcare have led to environmental contamination of water sources with elevated AMP levels. Current methods for detecting such contamination are costly, require sophisticated equipment, and depend on skilled personnel and unstable natural receptors. To address these limitations, we introduce AMP sensor for direct electrochemical detection of AMP in aqueous media. This sensor employs a molecularly imprinted polymer (MIP) integrated with a ruthenium oxide electrode, which serves as both a substrate transducer and an internal redox-active probe, eliminating the need for an external probe solution. The sensor exhibited a low limit of detection (LOD) of 6 nM and high recovery rates (98–114 %) in pond water samples, highlighting its sensitivity and practical application. This study demonstrates the potential of MIP-based electrochemical sensors for affordable, rapid, and accurate detection of antibiotic contaminants in water, contributing to improved tools for environmental and public health protection.

1. Introduction

Antibiotics constitute one of the most widely prescribed pharmaceuticals in human and animal medicines. Between 2000 and 2015 alone, global antibiotic consumption rose by 64 % with a predicted further increase of 200 % by 2030 [1]. This alarming trend in the increasing usage of antibiotics has led to their presence either as whole or residual compounds in aquatic environments, posing serious risks to aquatic flora and fauna [2,3]. Also, unregulated exposure to antibiotics has demonstrated toxic effects on animals and plants, disrupting vital metabolic processes involving renal and nerve cells, and impairing plant growth and photosynthesis [4–6]. This situation is exacerbated by the development of resistant bacterial strains due to their exposure to antibiotic residues in the environment, raising substantial public health concerns with 4.95 million deaths in 2019 [7]. Thus, leading international health institutions, such as the World Health Organization (WHO) and the United Nations Children's Emergency Fund (UNICEF), have identified antibiotic resistance as an urgent threat that necessitates robust collaborative efforts to combat [8–10].

To evaluate contamination levels and ensure water safety, current methods such as high-performance liquid chromatography [11–13], mass spectrometry [14–16], immunoassays [17,18], aptamer-based sensor [19–21], and surface-enhanced Raman spectroscopy [22,23] have been widely employed to detect AMP residues in water. Regrettably, they are accompanied by high costs, sophisticated analytical equipment, the need for skilled personnel, as well as unstable natural receptors (e.g., antibodies and enzymes) that are not suitable for field analyses [24]. To overcome these limitations, there is a pressing need to develop portable and simple sensing techniques that incorporate low-cost and stable biomimetic receptors, for on-site analysis.

Molecular imprinting is a synthesis strategy that is used to generate remarkably selective materials - molecularly imprinted polymers (MIPs), which mimic the functionality of natural antibodies [25]. MIPs as alternative receptors possess superior properties including, excellent chemical and thermal stability, cost-effective fabrication, and extended shelf life [26,27]. These attributes make MIPs ideal recognition elements in advanced chemical sensors. By combining MIPs and electrochemical transducers, effective electrochemical sensors that afford real-time monitoring, ease of usage, high sensitivity, and a lower cost than traditional methods can be achieved [26,28,29]. Moreover, the compatibility of electrochemical sensors with microfluidic systems and multiplexing technologies facilitates the large-scale fabrication of portable sensing platforms, positioning them as promising analytical tools for detecting and quantifying environmental pollutants [28,30].

Ampicillin (AMP), a β-lactam antibiotic, ranks third among the top ten most frequently sold fixed-dose antibiotic combinations globally and has elicited increasing concern due to its high utilization rates [31]. This widespread use, coupled with improper disposal practices in aquaculture, and healthcare, has resulted in the environmental contamination of water sources with elevated AMP concentrations [32,33]. Thus, AMP imprinting has been reported in literature where the MIPs were interfaced with various electrode transducers to develop MIP-based electrochemical sensors capable of selectively detecting AMP. For example, X. Shi et al. reported an electrochemically deposited poly(o-phenylenediamine) in the presence of AMP on a gold nanoparticle and single walled carbon nanotube modified glassy carbon electrode to fabricate an AMP-MIP that demonstrated high surface area and a limit of detection (LOD) of 1 nM [34]. Similarly, Y. Sun et al. developed a MIP-based sensor using pyrrole as functional monomer. The MIP was fabricated on a ZrO₂ nanofiber modified gold electrode, achieving a wide linear range and excellent repeatability [35]. Furthermore, Z. Liu's group employed bulk polymerization to generate AMP-MIP on Fe₃N–Co₂N modified carbon electrode using N,N′-dimethylacrylamide as the functional monomer and ethylene glycol dimethacrylate as the cross-linker [36]. The sensor demonstrated a high electrical conductivity and stability as well as large surface area. Moreso, a LOD of 0.4 nM was demonstrated in addition to a good recovery (97–102 %) when used in the analysis of pre-treated milk samples. Yet in another report, AMP-MIP was synthesized on the surface of a modified gold electrode as an electrochemical sensor for analysing AMP in various media, adopting dopamine as a functional monomer [37]. Following optimization, the authors reported the sensor's capacity to detect AMP at femtomolar concentration range.

Notwithstanding the outstanding performances of the sensors documented in the above reports, the monitoring of their performance requires the use of an additional external redox probe solution (e.g., ferricyanide) that helps to convert the molecular interaction on the sensor surface to a measurable signal. Unfortunately, most MIP-based electrochemical sensors targeted towards inactive target molecules depend on such detection principle i.e., monitoring the adsorption-dependent changes in the diffusion of redox probe molecules through the target-specific cavities preformed on the MIP surface [38,39]. However, the dependence on external redox probe introduces several limitations. This includes the complication of sensor design and the introduction of stability issues arising from potential interference from other electroactive species. In addition, employing a redox marker produces an indirect signal that reflects not only target presence but also polymer changes during sample interaction [40]. The existence of these limitations motivates the exploration of alternative approaches, such as incorporating internal redox centres into the electrode material [41,42].

Meanwhile, ruthenium oxide (RuO₂) electrodes offer numerous advantages in electrochemical analysis. Primarily, RuO₂ is esteemed for its steadfast catalytic efficacy, rendering it exceptionally suited for achieving high sensitivity in analytical applications [43]. Furthermore, it demonstrates remarkable thermodynamic stability, ensuring consistent performance of RuO₂ electrodes even under challenging experimental conditions [44]. Also, the expansive potential window of RuO₂ electrodes allows for their exploration in diverse redox processes [45]. Additionally, depending on the synthesis method, RuO₂ electrodes can exhibit a porous structure that provides a large surface area [46], crucial for enhancing charge-transfer characteristics and sensitivity in electrochemical measurements [47]. For example, the pH sensing electrodes based on RuO₂ presented a high sensitivity with minimal cross-sensitivity towards numerous cations and anions, making them well-suited for pH monitoring in complex water samples [48]. Moreover, RuO₂ exhibits versatile electrochemical behavior by possessing multiple accessible oxidation states [49,50], particularly valuable in MIP-based sensor configuration, as a single RuO₂ electrode can serve a dual purpose: an electrochemical transducer and an internal redox probe. This enables MIP-based electrochemical sensors to measure

signals directly, eliminating the need for external probe solutions. As a result, the measurement procedure is simplified and accelerated, reducing contamination risks and ensuring more reliable results. These improved electrochemical characteristics significantly enhance the overall sensor performance.

Despite these advantages, consolidating RuO₂ electrode with MIPs to implement real-life analysis of environmental samples had not received much attention from molecular imprinting community. To the best of our knowledge, the synthesis of MIPs on RuO₂ screen-printed electrodes (SPEs) and their subsequent application in electrochemical sensing platforms for antibiotic determination have not been previously reported.

This study aims to bridge the knowledge gap by developing an electrochemical sensor consisting of a RuO₂ electrode, serving a dual role as an electrochemical transducer and an internal redox probe. Prior to AMP-MIP synthesis, an appropriate functional monomer was selected among several electropolymerizable monomers by employing computer modeling that involved estimating binding energies using density functional theory (DFT)-based quantum chemical calculations. Most important, the performance of the AMP-MIP-based sensor (AMP sensor) was evaluated in a pond water sample to demonstrate its potential for practical on-site applications in environmental water analysis.

2. Experimental

2.1. Chemicals and materials

Ampicillin (AMP) sodium salt, amoxicillin (AMO), doxycycline (DOX), m-Phenylenediamine (mPD) were obtained from Sigma-Aldrich. Acetic acid 99.8 %, potassium dihydrogen phosphate (KH₂PO₄), disodium hydrogen phosphate dodecahydrate (Na₂HPO₄), and potassium chloride (KCl) were from Lach-ner. Sodium chloride (NaCl) was supplied by Honeywell, and methanol was purchased from Thermo Fisher Scientific Inc. The chemicals were received and stored under standard conditions. The aqueous solutions were prepared with ultra-pure water (Direct-Q 3 UV Water Purification system, resistivity 18.2 MΩ cm at 25 °C, Merck KGaA, Darmstadt, Germany). Phosphate-buffered saline (PBS) was prepared from KH₂PO₄, Na₂HPO₄, KCl and NaCl in ultrapure water. The polymer synthesis and all electrochemical measurements were conducted in PBS with a molar concentration of 10 mM and a pH value of 7.4. AMP sodium salt, a highly water-soluble form of AMP, was used as template and analyte. Analyte solutions were meticulously prepared using PBS and pond water.

The pond water was collected from a small and shallow pond located at latitude 59°23′44′′N and longitude 24°39′36′′E in Tallinn, Estonia. The water sample was filtered through filter paper to remove solid matter, such as debris, dirt, and other organic matter. The filtered sample was then poured into a glass bottle and stored at room temperature in a dark place to inhibit algae growth.

The Drop Sense RuO₂ screen-printed electrodes (SPEs) DRP-810 were obtained from Metrohm, a.s. in Spain. DRP-810 consists of a working electrode (WE) with a 4 mm diameter (approximately 12.56 mm²) made of RuO₂, a silver reference electrode (RE), and a carbon counter electrode (CE).

2.2. Functional monomers selection

Five electropolymerizable monomers, including 1,8-diaminonaphthalene (1,8-DAN), aniline (ANI), 3,4-ethylenedioxythiophene (EDOT), mPD, and pyrrole (PYR) were considered for the selection of a suitable functional monomer. The binding energy of complexes between each monomer and AMP with a 1:1 ratio was estimated. First, the structures of the individual compounds and monomer-template complexes underwent geometric optimization using Avogadro 1.2.0 software, employing the Universal Force Field (UFF) for energy minimization. Subsequently, binding energies were computed utilizing DFT method at

the B3LYP/6-31+G level of Gaussian'09 software.

2.3. Sensor preparation

The AMP sensor features an electrochemically deposited AMP-MIP film on the RuO$_2$ WE of the DRP-810 SPE, and connected to a potentiostat (Interface 1000™, Gamry Instruments, Inc., USA) enabling the detection of AMP in solution using linear sweep voltammetry (LSV). The AMP containing PmPD polymer film, denoted as PmPD/AMP, was synthesized on the WE by cyclic voltammetry (CV) in PBS solution containing mPD and AMP sodium salt at a potential range of −0.2 to 0.4 V with a scan rate of 100 mV/s vs the Ag/AgCl/3 M KCl external reference electrode. Subsequently, molecular imprints of AMP were generated after removing the entrapped AMP from PmPD/AMP film. This was achieved by immersing the modified electrode in a washing out solvent of acetic acid-methanol (volume ratio 1:19) for 30 min on vortex, resulting in AMP-MIP formation. A similar process was used for the reference film, non-imprinted polymers (NIPs), with the absence of AMP.

The sensor preparation stages were characterized by LSV in a PBS-based analyte solution, which utilized internal ruthenium oxide redox probe characteristics. The LSV was conducted in the potential range of −0.2 - 0.5 V vs external Ag/AgCl/3 M KCl reference, with a scan rate of 50 mV and a step size of 1 mV.

2.4. Evaluation of sensor performance

To conduct the rebinding investigation, sensors were incubated in PBS containing increasing analyte concentrations, followed by LSV. The anodic current peaks corresponding to each analyte concentration were normalized to represent the concentration-dependent sensor response (I$_n$) using Equation (1):

$$I_n = (I_0 − I) / I_0 \qquad (1)$$

where I$_0$ and I are the LSV current peaks measured after incubation in PBS buffer solutions or pond water without and with analyte, respectively. For similar analysis in pond water samples, the AMP sensor was incubated in pond water spiked with AMP concentrations and then transferred to PBS for LSV measurement (see section S1 for more details).

The selectivity of AMP sensor was evaluated in both PBS and pond water samples by comparing its response upon rebinding of AMP with those induced by other interfering antibiotics, including AMO and DOX. In this case, the AMP sensor's ability to recognize analyte molecules was evaluated by its relative response (RR), i.e. the response related to the respective "blank sensor" containing all components of AMP sensor except for AMP-MIP layer, which was replaced with a NIP layer:

$$RR = I_n(MIP)/I_n(NIP) \qquad (2)$$

where I$_n$(MIP) and I$_n$(NIP) represent the responses of AMP-MIP- and NIP-modified WEs of DRP-810, respectively, against the analytes.

The limits of detection (LOD) and quantification (LOQ) were determined from the linear regression of the sensor's response to low concentrations of the analyte in pond water, using Equations (3) and (4):

$$LOD = 3SD/b \qquad (3)$$

$$LOQ = 10SD/b \qquad (4)$$

where SD and b are the standard deviation of the residual and the slope of the regression line, respectively.

To evaluate the accuracy and reliability of the sensor, a series of recovery experiments were conducted in pond water samples. Thus, known amounts of the target antibiotic (AMP) were spiked into pond water samples and their normalized responses were recorded. Subsequently, the corresponding antibiotic concentrations were determined

using a previously established linear regression of the sensor's response to low concentrations of the analyte in pond water. The recovery percentage (%R) was then calculated using Equation (5):

$$\%R = \left(C_{measured} / C_{spiked} \right).100 \qquad (5)$$

where C$_{measured}$ (nM) is the concentration of the antibiotic estimated by the linear regression equation, and C$_{spiked}$ (nM) is the initial concentration of the antibiotic spiked into the sample. The experiment was performed in triplicates (n = 3) to evaluate the reproducibility.

3. Results and discussion

3.1. Sensor operating principle

In AMP sensor configuration, the RuO$_2$ electrode functions as both an electrochemical transducer and a redox probe, serving as an electrochemical indicator for monitoring target binding to the AMP-MIP-modified electrode surface. The working principle of the AMP sensor is illustrated in Fig. 1. During LSV, the RuO$_2$ electrode undergoes oxidation, prompting anions from the electrolyte to diffuse toward the electrode through the empty imprinted cavities of the AMP-MIP layer to compensate for the positive charge, thereby sustaining the current flow between the electrode and the solution within the electrochemical cell. If the solution contains AMP, its molecules rebind to the imprinted cavities of AMP-MIP obstructing the diffusion of anions towards the RuO$_2$ electrode surface, leading to a noticeable reduction in the measured current. The level of current reduction can be correlated with the concentration of AMP in the solution. Thus, the sensor detects the presence and quantity of AMP by measuring the resulting change in peak current observed during LSV.

3.2. Functional monomer selection

The selection of the functional monomer significantly influences MIP's performance, relying on the strength of interactions with the template molecule to form molecular memory based on its shape and arrangement of functional groups [51,52]. Hence, it is necessary to conduct a preliminary study of molecular complexes between a monomer and template molecule to design MIP with optimal performance. This study investigated electropolymerizable monomers containing functional groups that can form hydrogen bonds with oxygen and hydrogen atoms of template AMP: 1,8-DAN, ANI, EDOT, mPD, and PYR (Fig. 2).

Given that AMP molecule contains 4 oxygen atoms (O1, O2, O3, and O4) and 3 hydrogen atoms (H1, H2, and H3) with potential for hydrogen bonding, we estimated the binding energies between each monomer and the template by individually linking hydrogen atom of the amino group from each of the monomers 1,8-DAN, ANI, mPD or PYR to each oxygen atom of the template AMP (Table 1). Similarly, the binding energies between EDOT and the template AMP were calculated by linking oxygen atom of EDOT to each hydrogen atom of amino or hydroxyl group of AMP. Fig. 3 demonstrates possible points of interaction between AMP and mPD while other monomer-template interactions are depicted in Figs. S2(a–d) of SI. As seen in Table 1, mPD exhibited the greatest overall binding energy, signifying its capability to form robust hydrogen interactions with AMP. Consequently, further experimental work was carried out using mPD as a functional monomer.

3.3. AMP-MIP preparation and characterization

To assess the performance of AMP-MIP for the detection of AMP, initial experiments were conducted on gold slide before proceeding to the RuO$_2$ WE (see more in section S3). Gold was chosen due to its well-characterized electrochemical properties and stable surface chemistry [53,54]. The results in Fig. S3c indicate the formation of the polymer
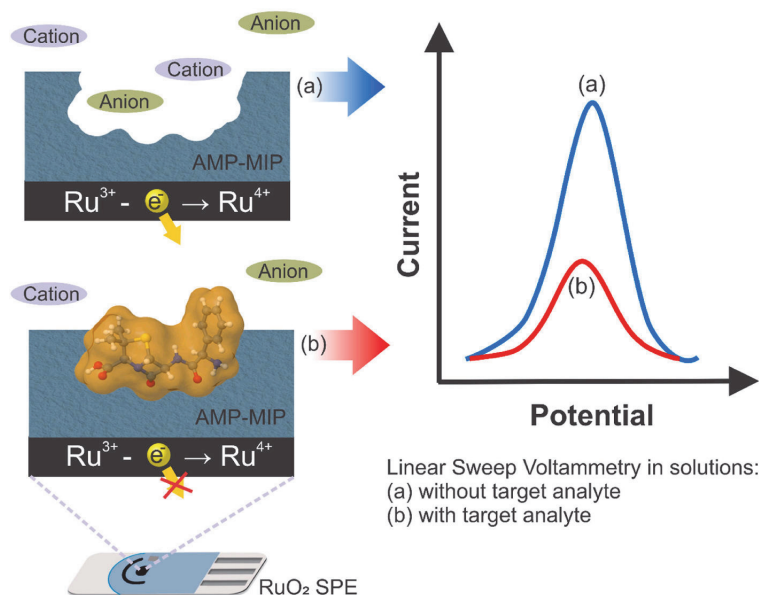
Fig. 1. Scheme showing the operating principle of AMP sensor. (a) In the absence of AMP, the charge is transferred through the binding cavity, providing a strong current peak (blue line). (b) After AMP rebinding, the non-conducting antibiotic molecules obstruct the charge transfer, resulting in a reduced current peak (red line). (For interpretation of the references to colour in this figure legend, the reader is referred to the Web version of this article.)
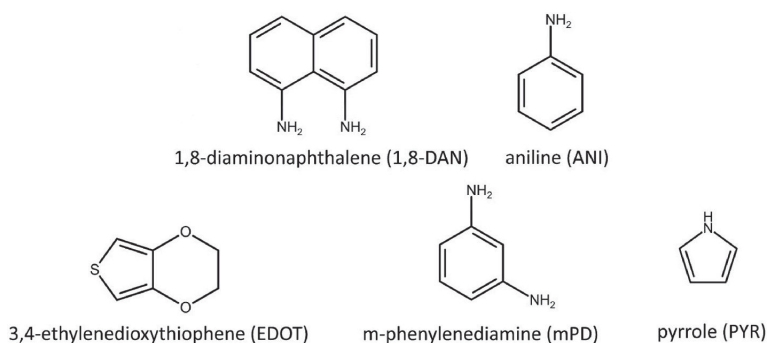
Fig. 2. Structural formula of electropolymerizable monomers examined as potential functional monomers for AMP-MIP synthesis.

Table 1
Hydrogen binding energy of monomers towards different oxygen (O) and hydrogen (H) atoms of AMP as calculated by Gaussian'09 software.

		mPD	ANI	1,8-DAN	PYR	EDOT
Binding energy (kJ/ mol)	O1	−231	−141	−146	−123	–
	O2	−182	−151	−149	−103	–
	O3	−351	−339	−286	−269	–
	O4	−327	−321	−282	−231	–
	H1	–	–	–	–	−278
	H2	–	–	–	–	−168
	H3	–	–	–	–	−107
	Total[a]	−1091	−952	−863	−726	−553

[a] A rough estimate of the overall binding energy was calculated as the sum of the individual binding energies in the 1:1 complex between AMP and the monomer.

film in the presence of AMP (PmPD/AMP), the efficiency of AMP washing out treatment to form AMP-MIP, and the subsequent rebinding behavior of AMP-MIP. This experiment was crucial in the AMP sensor development process as it demonstrated the initial selectivity of AMP-MIP, suggesting its potential effectiveness when later combined with the RuO₂ WE.

For the modification of the RuO₂ WE, CV was employed. This technique is particularly convenient for monitoring the electrochemical activity of RuO₂ WE upon its modification with the PmPD/AMP layer. By adjusting the number of CV cycles, the thickness of the layer could be finely tuned to ensure optimal synergy between the AMP-MIP and the RuO₂ WE, enhancing the sensor's performance in the end.

To assess the feasibility of electropolymerizing mPD on RuO₂ WE, a preliminary test was performed to confirm the electrodeposition of the polymer film over a potential range of −200 to 400 mV in PBS (Fig. 4). As can be seen in Fig. 4a, stable voltammograms, demonstrating the overlay of the 7 successive cycles, were obtained in the absence of mPD
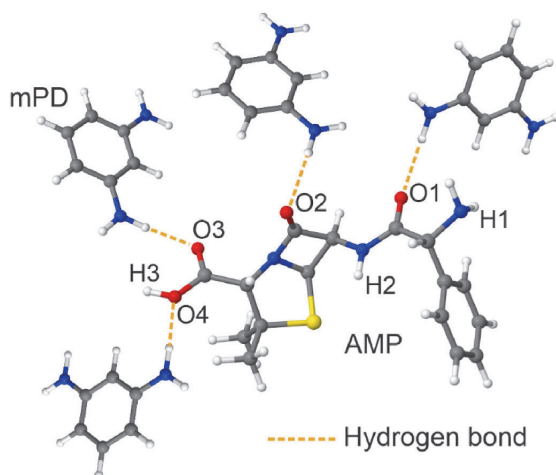
Fig. 3. Schematic representation of possible binding interaction positions between template AMP and mPD.

in PBS. The pair of anodic and cathodic peaks observed at 173 and 0 mV respectively, are attributed to the redox pair of Ru(III)/Ru(IV) (refer to Section S3 in Supplementary Information for more details).

After adding mPD to the PBS solution, a continuous decrease in both anodic and cathodic current peaks with each cycle were observed (Fig. 4b). This trend indicates the formation of a non-conductive film, which hinders charge transfer, providing clear evidence of the poly (mPD) (denoted as PmPD) film's presence and its impact on the electrochemical process on the RuO₂ WE surface.
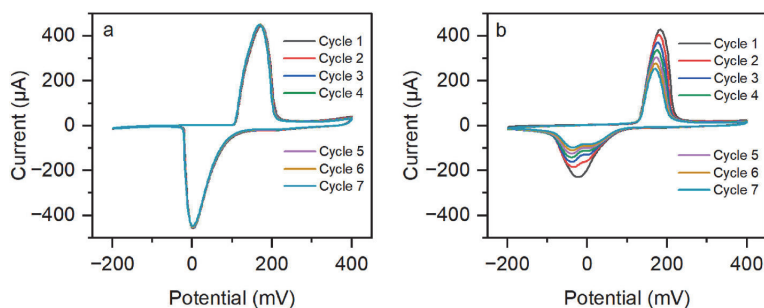
Furthermore, each stage of the AMP sensor preparation process was closely monitored by LSV, where the modifications of the RuO_2 electrode surface were expected to induce changes in charge transfer capability through the electrode surface. As shown in Fig. 5a, a marked reduction in peak currents was observed in the LSV following the electrochemical deposition of PmPD/AMP, indicating surface passivation by electrochemically inactive materials. However, upon treatment with a washing solution to form AMP-MIP, a partial recovery of the previously diminished peaks was observed. This indicates that the washing procedure engenders the removal of the trapped template molecules, thus forming molecular cavities in the polymer and facilitating charge transfer at the electrode/solution interface.

Conversely, similar treatments of the PmPD modified RuO_2 electrode showed no appreciable change in the LSV voltammograms, rather the signals following PmPD electrodeposition, NIP formation, and rebinding with AMP are closely related (Fig. 5b). This result supports, indirectly, that the current rise after treatment with the washing solution is likely due to AMP removal rather than a compromise in the quality of the PmPD layer. Thus, the imprinting of AMP in the PmPD film could be said to be successfully achieved.

3.3.1. Effect of polymer thickness

To determine the optimal thickness of the AMP-MIP layer, at which the sensor produces the strongest response towards AMP, the RuO_2 WE was modified with AMP-MIP films generated from increasing number of CV cycles (4–6 cycles). As seen, the AMP-MIP film formed from 5 CV cycles demonstrated the highest normalized response (I_n) and was thus selected as optimal for further study (Fig. 6a).

3.3.2. Effect of rebinding time

A rapid response time is a desirable characteristic for chemical sensors in environmental monitoring. Accordingly, to determine the optimal recognition time of AMP-MIP towards the target, several AMP sensors were each incubated in PBS containing 10 μM AMP for different

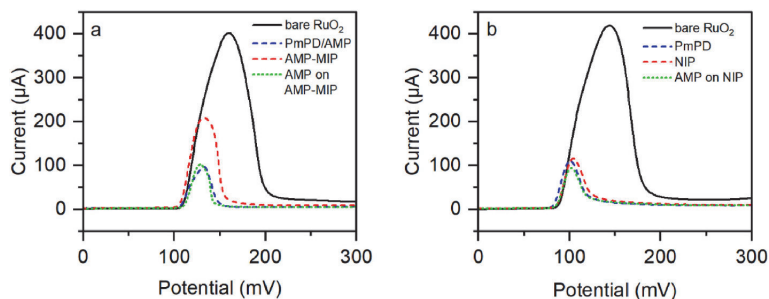**Fig. 4.** CV of RuO_2 WE in PBS (a) without and (b) with 5 mM mPD at a scan rate of 100 mV/s.

Fig. 5. LSV characterization of (a) AMP-MIP and (b) NIP film modification of RuO_2 WE. The data were recorded in PBS at scan rate of 50 mV/s.
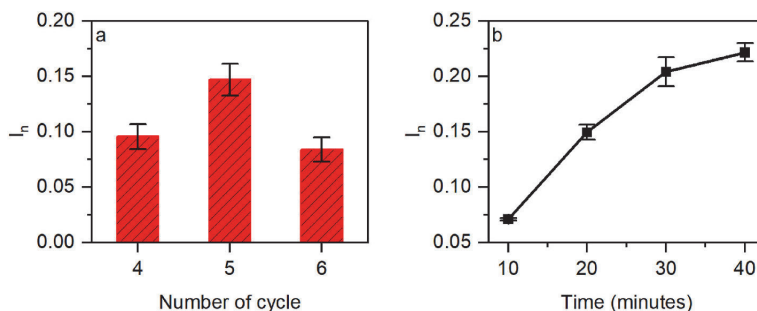
Fig. 6. Responses of AMP sensors (a) generated from different numbers of CV cycle and (b) generated from 5 CV cycles vs. the time of incubation (i.e. rebinding time). Sensor incubation was performed in PBS containing 10 μM AMP.

times, including 10, 20, 30, and 40 min (Fig. 6b). Evidently, a sharp increase in the response was observed with the increase in incubation time from 10 to 30 min. However, further incubation beyond 30 min showed a marginal growth in response. Consequently, 30 min was selected as the appropriate incubation time at which AMP sensor performs optimally and was used for further experiments.

3.4. Evaluation of sensor performance

3.4.1. Selectivity study

Two antibiotic candidates, AMO and DOX, were chosen to evaluate the sensor's ability to distinguish between different compounds (refer to Fig. 7 for their structures). The results presented in Fig. 8a demonstrate that the AMP sensor exhibits significantly higher response for the target compound, AMP. Specifically, the response was 2.4 times higher compared to AMO and 9.5 times higher compared to DOX in PBS. The relative responses (RRs) were also greater for AMP, reaching 4.2, compared to AMO at 2.1 and DOX at 1.6 (refer to Table S2).

Upon testing in pond water (Fig. 8b), the sensor showed even higher response values. This is likely due to the presence of diverse organic matter, microorganisms, potential pollutants, and inorganic substances such as minerals in natural pond water [55–57], which increase

background noise. In this context, the signal response of AMP sensor in the presence of AMP was 2.4 times higher than that for AMO and 5.2 times higher than for DOX. Likewise, the RRs were higher for AMP in comparison to both AMO and DOX (refer to Table S3). These findings indicate that the AMP sensor can effectively discriminate between AMP and other antibiotic molecules at high concentrations (10 μM) in both PBS and pond water samples.

Additionally, the sensor's performance was evaluated in pond water spiked with a low concentration (50 nM) of each antibiotic, mimicking real-world conditions as found for AMP in surface water at approximately 46 nM and in wastewater effluents in the range of 7–121 nM [58, 59]. As shown in Fig. 8c, the AMP sensor demonstrated the highest response towards AMP compared to AMO and DOX. The RRs were also higher for AMP, with a value of 2.4, compared to 1.7 for AMO and 1.6 for DOX (refer to Table S4). This underscores the significance of forming AMP-imprinted cavities within the AMP-MIP layer, which allows for the discriminatory recognition of the target over other antibiotics.

3.4.2. Detection limit

The successful implementation of a sensor in detecting low analyte concentrations is of paramount interest in MIP-based sensor development. Hence, further study was planned to evaluate the performance of
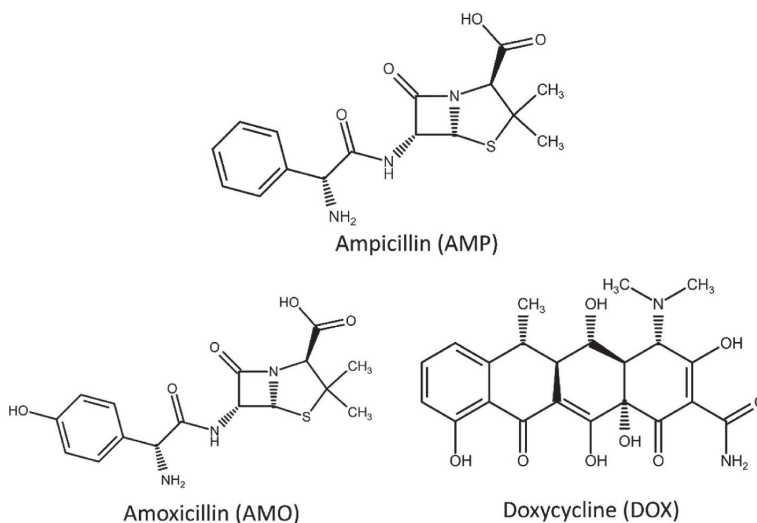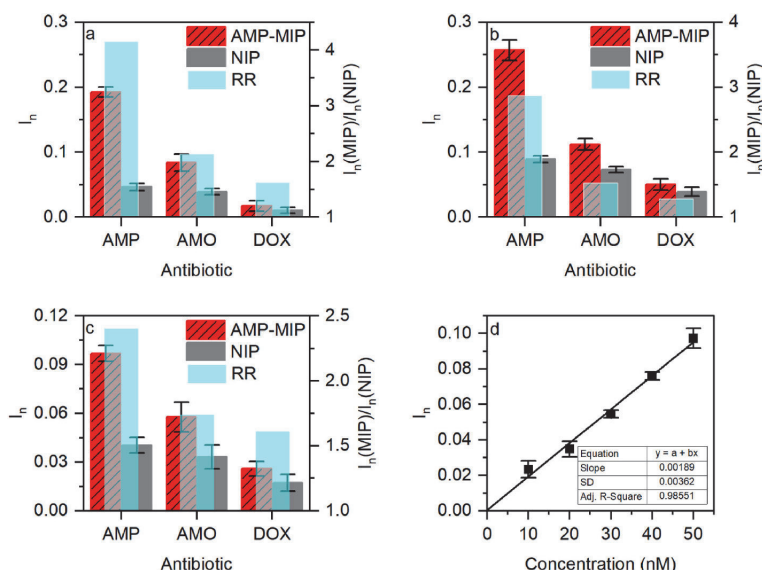

Fig. 7. Antibiotic molecules used in selectivity experiments, including AMO (365.4 g/mol) which belongs to the same class of aminopenicillin antibiotic as AMP (394.4 g/mol), and DOX (444.4 g/mol) that is a member of tetracycline antibiotic class.

Fig. 8. Responses of AMP-MIP and NIP-based sensors following incubation in different antibiotic solutions (AMP, AMO, DOX) at concentrations (a) 10 μM in PBS, (b) 10 μM in pond water, and (c) 50 nM in pond water. (d) Performance of AMP sensor at low analyte concentration (10–50 nM) in pond water. The solid line is a linear regression fit. The error bars represent the standard deviation of three measurements conducted using three independent AMP sensors.

the AMP sensor in low concentration range and to determine its quantitative limits, including LOD and LOQ. As shown in Fig. 8d, the response of the AMP sensor linearly increases with analyte concentrations up to 50 nM in pond water (referred to Fig. S5 for LSV responses). The LOD and LOQ values, calculated using Equations (3) and (4), are 6 nM and 19 nM respectively. This indicates the suitability of the sensor for analyzing AMP in environmental water samples, as AMP is found in surface water and wastewater treatment plant effluents within the nanomolar range [58,59].

To validate the accuracy and reliability of the sensor, a series of recovery experiments were conducted using AMP solutions of varying concentrations in pond water (as detailed in Table 2). The sensor showed good recoveries within the range of 98 %–114 %, confirming its robust performance.

4. Conclusion

The results obtained in this report showcase the uniqueness and significance of combining a MIP-based sensing element with an RuO$_2$ electrode for the development of an electrochemical sensor applicable in environmental monitoring. While the AMP-MIP provides a robust selectivity for AMP target, the RuO$_2$ electrode serves a dual purpose of a transducer and an internal redox probe that permits a direct detection of the non-electroactive analyte, deviating from the traditional requirement of an external probe solution. The strong discriminatory recognition of AMP in the presence of other aminopenicillin antibiotic and other antibiotics class in both buffer and pond water samples establishes the suitability of the sensor for the intended usage in environmental water. In addition, the LOD of 6 nM obtained in pond water samples accurately positions the sensor for potential deployment in the analysis of the target molecules since AMP presents itself within the nM concentration range in the aqueous environment. Lastly, the achieved recoveries (98–114 %) indicate the reliability of the sensor for accurate analysis beyond the margin of errors. Thus, by adopting the approach presented in this work, the potential for a sensitive, direct, accelerated, and accurate analysis of antibiotic pollutants in environmental water is achievable.

Table 2
Recoveries of AMP sensor in pond water samples as calculated by Equation (5).

Spiked AMP (nM)	Found AMP (nM)	Recovery (%)
20	23 ± 1	114 ± 7
35	34 ± 2	98 ± 5
50	52 ± 3	104 ± 6

CRediT authorship contribution statement

Vu Bao Chau Nguyen: Writing – review & editing, Writing – original draft, Investigation, Formal analysis. **Jekaterina Reut:** Writing – review & editing, Supervision. **Akinrinade George Ayankojo:** Writing – review & editing. **Vitali Syritski:** Writing – review & editing, Supervision, Resources, Project administration, Methodology, Funding acquisition, Formal analysis, Data curation, Conceptualization.

Declaration of competing interest

The authors declare the following financial interests/personal relationships which may be considered as potential competing interests: Vitali Syritski reports financial support was provided by Estonian Research Council. If there are other authors, they declare that they have no known competing financial interests or personal relationships that could have appeared to influence the work reported in this paper.

Appendix A. Supplementary data

Supplementary data to this article can be found online at https://doi.org/10.1016/j.talanta.2025.127580.

Data availability

Data will be made available on request.

References

[1] E.Y. Klein, T.P. Van Boeckel, E.M. Martinez, S. Pant, S. Gandra, S.A. Levin, H. Goossens, R. Laxminarayan, Global Increase and Geographic Convergence in Antibiotic Consumption between 2000 and 2015, vol. 115, Proceedings of the National Academy of Sciences, 2018, pp. E3463–E3470, https://doi.org/10.1073/pnas.1717295115.

[2] A.M. Sánchez-Baena, L.D. Caicedo-Bejarano, M. Chávez-Vivas, Structure of bacterial community with resistance to antibiotics in aquatic environments. A systematic review, IJERPH 18 (2021) 2348, https://doi.org/10.3390/ijerph18052348.

[3] X. Mu, Z. Huang, O.E. Ohore, J. Yang, K. Peng, S. Li, X. Li, Impact of antibiotics on microbial community in aquatic environment and biodegradation mechanism: a review and bibliometric analysis, Environ. Sci. Pollut. Res. 30 (2023) 66431–66444, https://doi.org/10.1007/s11356-023-27018-w.

[4] A. Elizalde-Velázquez, L.M. Gómez-Oliván, M. Galar-Martínez, H. Islas-Flores, O. Dublán-García, N. SanJuan-Reyes, Amoxicillin in the aquatic environment, its fate and environmental risk, in: M. Larramendy, S. Soloneski (Eds.), Environmental Health Risk - Hazardous Factors to Living Species, InTech, 2016, https://doi.org/10.5772/62049.

[5] P. Grenni, V. Ancona, A. Barra Caracciolo, Ecological effects of antibiotics on natural ecosystems: a review, Microchem. J. 136 (2018) 25–39, https://doi.org/10.1016/j.microc.2017.02.006.

[6] L. Liu, W. Wu, J. Zhang, P. Lv, L. Xu, Y. Yan, Progress of research on the toxicology of antibiotic pollution in aquatic organisms, Acta Ecol. Sin. 38 (2018) 36–41, https://doi.org/10.1016/j.chnaes.2018.01.006.

[7] C.J.L. Murray, K.S. Ikuta, F. Sharara, L. Swetschinski, G. Robles Aguilar, A. Gray, C. Han, C. Bisignano, P. Rao, E. Wool, S.C. Johnson, A.J. Browne, M.G. Chipeta, F. Fell, S. Hackett, G. Haines-Woodhouse, B.H. Kashef Hamadani, E.A.P. Kumaran, B. McManigal, S. Achalapong, R. Agarwal, S. Akech, S. Albertson, J. Amuasi, J. Andrews, A. Aravkin, E. Ashley, F.-X. Babin, F. Bailey, S. Baker, B. Basnyat, A. Bekker, R. Bender, J.A. Berkley, A. Bethou, J. Bielicki, S. Boonkasidecha, J. Bukosia, C. Carvalheiro, C. Castañeda-Orjuela, V. Chansamouth, S. Chaurasia, S. Chiurchiù, F. Chowdhury, R. Clotaire Donatien, A.J. Cook, B. Cooper, T. R. Cressey, E. Criollo-Mora, M. Cunningham, S. Darboe, N.P.J. Day, M. De Luca, K. Dokova, A. Dramowski, S.J. Dunachie, T. Duong Bich, T. Eckmanns, D. Eibach, A. Emami, N. Feasey, N. Fisher-Pearson, K. Forrest, C. Garcia, D. Garrett, P. Gastmeier, A.Z. Giref, R.C. Greer, V. Gupta, S. Haller, A. Haselbeck, S.I. Hay, M. Holm, S. Hopkins, Y. Hsia, K.C. Iregbu, J. Jacobs, D. Jarovsky, F. Javanmardi, A. W.J. Jenney, M. Khorana, S. Khusuwan, N. Kissoon, E. Kobeissi, T. Kostyanev, F. Krapp, R. Krumkamp, A. Kumar, H.H. Kyu, C. Lim, K. Lim, D. Limmathurotsakul, M.J. Loftus, M. Lunn, J. Ma, A. Manoharan, F. Marks, J. May, M. Mayxay, N. Mturi, T. Munera-Huertas, P. Musicha, L.A. Musila, M.M. Mussi-Pinhata, R.N. Naidu, T. Nakamura, R. Nanavati, S. Nangia, P. Newton, C. Ngoun, A. Novotney, D. Nwakanma, C.W. Obiero, T.J. Ochoa, A. Olivas-Martinez, P. Olliaro, E. Ooko, E. Ortiz-Brizuela, P. Ounchanum, G.D. Pak, J.L. Paredes, A.Y. Peleg, C. Perrone, T. Phe, K. Phommasone, N. Plakkal, A. Ponce-de-Leon, M. Raad, T. Ramdin, S. Rattanavong, A. Riddell, T. Roberts, J.V. Robotham, A. Roca, V.D. Rosenthal, K. E. Rudd, N. Russell, H.S. Sader, W. Saengchan, J. Schnall, J.A.G. Scott, S. Seekaew, M. Sharland, M. Shivamallappa, J. Sifuentes-Osornio, A.J. Simpson, N. Steenkeste, A.J. Stewardson, T. Stoeva, N. Tasak, A. Thaiprakong, G. Thwaites, C. Tigoi, C. Turner, P. Turner, H.R. Van Doorn, S. Velaphi, A. Vongpradith, M. Vongsouvath, H. Vu, T. Walsh, J.L. Walson, S. Waner, T. Wangrangsimakul, P. Wannapinij, T. Wozniak, T.E.M.W. Young Sharma, K.C. Yu, P. Zheng, B. Sartorius, A.D. Lopez, A. Stergachis, C. Moore, C. Dolecek, M. Naghavi, Global burden of bacterial antimicrobial resistance in 2019: a systematic analysis, Lancet 399 (2022) 629–655, https://doi.org/10.1016/S0140-6736(21)02724-0.

[8] Geneva: world, World Health Organization, Global antimicrobial resistance and use surveillance system (GLASS) report 2022. https://www.who.int/publications/i/item/9789240062702, 2022.

[9] World Health Organization, WHO reports widespread overuse of antibiotics in patients hospitalized with COVID-19. https://www.who.int/news/item/26-04-2024-who-reports-widespread-overuse-of-antibiotics-in-patients–hospitalized-with-covid-19, 2024. (Accessed 30 May 2024).

[10] UNICEF, A UNICEF guidance note on antimicrobial resistance. https://www.unicef.org/documents/amr-urgent-threat-drug-resistant-infections, 2023. (Accessed 30 May 2024).

[11] C. Kim, H.-D. Ryu, E.G. Chung, Y. Kim, Determination of 18 veterinary antibiotics in environmental water using high-performance liquid chromatography-q-orbitrap combined with on-line solid-phase extraction, J. Chromatogr. B 1084 (2018) 158–165, https://doi.org/10.1016/j.jchromb.2018.03.038.

[12] R.F. Straub, R.D. Voyksner, Determination of penicillin G, ampicillin, amoxicillin, cloxacillin and cephapirin by high-performance liquid chromatography—electrospray mass spectrometry, J. Chromatogr. A 647 (1993) 167–181, https://doi.org/10.1016/0021-9673(93)83336-Q.

[13] O. Opriş, M.-L. Soran, V. Coman, F. Copaciu, D. Ristoiu, Determination of some frequently used antibiotics in waste waters using solid phase extraction followed by high performance liquid chromatography with diode array and mass spectrometry detection, Open Chem. 11 (2013) 1343–1351, https://doi.org/10.2478/s11532-013-0263-y.

[14] R. Lindberg, P.-Å. Jarnheimer, B. Olsen, M. Johansson, M. Tysklind, Determination of antibiotic substances in hospital sewage water using solid phase extraction and liquid chromatography/mass spectrometry and group analogue internal standards, Chemosphere 57 (2004) 1479–1488, https://doi.org/10.1016/j.chemosphere.2004.09.015.

[15] M. Gros, S. Rodríguez-Mozaz, D. Barceló, Rapid analysis of multiclass antibiotic residues and some of their metabolites in hospital, urban wastewater and river water by ultra-high-performance liquid chromatography coupled to quadrupole-linear ion trap tandem mass spectrometry, J. Chromatogr. A 1292 (2013) 173–188, https://doi.org/10.1016/j.chroma.2012.12.072.

[16] F. Bruno, R. Curini, A.D. Corcia, M. Nazzari, R. Samperi, Method development for measuring trace levels of penicillins in aqueous environmental samples, Rapid Comm Mass Spectrometry 15 (2001) 1391–1400, https://doi.org/10.1002/rcm.381.

[17] G. Merola, E. Martini, M. Tomassetti, L. Campanella, New immunosensor for β-lactam antibiotics determination in river waste waters, Sensor. Actuator. B Chem. 199 (2014) 301–313, https://doi.org/10.1016/j.snb.2014.03.083.

[18] H. Lin, F. Fang, J. Zang, J. Su, Q. Tian, R. Kumar Kankala, X. Lin, A fluorescent sensor-assisted paper-based competitive lateral flow immunoassay for the rapid and sensitive detection of ampicillin in hospital wastewater, Micromachines 11 (2020) 431, https://doi.org/10.3390/mi11040431.

[19] J. Lin, A. Shi, Z. Zheng, L. Huang, Y. Wang, H. Lin, X. Lin, Simultaneous quantification of ampicillin and kanamycin in water samples based on lateral flow aptasensor strip with an internal line, Molecules 26 (2021) 3806, https://doi.org/10.3390/molecules26133806.

[20] J. Wang, K. Ma, H. Yin, Y. Zhou, S. Ai, Aptamer based voltammetric determination of ampicillin using a single-stranded DNA binding protein and DNA functionalized gold nanoparticles, Microchim. Acta 185 (2018) 68, https://doi.org/10.1007/s00604-017-2566-8.

[21] Z. Yu, A.L. Sutlief, R.Y. Lai, Towards the development of a sensitive and selective electrochemical aptamer-based ampicillin sensor, Sensor. Actuator. B Chem. 258 (2018) 722–729, https://doi.org/10.1016/j.snb.2017.11.193.

[22] Y.-T. Li, L.-L. Qu, D.-W. Li, Q.-X. Song, F. Fathi, Y.-T. Long, Rapid and sensitive in-situ detection of polar antibiotics in water using a disposable Ag–graphene sensor based on electrophoretic preconcentration and surface-enhanced Raman spectroscopy, Biosens. Bioelectron. 43 (2013) 94–100, https://doi.org/10.1016/j.bios.2012.12.005.

[23] S. Gao, J. Glasser, L. He, A filter-based surface enhanced Raman spectroscopic assay for rapid detection of chemical contaminants, JoVE (2016) 53791, https://doi.org/10.3791/53791.

[24] A.G. Ayankojo, J. Reut, A. Öpik, A. Tretjakov, V. Syritski, Enhancing binding properties of imprinted polymers for the detection of small molecules, Proc. Est. Acad. Sci. 67 (2018) 138–146, https://doi.org/10.3176/proc.2018.2.04.

[25] K. Mosbach, Molecular imprinting, Trends Biochem. Sci. 19 (1994) 9–14, https://doi.org/10.1016/0968-0004(94)90166-X.

[26] A. Herrera-Chacón, X. Cetó, M. del Valle, Molecularly imprinted polymers - towards electrochemical sensors and electronic tongues, Anal. Bioanal. Chem. 413 (2021) 6117–6140, https://doi.org/10.1007/s00216-021-03313-8.

[27] B. Önal Acet, T. İnanan, K. Salieva, B. Borkoev, M. Odabaşı, Ö. Acet, Molecular imprinted polymers: important advances in biochemistry, biomedical and biotechnology, Polym. Bull. (2024), https://doi.org/10.1007/s00289-024-05238-5.

[28] X. Zheng, S. Khaoulani, N. Ktari, M. Lo, A.M. Khalil, C. Zerrouki, N. Fourati, M. M. Chehimi, Towards clean and safe water: a review on the emerging role of imprinted polymer-based electrochemical sensors, Sensors 21 (2021) 4300, https://doi.org/10.3390/s21134300.

[29] A.G. Ayankojo, J. Reut, V. Syritski, Electrochemically synthesized MIP sensors: applications in healthcare diagnostics, Biosensors 14 (2024) 71, https://doi.org/10.3390/bios14020071.

[30] A.G. Ayankojo, J. Reut, V.B.C. Nguyen, R. Boroznjak, V. Syritski, Advances in detection of antibiotic pollutants in aqueous media using molecular imprinting technique—a review, Biosensors 12 (2022) 441, https://doi.org/10.3390/bios12070441.

[31] B. Bortone, C. Jackson, Y. Hsia, J. Bielicki, N. Magrini, M. Sharland, High global consumption of potentially inappropriate fixed dose combination antibiotics: analysis of data from 75 countries, PLoS One 16 (2021) e0241899, https://doi.org/10.1371/journal.pone.0241899.

[32] P.A. Segura, M. François, C. Gagnon, S. Sauvé, Review of the occurrence of anti-infectives in contaminated wastewaters and natural and drinking waters, Environ. Health Perspect. 117 (2009) 675–684, https://doi.org/10.1289/ehp.11776.

[33] J. Peris-Vicente, E. Peris-García, J. Albiol-Chiva, A. Durgbanshi, E. Ochoa-Aranda, S. Carda-Broch, D. Bose, J. Esteve-Romero, Liquid chromatography, a valuable tool in the determination of antibiotics in biological, food and environmental samples, Microchem. J. 177 (2022) 107309, https://doi.org/10.1016/j.microc.2022.107309.

[34] X. Shi, X. Ren, N. Jing, J. Zhang, Electrochemical determination of ampicillin based on an electropolymerized poly(o-phenylenediamine)/gold nanoparticle/single-walled carbon nanotube modified glassy carbon electrode, Anal. Lett. 53 (2020) 2854–2867, https://doi.org/10.1080/00032719.2020.1759619.

[35] Y. Sun, F. Shao, Y. Luo, H. Wang, Y. He, L. Sun, D. Xu, ZrO₂ nanofiber-based molecular imprinted electrochemical sensor for detection of ampicillin, J. Electrochem. Soc. 171 (2024) 096507, https://doi.org/10.1149/1945-7111/ad7764.

[36] Z. Liu, T. Fan, Y. Zhang, X. Ren, Y. Wang, H. Ma, Q. Wei, Electrochemical assay of ampicillin using Fe3N-Co2N nanoarray coated with molecularly imprinted

polymer, Microchim. Acta 187 (2020) 442, https://doi.org/10.1007/s00604-020-04432-2.

[37] T. Tao, X. Wei, Z. Ye, B. Zong, Q. Li, S. Mao, Dual recognition strategy-based transistor sensor array for ultrasensitive and multi-target detection of antibiotics, Adv. Funct. Mater. (2024) 2413485, https://doi.org/10.1002/adfm.202413485.

[38] A.G. Ayankojo, J. Reut, V. Ciocan, A. Öpik, V. Syritski, Molecularly imprinted polymer-based sensor for electrochemical detection of erythromycin, Talanta 209 (2020) 120502, https://doi.org/10.1016/j.talanta.2019.120502.

[39] O.T. Vu, Q.H. Nguyen, T. Nguy Phan, T.T. Luong, K. Eersels, P. Wagner, L.T. N. Truong, Highly sensitive molecularly imprinted polymer-based electrochemical sensors enhanced by gold nanoparticles for norfloxacin detection in aquaculture water, ACS Omega 8 (2023) 2887–2896, https://doi.org/10.1021/acsomega.2c04414.

[40] A. Yarman, F.W. Scheller, How reliable is the electrochemical readout of MIP sensors? Sensors 20 (2020) 2677, https://doi.org/10.3390/s20092677.

[41] P. Lach, A. Garcia-Cruz, F. Canfarotta, A. Groves, J. Kalecki, D. Korol, P. Borowicz, K. Nikiforow, M. Cieplak, W. Kutner, S.A. Piletsky, P.S. Sharma, Electroactive molecularly imprinted polymer nanoparticles for selective glyphosate determination, Biosens. Bioelectron. 236 (2023) 115381, https://doi.org/10.1016/j.bios.2023.115381.

[42] A. Garcia-Cruz, O.S. Ahmad, K. Alanazi, E. Piletska, S.A. Piletsky, Generic sensor platform based on electro-responsive molecularly imprinted polymer nanoparticles (e-NanoMIPs), Microsyst Nanoeng 6 (2020) 83, https://doi.org/10.1038/s41378-020-00193-3.

[43] H. Li, H. Sun, J. Ding, T. Wu, S. Cai, C. Wang, R. Yang, RuO2/rGO heterostructures as mimic peroxidases for colorimetric detection of glucose, Microchim. Acta 189 (2022) 261, https://doi.org/10.1007/s00604-022-05319-0.

[44] N. Hodnik, P. Jovanovič, A. Pavlišič, B. Jozinović, M. Zorko, M. Bele, V.S. Šelih, M. Šala, S. Hočevar, M. Gaberšček, New insights into corrosion of ruthenium and ruthenium oxide nanoparticles in acidic media, J. Phys. Chem. C 119 (2015) 10140–10147, https://doi.org/10.1021/acs.jpcc.5b01832.

[45] D. Majumdar, T. Maiyalagan, Z. Jiang, Recent progress in ruthenium oxide-based composites for supercapacitor applications, Chemelectrochem 6 (2019) 4343–4372, https://doi.org/10.1002/celc.201900668.

[46] N. Lenar, B. Paczosa-Bator, R. Piech, Optimization of ruthenium dioxide solid contact in ion-selective electrodes, Membranes 10 (2020) 182, https://doi.org/10.3390/membranes10080182.

[47] T. Roy, M.A. Salazar De Troya, M.A. Worsley, V.A. Beck, Topology optimization for the design of porous electrodes, Struct. Multidiscip. Optim. 65 (2022) 171, https://doi.org/10.1007/s00158-022-03249-2.

[48] K. Uppuluri, M. Lazouskaya, D. Szwagierczak, K. Zaraska, M. Tamm, Fabrication, potentiometric characterization, and application of screen-printed RuO2 pH electrodes for water quality testing, Sensors 21 (2021) 5399, https://doi.org/10.3390/s21165399.

[49] S. Chalupczok, P. Kurzweil, H. Hartmann, C. Schell, The redox chemistry of ruthenium dioxide: a cyclic voltammetry study—review and revision, International Journal of Electrochemistry 2018 (2018) 1–15, https://doi.org/10.1155/2018/1273768.

[50] J.W. Long, K.E. Swider, C.I. Merzbacher, D.R. Rolison, Voltammetric characterization of ruthenium oxide-based aerogels and other RuO$_2$ solids: the nature of capacitance in nanostructured materials, Langmuir 15 (1999) 780–785, https://doi.org/10.1021/la980785a.

[51] V.B.C. Nguyen, A.G. Ayankojo, J. Reut, J. Rappich, A. Furchner, K. Hinrichs, V. Syritski, Molecularly imprinted co-polymer for class-selective electrochemical detection of macrolide antibiotics in aqueous media, Sensor. Actuator. B Chem. 374 (2023) 132768, https://doi.org/10.1016/j.snb.2022.132768.

[52] V.B.C. Nguyen, J. Reut, J. Rappich, K. Hinrichs, V. Syritski, Molecularly imprinted polymer-based electrochemical sensor for the detection of azoxystrobin in aqueous media, Polymers 16 (2024) 1394, https://doi.org/10.3390/polym16101394.

[53] C. Malitesta, E. Mazzotta, R.A. Picca, A. Poma, I. Chianella, S.A. Piletsky, MIP sensors – the electrochemical approach, Anal. Bioanal. Chem. 402 (2012) 1827–1846, https://doi.org/10.1007/s00216-011-5405-5.

[54] X. Dong, C. Zhang, X. Du, Z. Zhang, Recent advances of nanomaterials-based molecularly imprinted electrochemical sensors, Nanomaterials 12 (2022) 1913, https://doi.org/10.3390/nano12111913.

[55] B. Oertli, D. Auderset Joye, E. Castella, R. Juge, D. Cambin, J.-B. Lachavanne, Does size matter? The relationship between pond area and biodiversity, Biol. Conserv. 104 (2002) 59–70, https://doi.org/10.1016/S0006-3207(01)00154-9.

[56] L. Clevenot, C. Carré, P. Pech, A review of the factors that determine whether stormwater ponds are ecological traps and/or high-quality breeding sites for Amphibians, Front. Ecol. Evol. 6 (2018), https://doi.org/10.3389/fevo.2018.00040.

[57] L. Ritter, K. Solomon, P. Sibley, K. Hall, P. Keen, G. Mattu, B. Linton, Sources, pathways, and relative risks of contaminants in surface water and groundwater: a perspective prepared for the Walkerton inquiry, J. Toxicol. Environ. Health 65 (2002) 1–142, https://doi.org/10.1080/152873902753338572.

[58] A.C. Faleye, A.A. Adegoke, K. Ramluckan, F. Bux, T.A. Stenström, Antibiotic residue in the aquatic environment: status in africa, Open Chem. 16 (2018) 890–903, https://doi.org/10.1515/chem-2018-0099.

[59] P. Kulkarni, N. Olson, G. Raspanti, R. Rosenberg Goldstein, S. Gibbs, A. Sapkota, A. Sapkota, Antibiotic concentrations decrease during wastewater treatment but persist at low levels in reclaimed water, IJERPH 14 (2017) 668, https://doi.org/10.3390/ijerph14060668.

Curriculum vitae

Personal data

Name:	Vu Bao Chau Nguyen
Date of birth:	02/01/1991
Place of birth:	Vietnam
Citizenship:	Vietnamese

Contact data

E-mail:	deannguyen91@gmail.com

Education

2021–2025	Tallinn University of Technology, PhD
2019–2021	Tallinn University of Technology, MSC
2015–2017	Ho Chi Minh City University of Technology, MSC
2009–2014	Ho Chi Minh City University of Technology, BSC
2007–2009	Nguyen Hien, High school

Language competence

Vietnamese	Native
English	Fluent
Chinese (Mandarin)	Good
Estonian	Basic

Professional employment

2015–2019	Mitalab Co., Vietnam, Application Specialist

Elulookirjeldus

Isikuandmed

Nimi:	Vu Bao Chau Nguyen
Sünniaeg:	02/01/1991
Sünnikoht:	Vietnam
Kodakondsus:	Vietnami

Kontaktandmed

E-post:	deannguyen91@gmail.com

Hariduskäik

2021–2025	Tallinna Tehnikaülikool, PhD
2019–2021	Tallinna Tehnikaülikool, MSC
2015–2017	Ho Chi Minhi Linna Tehnikaülikool, MSC
2009–2014	Ho Chi Minhi Linna Tehnikaülikool, BSC
2007–2009	Nguyen Hien, Keskkool

Keelteoskus

Vietnami keel	Emakeel
Inglise keel	Kõrgtase
Hiina keel	Kesktase
Eesti keel	Algtase

Teenistuskäik

2015–2019	Mitalab Co., Vietnam, Rakenduste Spetsialist